Franz Lichtenegger, BSc

Evaluation of different control concepts for an SDPF-SCR based exhaust gas after-treatment system

MASTER'S THESIS

for obtaining the degree of
Master of Science in Engineering
Master's Degree Programme Electrical Engineering

submitted at

Graz University of Technology

under the guidance of
Univ.-Prof. Dipl.-Ing. Dr.techn. Martin Horn
Institute of Automation and Control

Graz, October 2016

Acknowledgements

This master's thesis was conducted at AVL-List GmbH in Graz, Austria from November 2015 to November 2016.

At this point I would like to thank AVL-List GmbH, especially Dipl.-Ing. Alois Danninger for making it possible for me to carry out my research. I am also thankful for the excellent guidance and technical support over the whole time by my supervisor Dipl.-Ing. Armin Wabnig at AVL. I would also like to thank Rafael Candau Sanchez de Ybargueen, MSc, Dipl.-Ing. Christina Schwarz and Soeren Hage, MSc for many interesting and informative conversations.

For the technical support and many helpful comments on this text I would like to thank my supervisor Univ.-Prof. Dipl.-Ing. Dr.techn. Martin Horn at the Institute of Automation and Control at the University of Technology Graz.

Finally, my sincere thanks go to my family and my girlfriend Therese for their support, understanding and motivation over the course of the last six years.

Eidesstattliche Erklärung
Affidavit

Ich erkläre an Eides statt, dass ich die vorliegende Arbeit selbstständig verfasst, andere als die angegebenen Quellen/Hilfsmittel nicht benutzt, und die den benutzten Quellen wörtlich und inhaltlich entnommenen Stellen als solche kenntlich gemacht habe. Das in TUGRAZonline hochgeladene Textdokument ist mit der vorliegenden Masterarbeit identisch.

I declare that I have authored this thesis independently, that I have not used other than the declared sources/resources, and that I have explicitly indicated all material which has been quoted either literally or by content from the sources used. The text document uploaded to TUGRAZonline is identical to the present master's thesis.

Graz, am 28.10.2016 Franz Lichtenegger

Abstract

It is a known fact that global energy consumption is constantly increasing, especially due to the growing number of motor vehicles. However, the progression of global warming and environmental pollution gradually leads to a change of thinking in society and politics. More and more states are introducing even tougher emission limits for engines. And since engine modifications for further reduction of pollution often have negative effects on efficiency, exhaust gas after-treatment systems are necessary to meet these tough limits now and in the future.

Nowadays, different systems for reducing pollutant emissions are available. One of the most efficient in the reduction of nitrogen oxides is the SCR system which reduces nitrogen oxides to molecular nitrogen and water with ammonia. Further developments of exhaust gas filters and catalysts resulted in a diesel particle filter with SCR functionality (SDPF). The aim of this study is to investigate and evaluate different control concepts for exhaust gas after-treatment systems based on SDFP and SCR catalysts.

The introductory part of this thesis is about different emission legislations and the SCR process itself. Since the combination of SDPF and SCR offers many possible control strategies, three of them were chosen for further investigation.

The main part of this thesis focuses on the control design and the simulation of the concepts. Three different test cycles were used to analyse the control behaviour. The comparison of the simulation results showed that one of the investigated concepts clearly exhibits the most promising control behaviour.

Kurzfassung

Der Energieverbrauch weltweit steigt stetig an, nicht zuletzt auch auf Grund der wachsenden Zahl an Kraftfahrzeugen. Das Fortschreiten der Klimaerwärmung und der Umweltverschmutzung führen zum Umdenken in der Gesellschaft und Politik. Immer mehr Länder führen immer strengere Emissiongrenzwerte im Motorenbereich ein. Da innermotorische Maßnahmen zur Reduktion von Schadstoffen oft negative Auswirkungen auf die Effizienz haben, sind teilweise schon jetzt und vor allem in Zukunft Abgasnachbehandlungssysteme erforderlich, um die strengen Grenzwerte einhalten zu können.

Zur Reduktion von Schadstoffen im Abgas stehen heute verschiedene Systeme zur Verfügung. Eines der effizientesten Systeme zur Reduktion von Stickoxiden ist das SCR-System, welches mittels Ammoniak Stickoxide zu molekularem Stickstoff und Wasser reduziert. Weiterentwicklungen von Abgasfiltern und -katalysatoren haben zu Dieselpartikelfiltern mit SCR-Funktionalität (SDPF) geführt. Ziel dieser Arbeit ist es, verschiedene Regelungskonzepte für ein Abgasnachbehandlungssystem basierend auf einem SDPF und einem SCR-Katalysator zu untersuchen und zu evaluieren.

Im einführenden Teil dieser Arbeit wird auf die verschiedenen Emissionsgesetzgebungen eingegangen und der SCR-Prozess näher betrachtet. Da die Kombination von SDPF und SCR eine Vielzahl an Regelstrategien bietet, wurden die drei vielversprechendsten Konzepte für die weiteren Untersuchungen gewählt.

Der Hauptteil der Arbeit beschäftigt sich mit dem Reglerentwurf und der Simulation der Konzepte. Um das Regelverhalten analysieren zu können, wurden dabei drei verschiedene Testzyklen verwendet. Der Vergleich der Simulationsergebnisse zeigte eindeutig, dass eines der untersuchten Konzepte das vielversprechendste Regelverhalten aufweist.

Contents

List of Figures

List of Tables

Abbreviations, subscripts, chemical species and symbols

Abbreviations

ASC	Ammonia Slip Catalyst
BR	Batch Reactor
CARB	California Air Resources Board
CDPF	Catalysed or Coated Diesel Particle Filter
CSF	Catalysed Soot (Particle) Filter
CSTR	Continuous Stirred Tank Reactor
DEF	Diesel Exhaust Fluid
DOC	Diesel Oxidation Catalyst
DPF	Diesel Particulate Filter
EAS	Exhaust gas After-treatment System
ECE	Economic Commission for Europe
ECU	Engine Control Unit
EPA	Environmental Protection Agency
EU	European Union
ICE	Internal Combustion Engine
ISO	International Organization for Standardization
LNT	Lean NO_x Trap
NAC	NO_x Absorber Catalyst
NRSC	Non-Road Steady Cycle
NRTC	Non-Road Transient Cycle
NSC	NO_x Storage Catalyst
NSR	Nominal Stoichiometric Ratio
OP	Operation Point
PFR	Plug Flow Reactor
PM	Particulate Matter
SCR	Selective Catalytic Reduction
SDPF	Diesel Particulate Filter with SCR coating
SISO	Single Input Single Output
TSP	Total Suspended Particles
TWC	Three-Way-Catalyst
US	United States

Subscripts

ad	Adsorption
Air	Air
Amb	Ambience
c	Catalyst
$crit$	Critical
d	Desired
de	Desorption
$denox$	Denox
ds	Downstream
EG	Exhaust gas
equ	Equilibrium
fst	Fast
g	Gas phase
i	Reactant i
I	First
II	Second
j	Reaction rate j
k	k^{th} cell of CSTR cascade
max	Maximum
ox	Oxidation

PC	Precontrol	std	Standard
ref	Reference	us	Upstream
slw	Slow		

Chemical Species

$(NH_2)_2CO$	Urea	NH_3	Ammonia
CO	Carbon monoxide	NO	Nitric oxide
CO_2	Carbon dioxide	NO_2	Nitrogen dioxide
H_2O	Water	NO_x	Oxides of nitrogen
HC	Hydrocarbons	O_2	Molecular oxygen
HNCO	Isocyanic acid		
N_2	Molecular nitrogen		

Symbols

α	–	Feedratio
α_c	$\frac{\mathrm{W}}{\mathrm{m^2 \cdot K}}$	Heat transfer coefficient to ambient
β	–	Tradeoff index
ϵ	–	Coverage dependency
ϵ_g	–	Open frontal area of monolith
η	%	Conversion efficiency
λ	–	Excess-air ratio
ω_0	$\frac{\mathrm{rad}}{\mathrm{s}}$	Eigenfrequency
τ	s	Time constant
θ	–	Surface coverage fraction
Θ	$\frac{\mathrm{mol}}{\mathrm{m^2}}$	Surface density
θ_{crit}	–	Critical surface coverage fraction of ammonia
$\dot{m}$	$\frac{\mathrm{kg}}{\mathrm{s}}$	Mass flow
$\dot{n}$	$\frac{\mathrm{kmol}}{\mathrm{s}}$	Molar flow
a	$\mathrm{m^2}$	Surface
A	–	Temperature dependency
a_R	$\frac{\mathrm{m^2}}{\mathrm{m^3}}$	Reactive surface area of catalyst
c	$\frac{\mathrm{kmol}}{\mathrm{m^3}}$	Concentration
c_p	$\frac{\mathrm{J}}{\mathrm{kg \cdot K}}$	Heat capacity
E	K	Activation temperature of the reaction
GSA	$\frac{\mathrm{m^2}}{\mathrm{m^3}}$	Geometric surface area
J	ppm	Cost function
k_α	var.	Gain
K	var.	Frequency factor of the reaction
K_i	var.	Integral controller gain
K_l	var.	Gain injection time
K_p	var.	Controller gain

K_{equ}	$\frac{\mathrm{m}^{1.5}}{\mathrm{kmol}^{0.5}}$	Temperature dependent equilibrium constant
m	kg	Mass
M	Nm	Torque
M	$\frac{\mathrm{kg}}{\mathrm{kmol}}$	Molecular weight
M_p	–	Overshoot
n	–	Number of CSTR cells
n	$\frac{1}{\mathrm{min}}$	Rotational speed
p	Pa	Pressure
p	–	Weighting factor
q	–	Weighting factor
r	$\frac{\mathrm{kmol}}{\mathrm{m}^2}$	Reaction rate
R	$\frac{\mathrm{J}}{\mathrm{K \cdot kmol}}$	Universal gas constant
T	K	Temperature
T	s	Time
T_i	$\frac{\mathrm{s}}{\mathrm{rad}}$	Integral time constant
t_r	s	Rise time
T_t	s	discretisation time
T_t	s	Time delay
v_{space}	$\frac{\mathrm{m}^3}{\mathrm{s}}$	Space velocity
V	m^3	Volume
x	$\frac{\mathrm{mol}}{\mathrm{mol}}$	Substance amount fraction

1 Introduction

This chapter introduces the reader to the basic topics of this thesis. First of all, a short introduction to internal combustion engines will be given and the differences between gasoline and diesel engines will shortly be pointed out. Relating to the emission problems of internal combustion engines (ICE) and strict emission legislations the need of exhaust gas after-treatment system (EAS) should be shown. Furthermore the working principle of selective catalytic reduction (SCR) catalysts and diesel particle filter with SCR coating (SDPF) will be explained in short in order to give the reader the background knowledge for the next chapters and the main topic of this thesis: the evaluation of different control concepts of an SDPF-SCR based EAS.

1.1 Internal combustion engines

Today it is not possible to imagine a life without ICEs in most areas of the world. They are used in mobile as well as in stationary applications, for example [1, 2]:

Stationary applications:

- Power and heat supply stations
- Emergency power supplies
- Power sets

Mobile applications:

- Passenger cars
- Commercial vehicles
- Trucks
- Busses
- Motorbikes
- Agriculture vehicles

- Construction machines
- Locomotives
- Aircrafts
- Watercrafts

In this thesis, the focus is on mobile applications, especially on engines for commercial vehicles and trucks. The number of registered motor vehicles worldwide has passed the 1 billion line in 2010 [3]. In 2014 about 90 million motor vehicles were produced [4]. This shows again how important mobility is today.

The increasing number of cars, commercial vehicles, trucks et cetera leads to a rise of the consumption of resources like crude oil and also to a higher pollution of the earth's atmosphere. Furthermore, the combustion of fuel produces CO_2, which is a greenhouse gas. Now that the first effects of global warming can be seen, the reduction of CO_2 production is getting more and more important. Even if the number of registered electric driven vehicles reached 740.000 in 2015, there will still be a need of motor vehicles driven by ICEs in the next years and decades [5]. So it can be seen that not only the emission of pollutants has to be reduced, but also the CO_2 production. In some areas these two aims are contradictory.

CO_2 emissions can only be reduced if the fuel consumption is reduced[1]. Some engine modifications for lower NO_x emissions like the exhaust gas recirculation lead to adverse combustion conditions and, as a consequence, to higher fuel consumption [1]. With EAS pollutant emissions can be reduced and the efficiency of ICEs can be improved by engine modifications.

1.2 Diesel engines

The diesel engine is a combustion engine with self ignition. Due to the compression of air in the combustion chamber, the temperature rises. At this high temperature the injected diesel fuel, begins to ignite. Via combustion of the fuel and the resulting heat, the diesel engine converts the chemical energy into mechanical energy [6].

Diesel engines have many advantages such as low fuel consumption, relatively low pollution emissions and high efficiency. Big and low running engines reach real efficiency values up to 50% [6].

1.2.1 Emissions of diesel engines

As the thesis is about the control of EAS, it is necessary to look at the emissions of a diesel engine. Today, many different engine modifications are possible, so the raw

[1] CO_2 emissions are directly proportional to fuel consumption

emissions can differ from engine to engine. Figure 1.1 shows typical raw emissions of a passenger car diesel engine. For more detailed information on diesel engines please refer to [1, 2, 6, 7, 8].

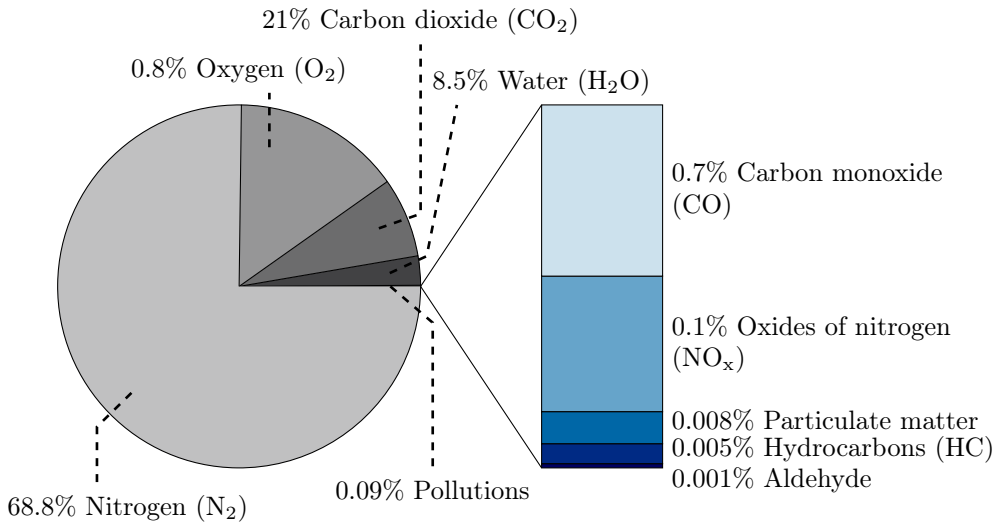

Figure 1.1: Raw emissions of a diesel engine [1]

1.3 Gasoline engines

Major differences between diesel and gasoline engines are the ignition and the preparation of the air / fuel mixture. The gasoline engine is a combustion engine with spark ignition. Optimally, a homogeneous air / fuel mixture is ignited in the combustion chamber by a spark plug. The resulting heat- and pressure increase is then converted into mechanical energy [6].

The mixture formation in gasoline engines has changed over the last decades. Firstly, the mixture formation by a carburettor was replaced by intake-manifold fuel injection. To further increse efficiency, the direct fuel injection was invented and introduced [9].

1.3.1 Emissions of gasoline engines

Figure 1.2 shows typical raw emissions of a passenger car gasoline engine at $\lambda = 1$. In comparison to diesel engines, gasoline engines have very high pollution emissions. As it can be seen in 1.2, the main components are carbon monoxide, oxides of nitrogen and hydrocarbons. For gasoline engines which operate at $\lambda = 1$ the pollution emissions can be reduced up to 99% by three-way catalytic converters [1]. For more detailed information on gasoline engines please refer to [1, 6, 7, 8, 9].

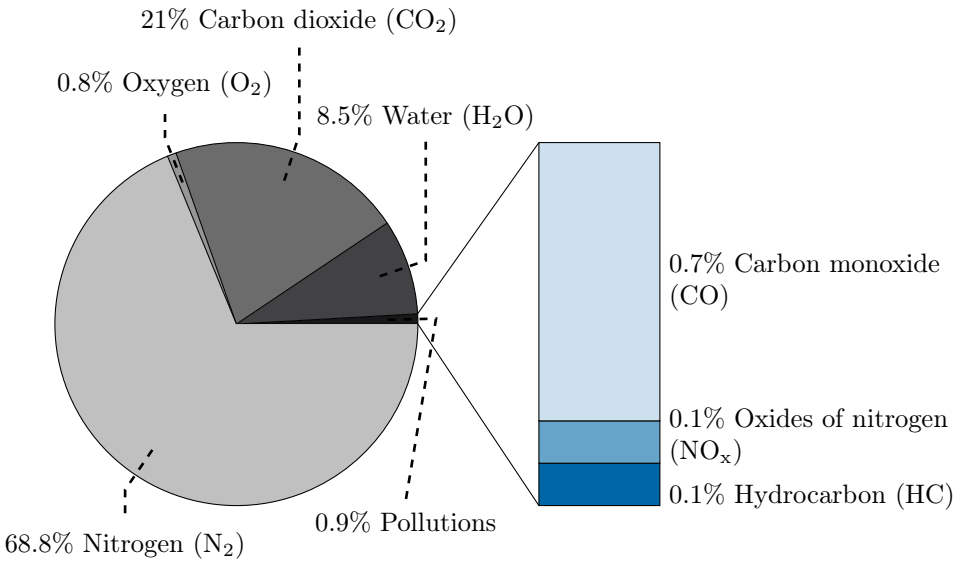

Figure 1.2: Raw emissions of an gasoline engine [1]

1.4 Legislation

The first laws for the reduction of pollutant emissions were introduced in California in the 1960s. Since then, more and more states introduced similar regulations and over the years, the legislation got more and more strict. Today all industrial countries have emission laws. Figure 1.3 shows a global map with the countries and their current legislation [6].

It can be seen that there are four different basic regulations:

- US CARB (California Air Resources Board)
- US EPA (Environmental Protection Agency)
- EU (European Union)
- Japan

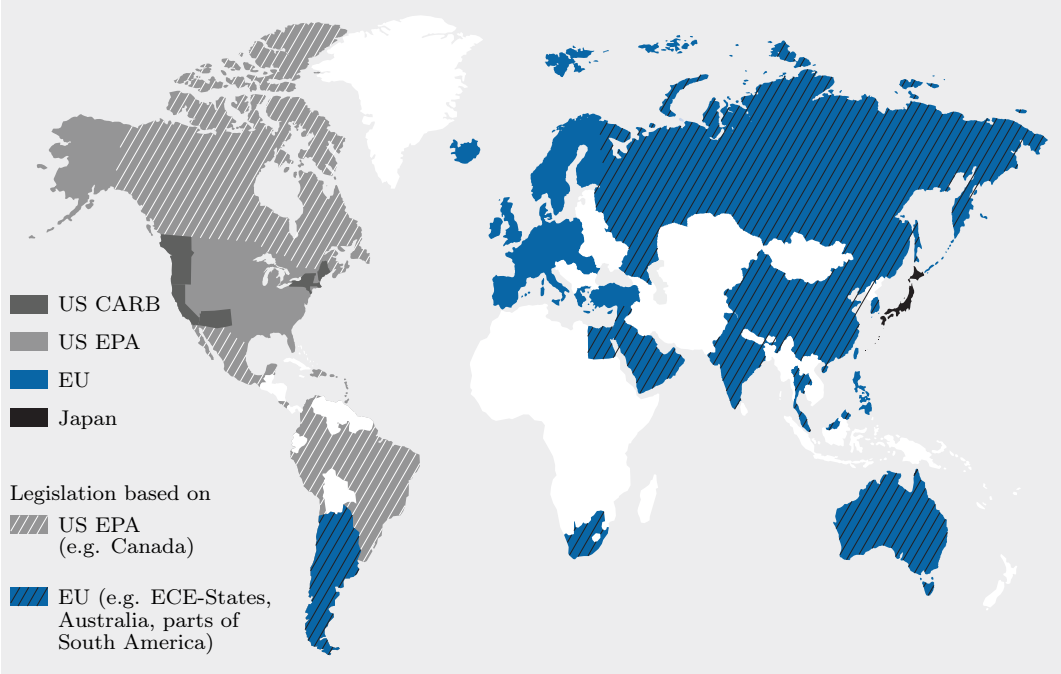

Figure 1.3: Global map of emissions legislations [6]

Some countries have their own laws based on one of these four regulations. All legislations have a classification of motor vehicles and differentiate between:

- Personal cars
- Light duty vehicles, light duty trucks
- Medium duty vehicles, medium duty trucks
- Heavy duty vehicles, heavy duty trucks
- Non-road vehicles

In Europe, the EURO 6 applies to p and light duty vehicles since 2015, while the EURO VI applies to heavy duty vehicles since 2013[2]. Figure 1.4 illustrates the EU emission limits for heavy duty vehicles. The diagram shows the decrease of the limits for carbon monoxide (CO), oxides of nitrogen (NO_x), particulate matter (PM) and hydrocarbons (HC) emissions over the last three decades. It can be seen that with EURO VI the limits are very strict. For example, the PM limit is now about 98% lower than the limit in EURO I. For detailed information about the legislations please refer to [1, 6, 10, 11, 12, 13].

[2]Europe only differentiates between personal cars, light duty vehicles, heavy duty vehicles and non-road vehicles

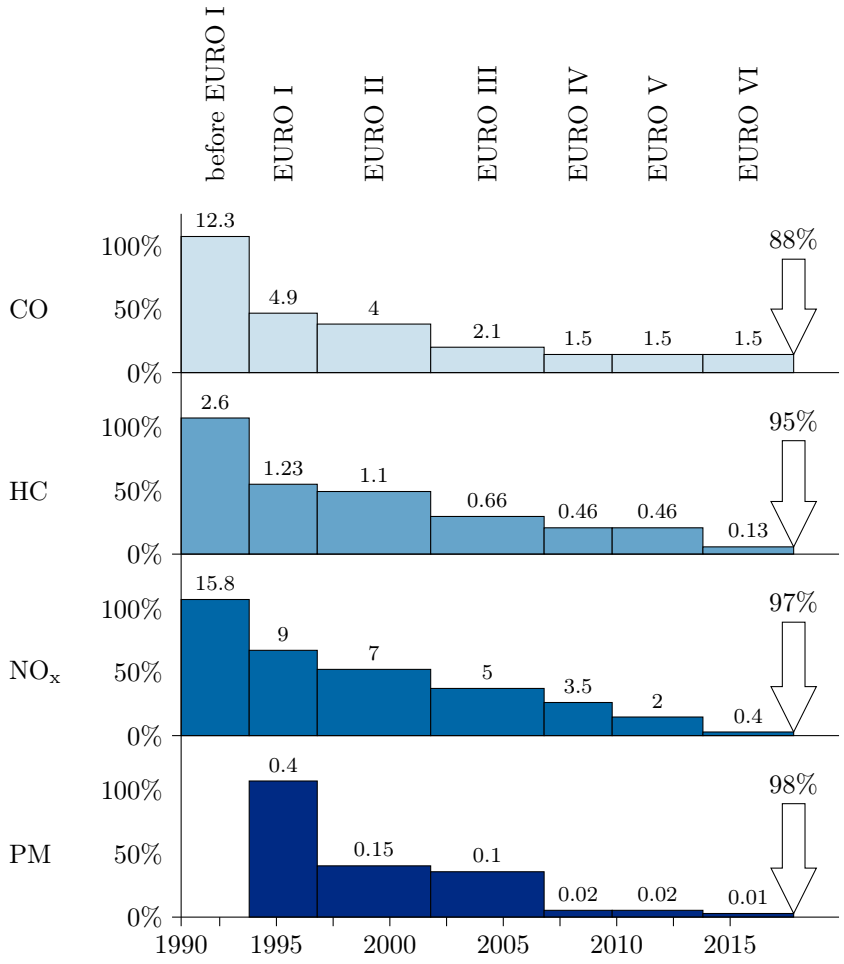

Figure 1.4: EU emission limits for heavy duty trucks [10, 11, 12, 13]

1.5 Exhaust gas after-treatment systems

The production of pollution emission has different reasons. Among other things, the main causes are:

- Industrial sector
- Traffic
- Agriculture
- Small consumer (households etc.)
- Energy supply

Traffic plays a big part in contributing to the pollution of the atmosphere. In the year 2013, traffic caused about 24% of the emitted TSP (Total Suspended Particles)[3] in Austria. About 56% of the emitted NO_x[4], 16% of emitted CO and 7% of the emitted HC[5] was caused by traffic [14].

This shows that strict legislations like the EURO VI or EURO 6 are necessary. The tough limits can only be reached if both, engine modifications and EAS, are used to reduce pollution emissions. Furthermore, the CO_2 emissions of ligth duty vehicles will also be limited in 2017 in Europe, Japan and Korea[6]. As already mentioned, the reduction of CO_2 and the pollution emissions with engine modifications are often contradictory. With EAS, these problems can be solved.

The main components of the pollutant emissions are CO, NO_x, PM and HC. There are some existing systems for reducing these pollutions. The most important are:

- **Three-Way-Catalyst (TWC):**
  The main components of the pollutant emissions of an gasoline engine are carbon monoxide (CO), oxides of nitrogen (NO_x) and hydrocarbons (HC). The TWC is a catalyst which oxidises CO and HC with the oxygen in the NO_x. Therefore the engine has to operate within areas of $\lambda = 1$. This catalyst is useful for gasoline engines only and reduces up to 99% of the pollutions to harmless CO_2, H_2O and N_2 [2, 8].

- **Diesel Oxidation Catalyst (DOC):**
  Diesel engines are operating with excess air ($\lambda >> 1$). So the exhaust gas contains molecular oxygen (O_2). This is the reason why TWC can not be used in combination with diesel engines. DOCs are two-way catalysts which oxidise CO and HC with O_2 to harmless CO_2 and H_2O. They also oxidise parts of the particulate matter and NO to NO_2. This reduces the mass of PM and increases the NO_2 / NO ratio, which has positive effects on other parts of the EAS, for example a DPF, an SDPF or an SCR can trade on higher NO_2 rates. Additionally the DOC is used as a catalytic burner to rise the exhaust gas temperature if needed[6] [1].

[3] TSP includes all airborne particles such as different sizes of PM
[4] traffic inclusive fuel export
[5] HC emissions without methane
[6] Higher exhaust gas temperatures are needed to start the DPF regeneration

- **Lean NO_x Trap (LNT[7]):**
  LNT are used in combination with lean combustion engine concepts. NO_2 from the exhaust gas is stored by reacting with the LNT coating. The resulting chemical compound is reversible. In a first step, the NO_2 is stored. In a second step the LNT has to be regenerated. The regeneration starts under rich conditions where the resulting CO, H_2 and various hydrocarbons are used as reducing agents. Poisoning through sulphur and the moderate conversion efficiency rates are two of the major deficiencies of the LNT [1, 8].

- **Diesel Particulate Filter (DPF):**
  Today most of the used DPF are ceramic wall flow filters. In this filter, the particle loaded exhaust gas flows through the porous filter walls. Up to 99.9% of the PM mass can be filtered from the exhaust gas. From time to time, the DPF has to be regenerated because the deposition of the soot particles leads to higher back pressure and hence to lower efficiency of the engine. For the regeneration, the exhaust gas temperature needs to be increased. There are some possibilities to do that. One option is to inject fuel infront of the DOC. The oxidation of the fuel by the DOC causes a rise of the exhaust gas temperature. At temperatures above 600°C the soot in the DPF gets burned[8] [1, 2].

- **Catalysed Soot (Particle) Filter (CSF[9]):**
  An SCF is basically a DPF with an additional catalytic coating. In this catalyst the soot reacts with the NO_2 at temperatures of about 350°C. The catalytic coating of the SCF has several functions: It decreases the regeneration temperature, oxidises CO and hydrocarbons and also oxidises NO to NO_2. The resulting NO_2 is then used to continuously burn the stored soot[10]. When the soot loading of the SCF reaches a limit, the active regeneration has to be started [2].

- **Selective Catalytic Reduction (SCR):**
  Using SCR catalysts is one of the most efficient options to remove NO_x from exhaust gas. Two of the greatest advantages are the high conversion rates and that they can remove NO_x continuously. Ammonia (NH_3) is used as reducing agent, which reacts with the NO_x and forms harmless molecular nitrogen (N_2) and water (H_2O). SCR systems can, depending on the operation point (OP), reach conversion rates of about 90% [6]. Because the SCR catalyst is one of the main parts of the investigated EAS in this thesis, detailed information will be provided in 1.6.

[7] LNT are also known as NO_x Storage Catalyst(NSC) or NO_x Absorber Catalyst (NAC)
[8] This is called active regeneration
[9] CSF are also known as Catalysed or Coated Diesel Particle Filter (CDPF)
[10] This is called passive regeneration

- **Diesel Particulate Filter with SCR coating (SDPF):**
  SDPF are DPF with an additional SCR coating. The SDPF can also, like the SCR, reduce NO_x from exhaust gas by using NH_3 as a reducing agent. Advantages of the SDPF are lower costs, lower construction volume[11] and a faster achievement of the operation temperature due to the lower heat capacity of the overall system and the fact that the SDPF is often placed closer to the engine [15]. Because the SDPF is also one of the main parts of the investigated EAS in this thesis, there will be detailed information in 1.7.

- **Ammonia Slip Catalyst (ASC):**
  Not all of the NH_3, which is used to reduce the NO_x emissions within SCR based EAS, is reacting with the NO_x as some NH_3 leaves the SCR catalyst. NH_3 is toxic in higher concentrations and can cause chemical burn of the eyes, the respiratory tract and the skin. Furthermore, even little concentrations can lead to unpleasant smells. To reduce NH_3 tailpipe emissions, the ASC is used, which reduces most of the NH_3 to N_2 and water.

Many different arrangements of the mentioned catalysts and filters are possible. Figure 1.5 shows some possible concepts for the arrangement of EAS, while in this thesis the bottom concept will be the main focus.

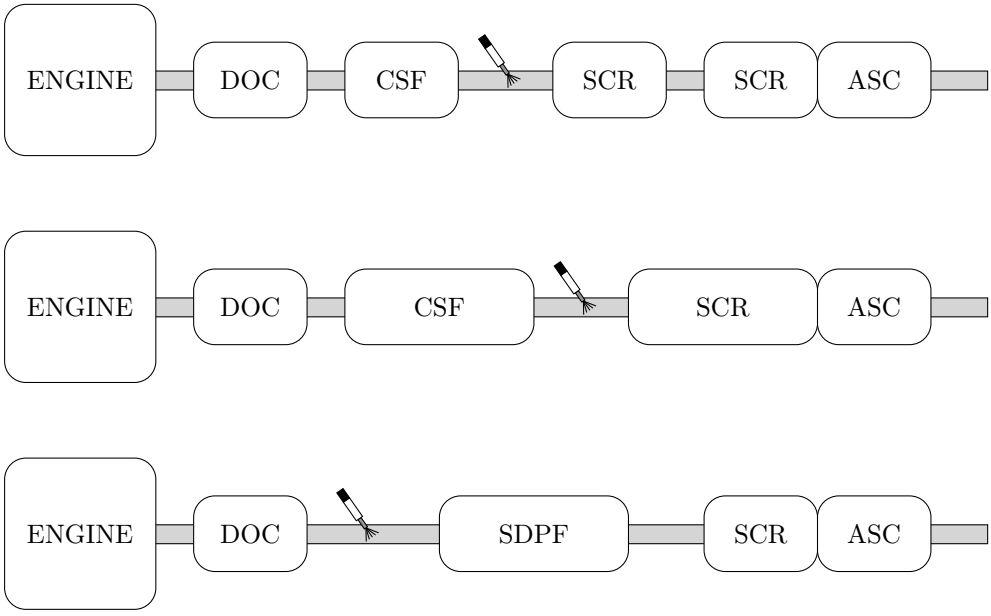

Figure 1.5: Different EAS concepts [15]

[11] Due to the SCR function of the SDPF, the volume of the following SCR can be reduced

1.6 Introduction to SCR

As mentioned in the previous section, there are some approaches to reduce the NO_x emissions of motor vehicles. One of the most efficient is the SCR technology. SCR systems have been known since the 1970s and have been used in stationary applications like coal power stations or waste incineration plants. Today, the SCR technology is also used in mobile applications. The reason can be found in the strict regulations of pollution emissions such as the EURO VI for heavy duty trucks and EURO 6 for passenger cars and light duty vehicles. For mobile applications, the SCR systems has to face new challenges, e.g. constantly changing operation conditions and wide ranges of the exhaust gas temperature and the space velocity. Size and weight are often limited which is another problem [16]. These challenges and new exhaust gas after-treatment concepts and arrangements require new control strategies. As already shown in section 1.5 with SCR systems as a part of the EAS, the focus of engine modifications can be on increasing the efficiency and decreasing the PM emission of the engine.

1.6.1 Description of the SCR process

As indicated before, SCR means selective catalytic reduction. *Selective* in this case means that the reducing agent selectively reacts with the oxygen of the NO_x although there is molecular oxygen (O_2). NH_3 has established itself as reducing agent because it shows the highest selectivity. However, NH_3 is highly toxic, so it is hardly possible to carry and include it in mobile applications safely. Today the most common reducing agent is a aqueous solution with 32.5% urea[12] named AdBlue™ [13]. To get the desired NH_3, the followed steps have to be taken:

- Evaporation of the aqueous urea solution
- Thermolysis
- Hydrolysis

Thermolysis

With the dosing unit, the AdBlue™ is injected into the tailpipe and mixed with the exhaust gas in front of the SCR catalyst. Sometimes a special mixing unit is used to get a homogeneous exhaust gas urea mixture [17]. Due to the evaporation of the water, the solid urea starts to melt. In a further step the molten urea decomposes in ammonia and isocyanic acid[14]. This decomposition is called thermolysis. The chemical equation

[12] The chemical notation of urea is $(NH_2)_2CO$
[13] AdBlue™ is a brand name. In North America it is called Diesel Exhaust Fluid (DEF)
[14] The chemical notation of isocyanic acid is HNCO

of this process can be written as

$$(NH_2)_2\,CO \rightarrow NH_3 + HNCO.$$

Hydrolysis

As already mentioned, due to the thermolysis, isocyanic acid and ammonia is generated. After this reaction the isocyanic acid reacts with water and forms NH_3 and CO_2. This reaction is called hydrolysis and it can be described by

$$HNCO + H_2O \rightarrow NH_3 + CO_2.$$

After the thermolysis and the hydrolysis two NH_3 molecules are formed out of one urea molecule. These two ammonia molecules can be used for the next step, the reduction of NO_x in the exhaust gas. The following processes and reactions are important for this step:

- Adsorption / Desorption
- Standard SCR reaction
- Fast SCR reaction
- Slow SCR reaction

Adsorption / desorption

The surface of the SCR catalyst can adsorb and desorb ammonia. This leads to a so called NH_3 loading. The current loading results from the balance between the adsorption and the desorption of ammonia. The NH_3 loading is also a very important parameter for the control of the SCR catalyst. In literature the chemical equation

$$NH_3 + S \leftrightarrow NH_3\,(S)$$

describes the adsorption respectively the desorption of the ammonia [6, 7]. For the reaction of the NO_x with the NH_3 the following three equations are relevant in principle. Important is that for these reactions the adsorbed NH_3 is used. The reason for that is that the reactions take place on the surface of the catalyst where the catalytic coating exists.

Standard SCR reaction

The standard SCR reaction equation is given by

$$4NO + 4NH_3 + O_2 \rightarrow 4N_2 + 6H_2O.$$

It can be seen that with this reaction only NO will be reduced. For each NO molecule an NH_3 molecule is used.

Fast SCR reaction

The fast SCR reaction equation can be described by

$$NO + NO_2 + 2NH_3 \rightarrow 2N_2 + 3H_2O.$$

This is the desired reaction because it is the fastest. The reaction happens preferably when the ratio between NO_2 and NO is near one. As already mentioned in section 1.5, the DOC oxidises NO to NO_2. This contributes to an NO_2 to NO ratio near one and thus to a fast NO_x reduction and high conversion rates [7].

Slow SCR reaction

The slow SCR reaction reduces NO_2 only. It is given by

$$6NO_2 + 8NH_3 \rightarrow 7N_2 + 12H_2O.$$

This reaction is very slow in comparison to the fast and the standard SCR reaction. Therefore, and because of higher consumption of ammonia, this reaction is not the desired one. An NO_2 to NO ratio greater than one has to be avoided.

Another important process is the oxidation of NH_3 at high temperatures [7]. This process decreases the available amount of ammonia. In literature this reaction is described by

$$4NH_3 + 3O_2 \rightarrow 2N_2 + 6H_2O. \tag{1.1}$$

If too much AdBlue^{TM} is injected, the resulting ammonia can not get adsorbed respectively the adsorbed ammonia desorbs before it reacts with NO_x. This leads to an ammonia slip. Ammonia is toxic and has a very low odor threshold. So also a small ammonia slip leads to a disturbance of the environment. Therefore an ASC is situated after the SCR catalyst to reduce the NH_3 slip. It oxidises the NH_3 to N_2 and H_2O according to equation 1.1. In figure 1.6 the described SCR process is depicted.

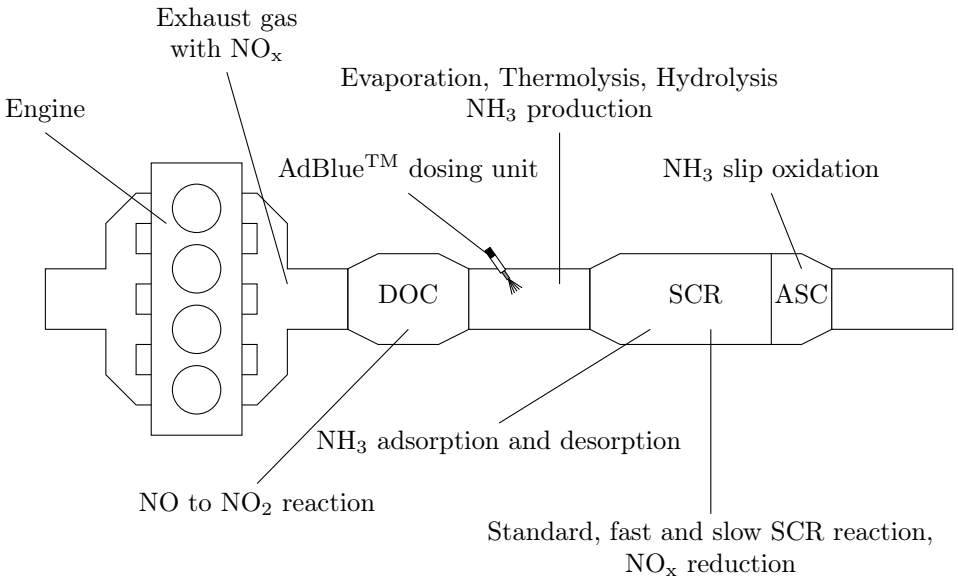

Figure 1.6: Concept of selective catalytic reduction

1.7 Introduction to SDPF

As already mentioned the SDPF is basically a DPF with an additional SCR coating. So it is not only used to filter PM but also to reduce NO_x emissions by its SCR functionality. Within this thesis the focus is on the reduction of the NO_x emissions. The process is the same as with SCR catalysts but there are some interesting influences between the loaded soot and the SCR reactions which are described in section 1.7.2.

1.7.1 Advantages of SDPF based EAS

Exhaust gas aftertreatment systems with an SDPF have many advantages compared to systems which only use SCR catalysts to reduce NO_x emissions. Due to the SCR functionality of the SDPF, the volume of the following SCR catalyst can be reduced. This leads to lower weight and also lower costs. The overall volume also decreases [18]. Each component in the EAS increases the back pressure. Due to the reduction of the SCR volume when SDPF using, the back pressure can be reduced[15], which is a big advantage because higher back pressures lead directly to a lower engine efficiency and thus to higher fuel consumption. One of the greatest benefits is that the overall heat capacity decreases[16]. This causes the EAS to reach the operation temperature faster at cold start and in low load conditions. Also, the fact that the SDPF is often situated

[15]Of course there are also other reasons which have a influence on the back pressure like, for example, porosity

[16]Lower catalyst volume leads to a lower heat capacity

near the engine effects that the operation temperature is reached earlier. So the SDPF takes over the task of reducing the NO_x emissions at low load conditions and cold start. The SCR covers the high load conditions when the SDPF is not able to reduce all the NO_x in the exhaust gas [18, 19].

1.7.2 Influences between soot loading and SCR reactions

As already indicated, the DPF and the SCR functionality influence each other. The impact of the soot on the SCR reactions is very small and hardly matters. But some studies showed that the NO_x conversion is slightly higher in the presence of soot at higher temperatures. One reason could be that the soot inhibits the NH_3 oxidation. At lower temperatures, the NO_x conversion decreases when the SDPF is loaded with soot due to the fact that the soot blocks active sites [20]. The SCR reactions have more significant influences on the DPF. As already mentioned in section 1.5 the loaded soot can also be reduced by oxidation with the oxygen of the NO_2, which is called passive regeneration. But the standard and the fast SCR reaction dominate and so there is not enough NO_2 to burn the soot. This means that the passive regeneration is inhibited by the SCR reactions. Upstream the SDPF an NO_2 to NO ratio greater than one is desired, because the NO_2 excess leads to soot oxidation. The oxidation effects that the resulting NO_2 to NO ratio gets closer to one, which is preferred for the SCR reactions [21].

2 Mathematical models

For the evaluation of the different control concepts, models of the SCR catalyst and the SDPF, provided by the AVL List, are used. The SCR model is a control oriented model for the use on an embedded system like an engine control unit (ECU). In [16] the SCR model is described in detail. Within this thesis there will be only a short description. The SDPF model is a detailed physical model for concept studies and simulations. The next sections will give a overview of these two respective models.

2.1 SCR model

For modeling a catalyst like the SCR, different chemical reactor models are known in literature, for example the batch reactor (BR), the plug flow reactor (PFR) or the continuous stirred tank reactor (CSTR). These chemical reactors can also be combined to get closer to the real behaviour. For the SCR catalyst the PFR would be the ideal reactor model. Due to the high computational effort the PFR is approximated by a CSTR cascade. Therefore the SCR model is discretised in n CSTR cells along the flow direction of the exhaust gas. To get an efficient SCR model some simplifications and assumptions are made, which are described in [16]. With these simplifications the k-th cell of the SCR model can be described by the following equations.

$$\begin{aligned}\frac{d}{dt}c_{NO,k} =& \frac{n}{V_c \cdot \epsilon_g} \cdot \frac{\dot{m}_{EG} \cdot R}{p_{EG} \cdot M_{EG}} \cdot (T_{EG,k-1} \cdot c_{NO,k-1} - T_{c,k} \cdot c_{NO,k}) \\ &+ a_R \cdot (-4 \cdot r_{std,k} - 2 \cdot r_{fst,k} - r_{NO,g,k})\end{aligned}$$

$$\begin{aligned}\frac{d}{dt}c_{NO_2,k} =& \frac{n}{V_c \cdot \epsilon_g} \cdot \frac{\dot{m}_{EG} \cdot R}{p_{EG} \cdot M_{EG}} \cdot (T_{EG,k-1} \cdot c_{NO_2,k-1} - T_{c,k} \cdot c_{NO_2,k}) \\ &+ a_R \cdot (-2 \cdot r_{fst,k} - 6 \cdot r_{slw,k} + r_{NO,g,k})\end{aligned}$$

$$\begin{aligned}\frac{d}{dt}c_{NH_3,k} =& \frac{n}{V_c \cdot \epsilon_g} \cdot \frac{\dot{m}_{EG} \cdot R}{p_{EG} \cdot M_{EG}} \cdot (T_{EG,k-1} \cdot c_{NH_3,k-1} - T_{c,k} \cdot c_{NH_3,k}) \\ &+ a_R \cdot (-r_{ad,k} + r_{de,k} - 4 \cdot r_{ox,g,k})\end{aligned}$$

$$\begin{aligned}\frac{d}{dt}c_{O_2,k} =& \frac{n}{V_c \cdot \epsilon_g} \cdot \frac{\dot{m}_{EG} \cdot R}{p_{EG} \cdot M_{EG}} \cdot (T_{EG,k-1} \cdot c_{O_2,k-1} - T_{c,k} \cdot c_{O_2,k}) \\ &+ a_R \cdot (-0.5 \cdot r_{NO,g,k})\end{aligned}$$

$$\frac{d}{dt}\theta_{NH_3,k} = \frac{1}{\Theta_{NH_3}} \cdot (r_{ad,k} - r_{de,k} - 4 \cdot r_{fst,k} - 8 \cdot r_{slw,k} - 4 \cdot r_{ox,k})$$

$$\frac{d}{dt}T_{c,k} = \frac{n}{m_c \cdot c_{p,c}} \cdot (\dot{m}_{EG} \cdot c_{p,EG} \cdot (T_{EG,k-1} - T_{c,k}) + \alpha_c \cdot a_c \cdot (T_{Amb} - T_{c,k}))$$

It can be seen that each cell has six state variables ($c_{NO,k}, c_{NO_2,k}, c_{NH_3,k}, c_{O2,k}, \theta_{NH_3,k}, T_{c,k}$) where the first four variables describe the concentration of the different gas species and the last two the ammonia loading and the catalyst temperature. The entire model therefore has n times six state variables, which are also the output variables of the model. The input variables of the model are the mass flow of the exhaust gas $\dot{m}_{EG}$, the ambient temperature T_{Amb}, the pressure of the exhaust gas p_{EG}, the temperature of the exhaust gas $T_{EG,us}$ and the concentrations of the different gas species of the exhaust gas upstream the SCR ($c_{NO,us}, c_{NO_2,us}, c_{NH_3,us}, c_{O2,us}$). For the first cell ($k = 1$) there is no previous cell. Thus the input variables are used instead of the state variables of the previous cell. For example

$$\begin{aligned}\frac{d}{dt}c_{NO,1} =& \frac{n}{V_c \cdot \epsilon_g} \cdot \frac{\dot{m}_{EG} \cdot R}{p_{EG} \cdot M_{EG}} \cdot (T_{EG,us} \cdot c_{NO,us} - T_{c,1} \cdot c_{NO,1}) \\ &+ a_R \cdot (-4 \cdot r_{std,1} - 2 \cdot r_{fst,1} - r_{NO,g,1})\,.\end{aligned}$$

Additionally, reaction rates are needed to model the equation above. The following equations are given for the k-th cell.

For the adsorption of ammonia on the catalyst surface the reaction equation

$$NH_3 + S \rightarrow NH_3\,(S)\,.$$

applies. The associated reaction rate equation is given by

$$r_{ad,k} = K_{ad} \cdot e^{-\frac{E_{ad}}{T_{c,k}}} \cdot c_{NH_3,k} \cdot (1 - \theta_{NH_3,k})\,.$$

The reaction equation and the reaction rate equation for the desorption of ammonia from the catalyst surface can be described by

$$NH_3 + S \rightarrow NH_3\,(S) \quad \text{and}$$

$$r_{de,k} = K_{de} \cdot e^{-\frac{E_{de} \cdot \left(1 - \epsilon \cdot \theta_{NH_3,k}\right)}{T_{c,k}}} \cdot c_{NH_3,k} \cdot \theta_{NH_3,k}$$

As already mentioned in section 1.6.1, the reaction equations for the standard, the fast and the slow SCR reaction are considered by

$$4NO + 4NH_3 + O_2 \rightarrow 4N_2 + 6H_2O$$

$$NO + NO_2 + 2NH_3 \rightarrow 2N_2 + 3H_2O \quad \text{and}$$

$$6NO_2 + 8NH_3 \rightarrow 7N_2 + 12H_2O.$$

Therefore the corresponding reaction rate equations are defined according to

$$r_{std,k} = K_{std} \cdot e^{-\frac{E_{std}}{T_{c,k}}} \cdot c_{NO,k} \cdot \theta_{crit} \cdot \left(1 - e^{-\frac{\theta_{NH_3,k}}{\theta_{crit}}}\right)$$

$$r_{fst,k} = K_{fst} \cdot e^{-\frac{E_{fst}}{T_{c,k}}} \cdot c_{NO,k} \cdot c_{NO_2,k} \cdot \theta_{crit} \cdot \left(1 - e^{-\frac{\theta_{NH_3,k}}{\theta_{crit}}}\right) \quad \text{and}$$

$$r_{slw,k} = K_{slw} \cdot e^{-\frac{E_{slw}}{T_{c,k}}} \cdot c_{NO_2,k} \cdot \theta_{crit} \cdot \left(1 - e^{-\frac{\theta_{NH_3,k}}{\theta_{crit}}}\right).$$

As an undesired side reaction the ammonia is oxidised in the catalyst. The oxidation can be separated into an oxidation on the catalyst surface and an oxidation in the gas phase. The reaction equation of the surface oxidation is given by

$$4NH_3\,(S) + 3O_2 \rightarrow 2N_2 + 6H_2O.$$

Therefore the associated reaction rate equation is considered by

$$r_{ox,k} = K_{ox} \cdot e^{-\frac{E_{ox}}{T_{c,k}}} \cdot \theta_{NH_3,k}.$$

The oxidation of ammonia in the gas phase is described by the reaction equation

$$4NH_3 + 3O_2 \rightarrow 2N_2 + 6H_2O.$$

and the corresponding reaction rate equation

$$r_{ox,g,k} = K_{ox,g} \cdot e^{-\frac{E_{ox,g}}{T_{c,k}}} \cdot c_{NH_3,k}.$$

Another important reaction in SCR catalysts is the NO oxidation to NO_2 respectively the NO_2 reduction to NO. As already mentioned in section 1.5, the oxidation of NO to NO_2 is the desired reaction because of its positive effects on the reduction of nitrogen oxides. The oxidation causes higher NO_2 to NO ratios, which is an advantage for the fast SCR reaction. The oxidation can be described by the reaction equation

$$2NO + O_2 \rightarrow 2NO_2$$

and the reaction rate equation

$$r_{NO,k,I} = K_{NO,I} \cdot T_{c,k}^{A_{NO,I}} \cdot e^{-\frac{E_{NO,I}}{T_{c,k}}} \cdot \left(c_{NO,k} \cdot c_{O_2,k}^{0.5} - \frac{c_{NO_2,k}}{K_{equ}\left(T_{c,k}\right)} \right) \cdot \left(1 - \theta_{NH_3,k}\right).$$

The reduction of NO_2 to NO is given by its reaction equation

$$2N0_2 \rightarrow 2NO + O_2$$

and its related reaction rate equation

$$r_{NO,k,II} = -K_{NO,II} \cdot T_{c,k}^{A_{NO,II}} \cdot e^{-\frac{E_{NO,II}}{T_{c,k}}} \cdot \left(c_{NO_2,k} - K_{equ}\left(T_{c,k}\right) \cdot c_{NO,k} \cdot c_{O_2,k}^{0.5}\right) \cdot \left(1 - \theta_{NH_3,k}\right) \quad .$$

NO oxidation and NO_2 reduction can be seen as one reversible reaction. The reaction rate equations can be summarised to

$$r_{NO,g,k} = \begin{cases} r_{NO,k,I} & \text{for} \quad \left(c_{NO,k} \cdot c_{O_2,k}^{0.5} - \frac{c_{NO_2,k}}{K_{equ}\left(T_{c,k}\right)} \right) \geq 0 \\ r_{NO,k,II} & \text{for} \quad \left(c_{NO,k} \cdot c_{O_2,k}^{0.5} - \frac{c_{NO_2,k}}{K_{equ}\left(T_{c,k}\right)} \right) < 0 \end{cases} .$$

The constant K_{equ} depends on the temperature and can be calculated by

$$K_{equ}\left(T_{c,k}\right) = \sqrt{\left(\frac{p_{EG}}{R \cdot T_{c,k}} \right)^{-1}} \cdot e^{\left(-9.259 + \frac{6848}{T_{c,k}} + 0.2791 \cdot \frac{T_{c,k}}{1000} - 0.02245 \cdot \left(\frac{T_{c,k}}{1000}\right)^2 - 0.4139 \cdot ln\left(\frac{T_{c,k}}{1000}\right) \right)}.$$

The here shown continuous model is separated into two parts to allow a cell number variable implementation in Matlab-Simulink®. These two parts are the mass and heat flow phenomena and the chemical reaction kinetics. For the simulations and investigations within this thesis a discretized version of the shown model is implemented.

2.2 SDPF model

As already mentioned, the SDPF is a DPF with SCR functionality. As a first step of concept investigation within this thesis, only the NO_x reduction properties of the SDPF are considered. This means that the SDPF will not be loaded with soot during the simulations and therefore, the influence of the DPF functionality will not be considered. This will be part of further investigations.

The mathematical equations of the SDPF model are basically the same as those of the SCR model (refer to section 2.1). Additionally, equations for the DPF function and mutual influences with the SCR functionality are also included in the model. However, the consideration of these effects will go beyond the scope of this thesis. Therefore, these equations will not be used and due to readabilty not be shown within this thesis.

The reason for using a SDPF model and not two SCR models in a row is that the parameterisation of the SCR and the SDPF model is different.

2.3 Important relations

For the control of the NH_3 loading a stoichiometric factor named feedratio α is used. It is defined as

$$\alpha = \frac{\dot{n}_{NH_3,SDPF,us}}{\dot{n}_{NO_x,SDPF,us}}$$

according to the fast and the standard SCR reaction which are the dominant reactions in the SCR process where $\dot{n}_{NH_3,SDPF,us}$ is the molar flow of NH_3 in front of the SDPF and $\dot{n}_{NO_x,SDPF,us}$ the molar flow of NO_x [16].

One of the most important quality criteria for evaluating the SDPF or SCR performance is the conversion efficiency. It can be defined for the conversion of NO_x or NH_3. The NO_x conversion efficiency of the overall system is defined by

$$\eta_{NO_x} = \frac{\dot{n}_{NO_x,SDPF,us} - \dot{n}_{NO_x,SCR,ds}}{\dot{n}_{NO_x,SCR,us}} \cdot 100\%$$

where *us* means upstream an in front of the catalyst and *ds* downstream and after the catalyst [16].

The NH_3 conversion efficiency is given by

$$\eta_{NH_3} = \frac{\dot{n}_{NH_3,SDPF,us} - \dot{n}_{NH_3,SCR,ds}}{\dot{n}_{NH_3,SCR,us}} \cdot 100\%.$$

As an additional quality criterion the so called NH_3 slip, which is the NH_3 concentration $x_{N_3,ds}$ downstream the catalyst is often used [16].

Sometimes it is necessary to calculate the absolute NH_3 loading of the catalyst. For better understanding, the equation is shown with the units. The absolute NH_3 loading is defined by

$$m_{\theta,NH_3}\,[g] = \theta_{NH_3}\,[-] \cdot \Theta_{NH_3}\left[\frac{mol}{m^2}\right] \cdot GSA\left[\frac{m^2}{m^3}\right] \cdot V_c\left[m^3\right] \cdot M_{NH_3}\left[\frac{g}{mol}\right]$$

where Θ_{NH_3} is the maximum NH_3 storage capacity of the catalyst, GSA the geometric surface area of the catalyst, V_c the volume of the catalyst and M_{NH_3} the molar weight of NH_3.

Also important is the relation between the mass flow and the concentration of a gaseous species. For example, regarding NH_3, it is defined by

$$\dot{m}_{NH_3} = \frac{M_{NH_3}}{M_{Air}} \cdot \dot{m}_{EG} \cdot x_{NH_3,us}$$

where the simplification $M_{Air} = M_{EG}$ is assumed [16].

3 Control concepts

This section shows existing control concepts for SCR based EAS. Mainly, there are two different types which are open-loop and closed-loop control strategies. This section points out the differences between these two types and shows the benefits of closed-loop control strategies. Especially the model based closed-loop control concept invented by AVL List is discussed in detail.

Based on this specific control concept, different concepts for controlling an SDPF-SCR based EAS are introduced, three of which will be discussed, investigated and compared in the next sections.

3.1 Existing control concepts for SCR systems

In recent years, different control strategies were invented. With open-loop control concepts it was able to meet the emission legislations like EURO 4 and EURO 5. Strict emission limits nowadays and in the future, respectively in-use compliance requirements, ask for high SCR system performances. Therefore, closed-loop control strategies and model based control concepts seem to be a suitable solution [22].

3.1.1 Open-loop control strategy

As already mentioned, open-loop control strategies show acceptable performance for EURO 4 and EURO 5 emission legislations, where NO_x reduction rates of about 80% are required. Open-loop or feedforward control strategies are able to reach such reduction rates. The block scheme of a possible open-loop SCR control strategy is illustrated in figure 3.1. It mainly consists of three different parts: the engine-out NO_x prediction, the tailpipe NO_x target and the open-loop control. With the engine-out NO_x prediction block, the NO_x emissions of the engine (in front of the SCR) are predicted. In some cases the engine-out NO_x concentration is measured by an NO_x sensor. The tailpipe NO_x target block specifies the desired NO_x concentration after the SCR catalyst. By subtracting the NO_x reference from the NO_x prediction, the NO_x reduction is then calculated. In the open-loop control block the needed amount of NH_3 is calculated by the stoichiometric ratio. It can be seen that the thereby determined amount of NH_3 is limited by a so called NSR[17] map. This limitation is responsible for preventing NH_3 slip. The open-loop control block also includes a desorption compensation. With

[17]Nominal Stoichiometric Ratio (NSR)

rising catalyst temperatures, the stored NH_3 desorbs, leading to NH_3 slip. To solve this problem, the desorption compensation reduces the amount of the urea dosage when the temperature rises [22].

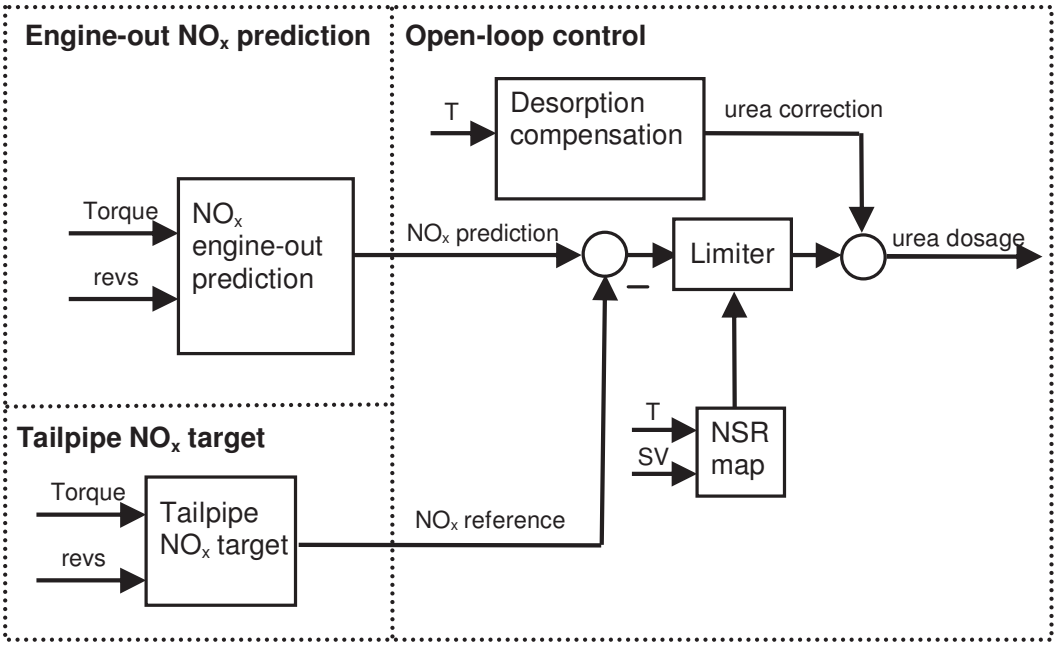

Figure 3.1: Block scheme of an open-loop SCR control strategy [22]

Beside the NO_x reduction, additional challenges like the minimization of NH_3 slip, transient conditions, robustness against urea dosing inaccuracy, catalyst ageing and NO_x engine-out variations have to be mastered by the used control strategies in order to meet current emission standards. Also, the calibration effort and the costs have to be considered. Open-loop control concepts have shown not to be suitable to face these challenges and are therefore not the ideal way of solving said problems [22].

3.1.2 Closed-loop control strategy

Figure 3.2 shows a block scheme of a possible closed-loop control strategy. Beside the engine-out NO_x prediction block, this control system has three more important blocks: the surface coverage control, the NH_3 slip feedback control and the control mode switching and adaptation block. At high and rising catalyst temperatures, the system shows faster dynamics and a lower maximum NH_3 storage capacity. Adsorption and desorption of NH_3 happens faster than at low catalyst temperatures. Therefore,

an NH_3 slip feedback controller can be used where an NH_3 sensor downstream the SCR provides feedback information [22].

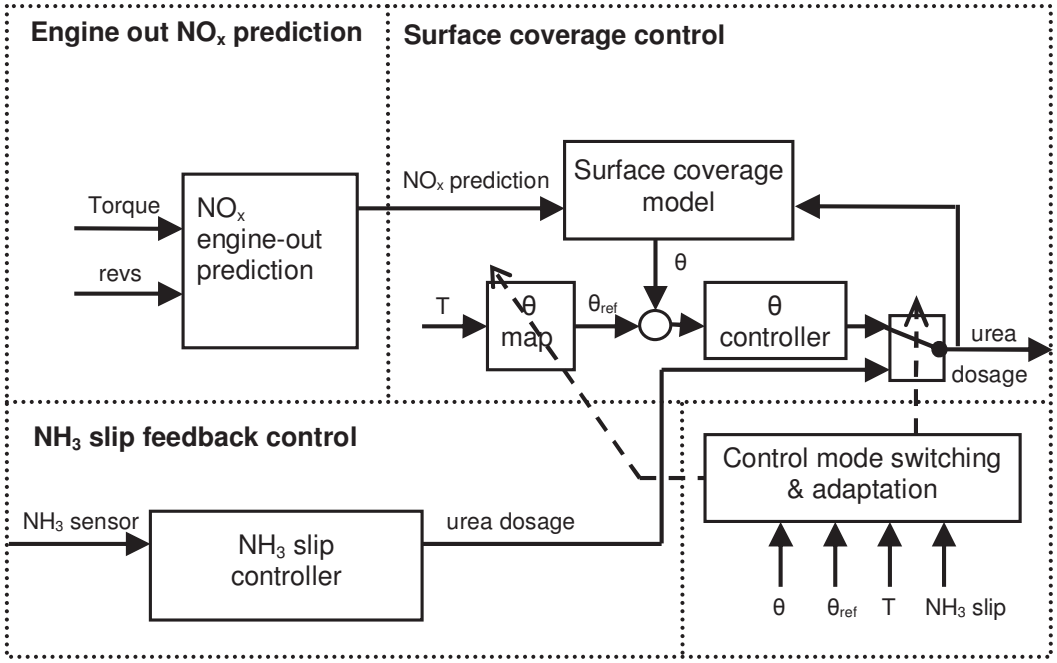

Figure 3.2: Block scheme of a closed-loop SCR control strategy [22]

At low temperatures the slow catalyst dynamics prevent an NH_3 slip feedback control because urea dosing variations can not be tracked with the sensor downstream the SCR. The effect on the gas concentrations downstream the SCR is filtered by the slow reaction kinetics and the NH_3 storage [22].

For low catalyst temperature conditions the surface coverage control takes over the urea dosing. Since the surface coverage can not be measured, this strategy is an open-loop control strategy. For controlling the NH_3 surface coverage or the NH_3 loading, a surface coverage model is used as an observer. The controller and the model form a closed-loop. The thereby determined urea dosing is used for the real SCR system [22].

The third important block is the control mode switch and adaptation block, which determines whether the surface coverage control or the NH_3 slip feedback control sets the urea dosage. Furthermore, it adapts the NH_3 loading reference map [22].

3.1.3 Model-based closed-loop control strategy (Concept 0)

As the basis for the investigated control concepts in this thesis a model-based closed-loop control concept from AVL List was used. This concept controls the NH_3 loading

of the SCR catalyst. Therefore a model of the SCR system is used as an observer to predict NH_3 loading and other important parameters. In a strict sense, this concept is an open-loop control concept because the feedback information comes from the model and not from a real sensor. The real sensor information is used for adaptations of the urea dosage.

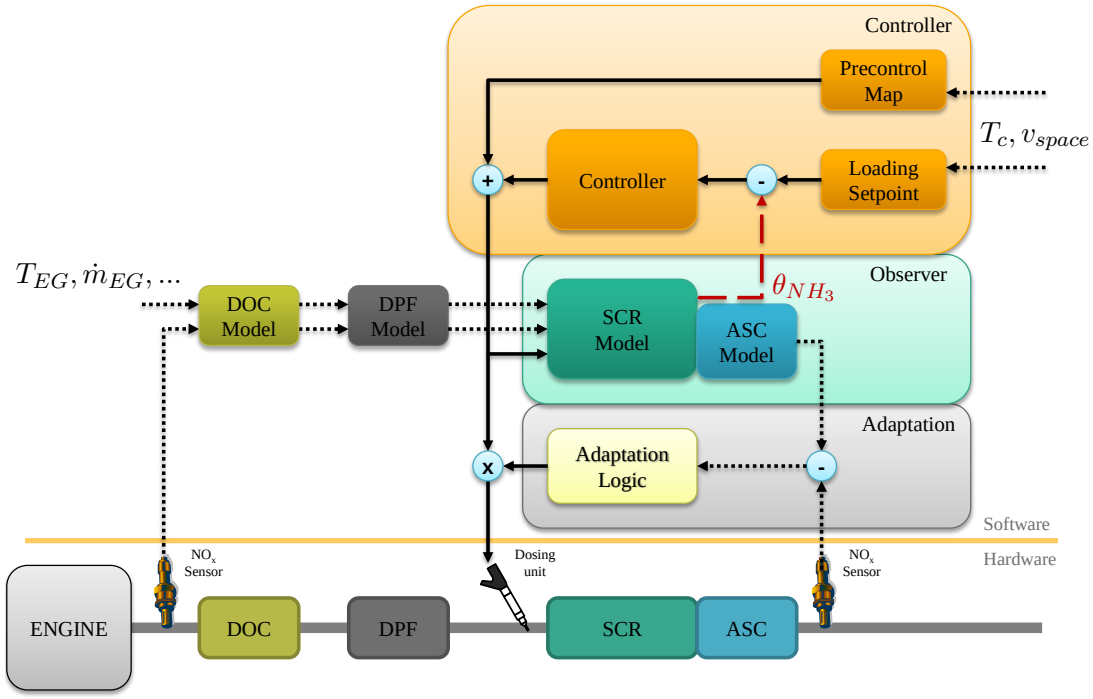

Figure 3.3: Block scheme of the model-based closed-loop SCR control concept from AVL List

Figure 3.3 shows a block scheme of the model-based closed-loop SCR control concept by AVL List. The control block consists of three different main parts: the loading setpoint map, the NH_3 dosing feedforward control map which is called precontrol map and the PI-controller. Because the system is strongly nonlinear, a gain-scheduled PI-controller is needed. Therefore the control parameters K_p and T_i are changed by the catalyst temperature T_c and the exhaust gas mass flow $\dot{m}_{EG}$, more precisely by the space velocity v_{space}. The changing of the parameter is done by a map. Also the loading setpoint map and the NH_3 dosing precontrol map are maps where the catalyst temperature and the space velocity are used as input parameters. With the loading setpoint map for each OP, a desired NH_3 loading is given. The precontrol map serves as feed forward control with the advantage that the controller only has to compensate the deviation between the desired and the current NH_3 loading.

3.2 Control concepts for SDPF-SCR systems

Based on the existing control concept which is described in section 3.1.3 many different new concepts for controlling an SDPF-SCR based EAS have been developed as part of this thesis. In this section, all these different concepts are introduced and discussed in terms of their advantages and disadvantages. Concepts with similar approaches are summarized.

3.2.1 Concept 1.1

The first concept is very similar to the original one for controlling an SCR based EAS. Thereby the relative NH_3 loading of the SDPF and the SCR model is summed up. This overall relative NH_3 loading is controlled exactly as it was in concept 0. Figure 3.4 shows the block scheme of concept 1.1

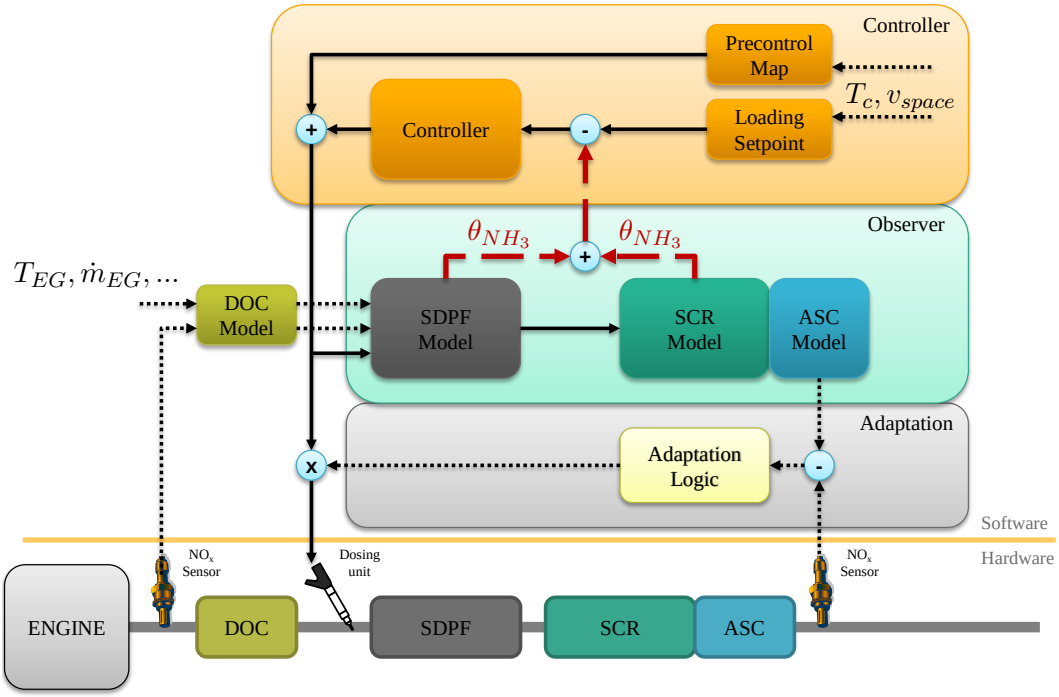

Figure 3.4: Block scheme of concept 1.1

The main advantages here is that it is a proven concept with an existing calibration workflow. The calibration workflow from concept 0 can easily be adapted. Compared to other concepts it is a simple control approach.

On the other hand, the disadvantages are that the transient temperature behaviour and the loading distribution of the SDPF and the SCR are not considered. The biggest drawback is that summing up two relative NH_3 loadings makes no sense. Because of

the different maximum NH_3 loading capacities of the SDPF and the SCR, one specific value for the sum of the two relative NH_3 loadings may imply different values for the overall absolute NH_3 loading.

3.2.2 Concept 1.2 (A)

Figure 3.5 illustrates the block scheme of concept 1.2. It can be seen that it has the same structure as the first one. The difference between these two concepts is that not the relative NH_3 loading is summed up, but the absolute value. Compared to the previous concept summing up absolute values does indeed make sense.

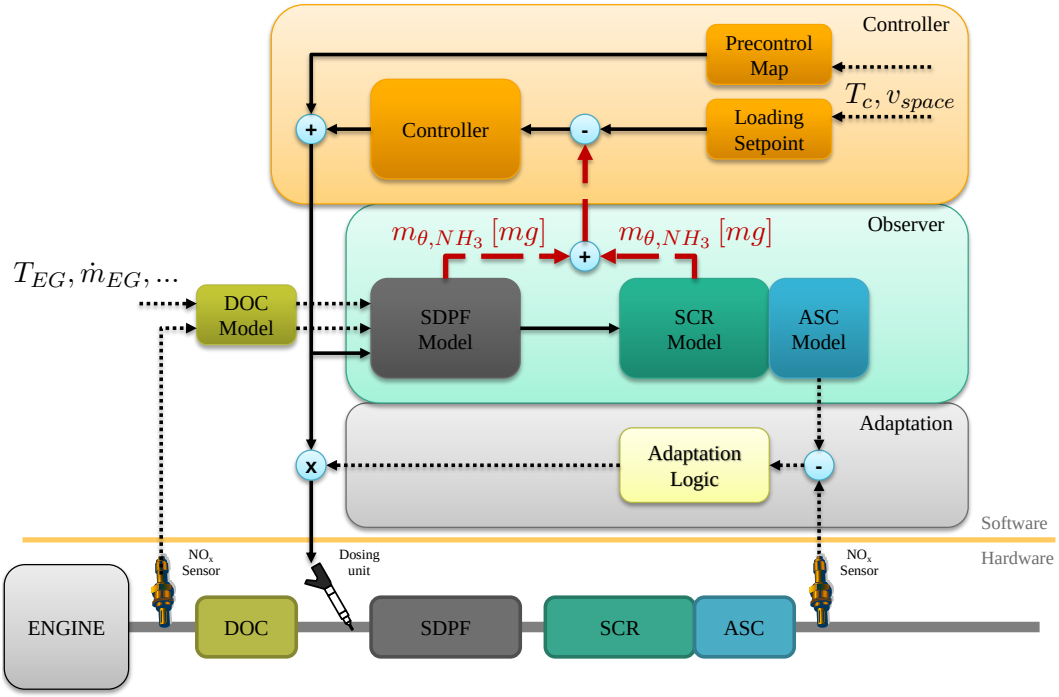

Figure 3.5: Block scheme of concept 1.2

This concept has the same advantages as the previous one. Also, the disadvantages are the same with the exception of summing up the NH_3 loadings. As already said, within this concept this makes sense because it sums up the absolute values and not the relative ones.

3.2.3 Concept 1.3

This concept differs in modeling the real hardware, in contrary to the previous two concepts. Here, the SDPF and the SCR are modeled as one unit with one relative NH_3

loading. Just as in the other concepts, the relative loading is controlled. Figure 3.6 shows the block scheme of this concept.

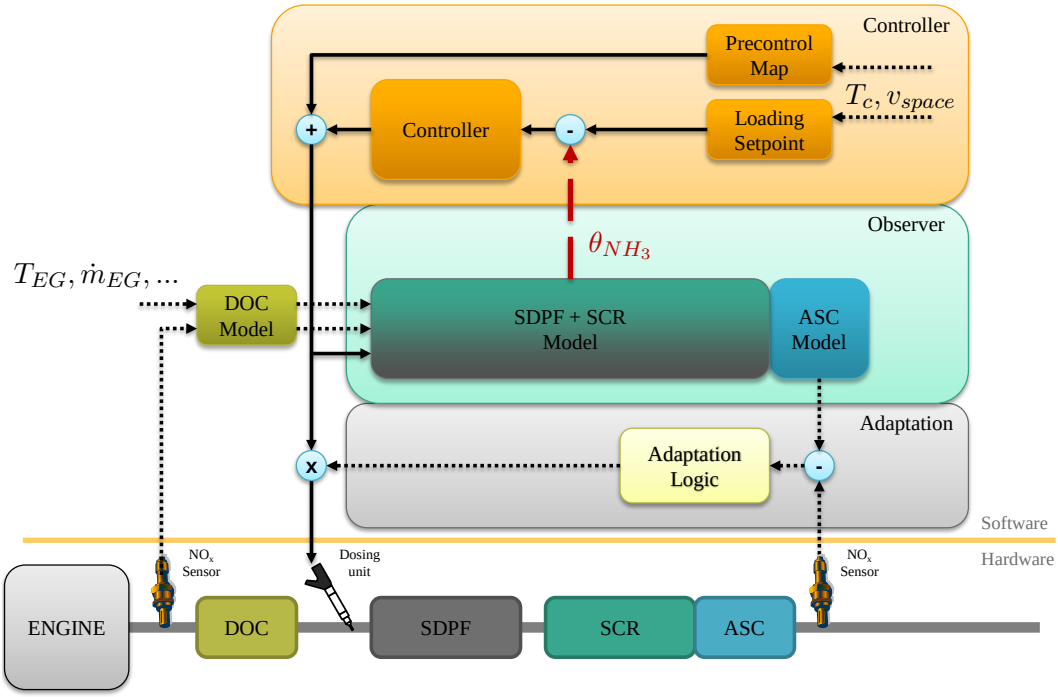

Figure 3.6: Block scheme of concept 1.3

Since the control approach is the same as in the concepts described before, the advantages remain the same. An additional benefit is the lower calibration effort because there is only one single ECU model which represents the SDPF and the SCR. Big disadvantages of combining the SDPF and the SCR to one model only however are that the different behaviours and different catalyst temperatures, due to the positions of the catalysts, are not considered.

The first three concepts have in common that the overall NH_3 loading is controlled. Therefore, it is of course not possible to consider the loading distribution between the SDPF and the SCR.

3.2.4 Concept 2

Figure 3.7 shows the block scheme of concept 2. Within this concept only the relative NH_3 loading of the SDPF is controlled while the loading of the SCR is not considered. The idea behind this concept is that occurring NH_3 slip of the SDPF is used for NO_x reduction in the SCR. The main disadvantage of this concept is, as said before, that the SCR is not considered. Therefore not only undesired NH_3 slip downstream the EAS can occur, but also the NO_x conversion efficiency might not be optimal.

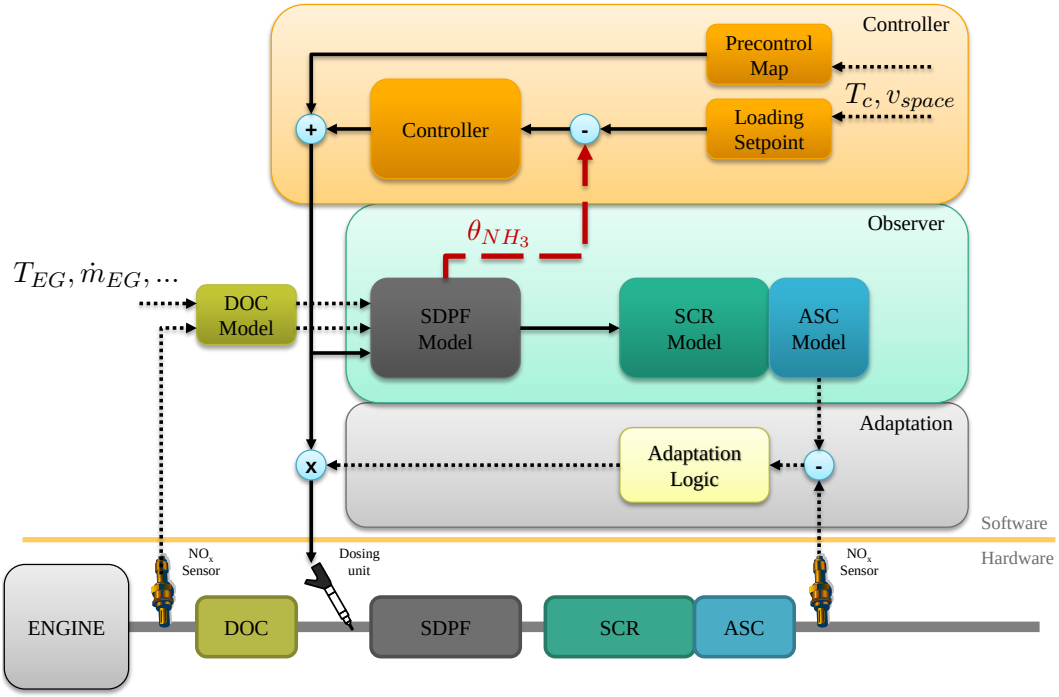

Figure 3.7: Block scheme of concept 2

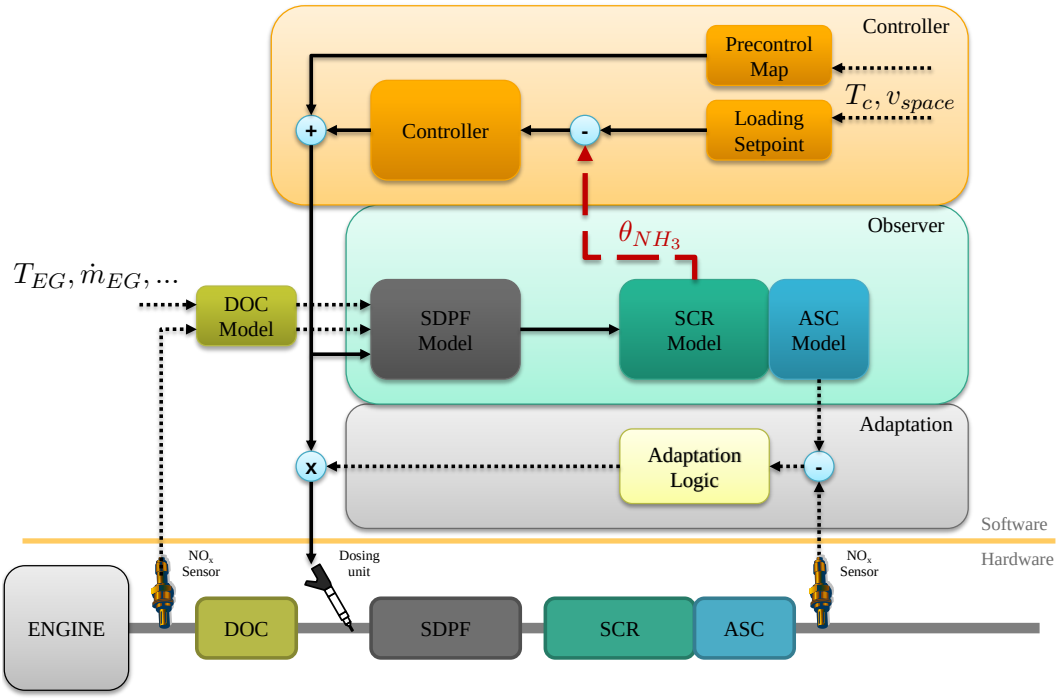

Figure 3.8: Block scheme of concept 3.1

3.2.5 Concept 3.1 (B)

Figure 3.8 illustrates the block scheme of concept 3.1. As it can be seen in the graphic, the relative NH_3 loading of the SCR is controlled. The idea here is that an urea dosing leads to an NH_3 loading of the SDPF and further more to an NH_3 slip. Due to this NH_3 slip the SCR gets loaded with ammonia.

The validated control concept and the existing calibration workflow are positive arguments for this concept. On the other hand, the demanded NH_3 loading of the SCR catalyst can be very low where the loading control is very sensitive. Another drawback is that a time delay occurs between urea dosage and the change of the loading of the SCR due to the SDPF limiting the overall system dynamic.

3.2.6 Concept 3.2 (C)

This concept is basically an extension of the previous concept. The NH_3 loading of the SCR is controlled but a second controller regulates the NH_3 slip of the SDPF. The controller used here is a cascaded PI-controller. Figure 3.9 illustrates the block scheme of concept 3.2.

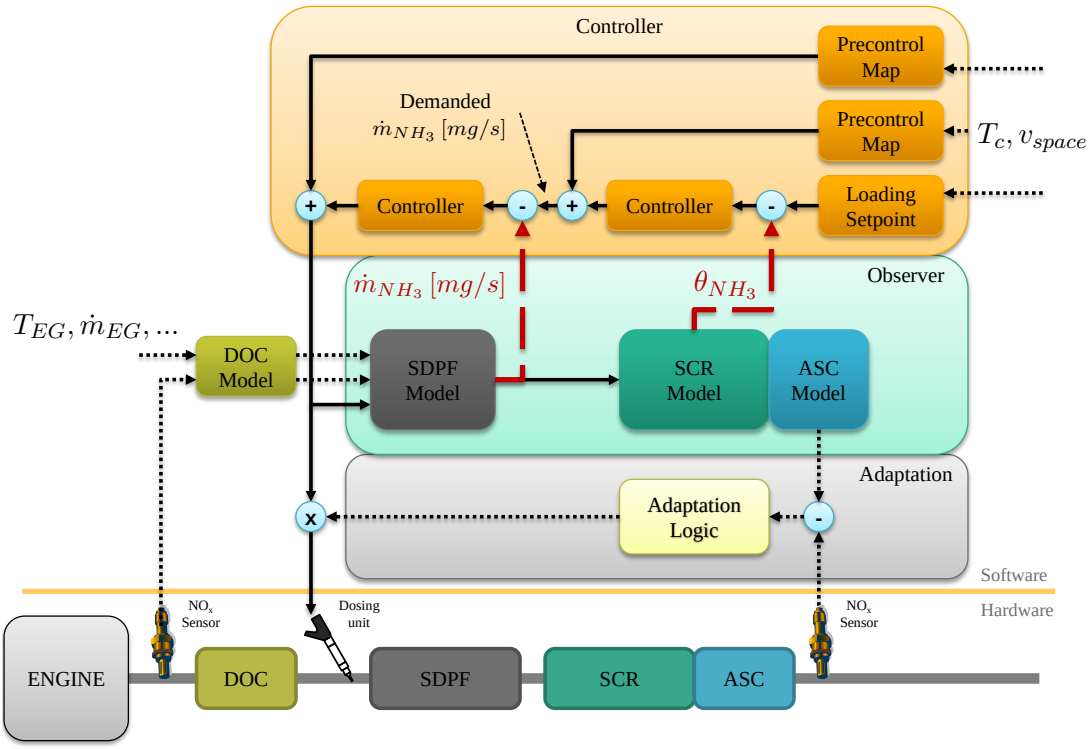

Figure 3.9: Block scheme of concept 3.2

The big advantage of this concept compared to the previous one is that it also con-

siders the SDPF. Due to the control of the NH_3 slip of the SDPF, the time delay can be shortened and the SCR controller does not produce such a big overshoot. Furthermore it is easy to improve the concept by installing an NO_x or NH_3 sensor downstream the SDPF later on.

Nevertheless this concept has a huge disadvantage compared to concept 3.1. Two scheduled PI-controllers and two different precontrol maps require a lot more calibration effort. Furthermore there is still a time delay which makes it hard to control the system.

3.2.7 Concept 3.3

Compared to the previous one this concept gathers information about the NH_3 slip from an NH_3 sensor between the SDPF and the SCR. Figure 3.10 shows the block scheme of this concept.

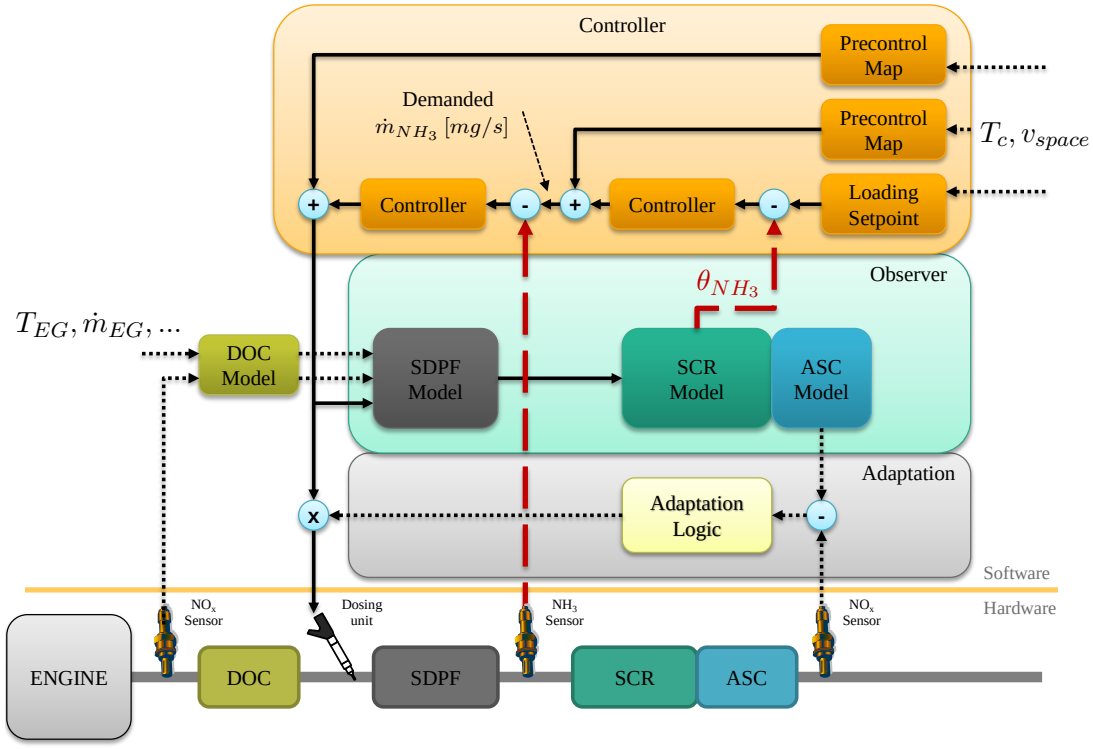

Figure 3.10: Block scheme of concept 3.3

In comparison to the previous concepts there is one main advantage which is the truly measured NH_3 slip. However, there are also disadvantages, namely the higher costs, the cross-sensitivity of the NH_3 sensor with NO_x and a poor accuracy due to the cross-sensitivity.

3.2.8 Concept 4

Figure 3.11 shows the block scheme of concept 4. This concept uses two different controllers. The first one controls the NH_3 loading of the SDPF and the second one the loading of the SCR catalyst.

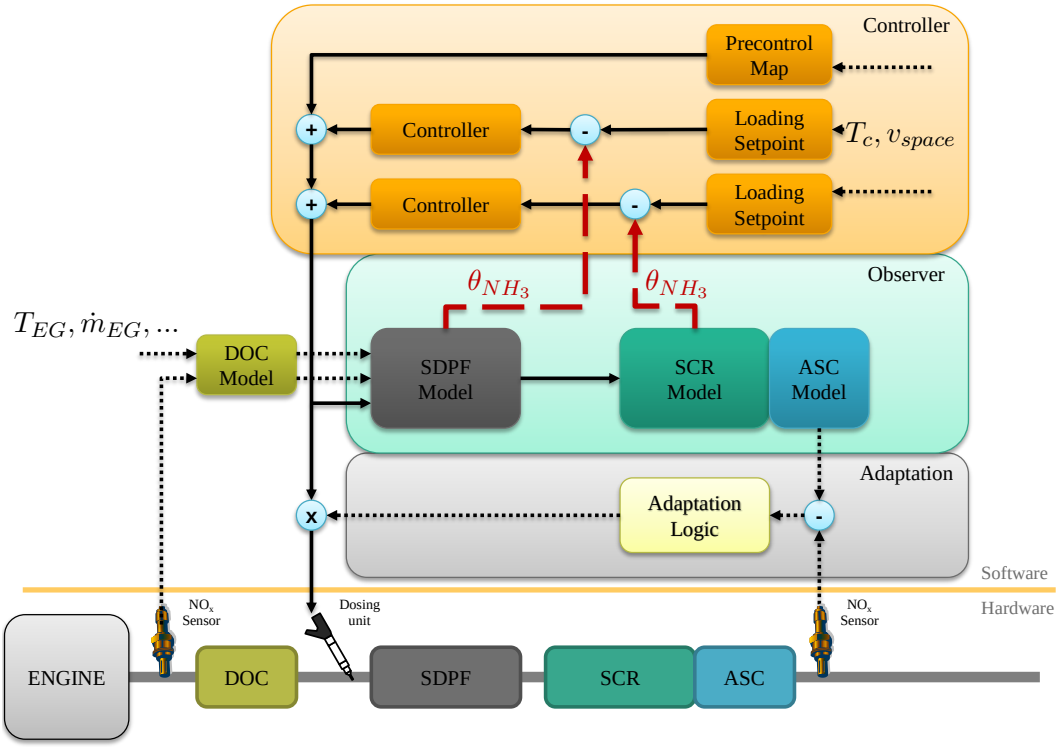

Figure 3.11: Block scheme of concept 4

The main advantages of this concept are that each catalyst is controlled individually and that the different catalyst temperatures are considered properly. However, there are serious disadvantages like the increased calibration effort and especially the fact that the two controllers are working against each other.

3.2.9 Concept 5

This concept uses an additional NO_x sensor to obtain feedback information. With this sensor the desired NH_3 loading can be adapted with an additional feedback controller, using the cross sensitivity of this sensor with NH_3. Figure 3.12 illustrates the block scheme of concept 5.

One of the advantages is that this concept allows a real NH_3 slip feedback control of the SDPF at high SCR efficiency operating modes. Nevertheless, the disadvantages prevail. The additional sensor rises costs and the additional feedback controller leads

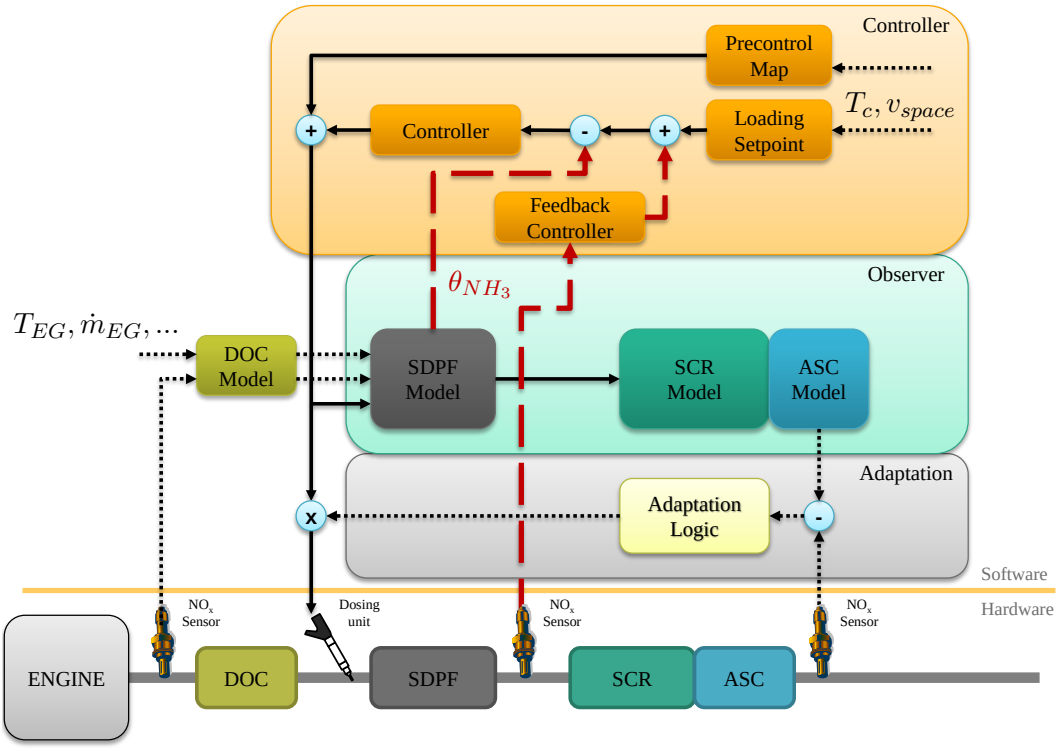

Figure 3.12: Block scheme of concept 5

to a higher calibration effort. Furthermore, the NO_x sensor accuracy to measure NH_3 is low and the NH_3 loading of the SCR catalyst is not considered.

3.2.10 Concept 6

Figure 3.13 shows the last concept that is discussed. This concept uses an additional urea dosing unit. The first dosing unit is controlled by a precontrol map, while the second one makes a fast and exact control of the relative NH_3 loading of the SCR possible. This factor is very beneficial. For example, the urea dosing at the SDPF can be released much earlier during the heat-up phase and the urea dosing in front of the SDPF can be decreased in high efficiency areas of the SCR catalyst. Thus, the influences of urea dosing to the DPF performance of the SDPF can be reduced or even avoided.

The disadvantages of this concept are that two dosing units are necessary and that this hardware configuration is not applicable at the moment.

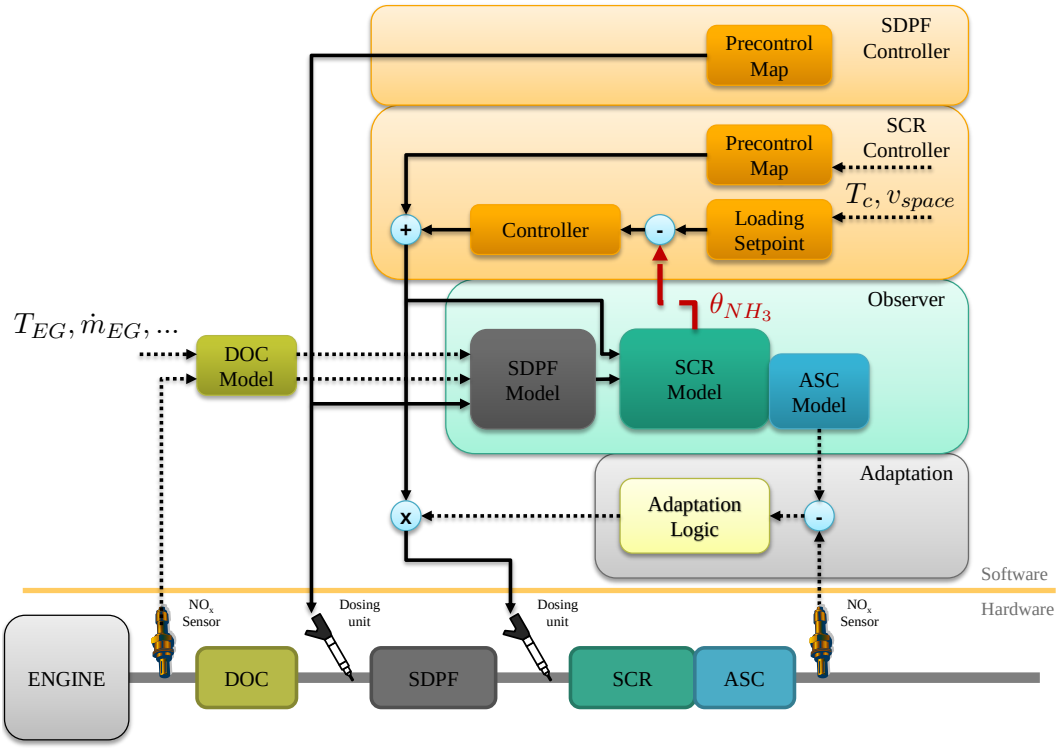

Figure 3.13: Block scheme of concept 6

3.3 Selection of three promising concepts

The previous section dealt with an overview of different concepts for controlling an SDPF-SCR based EAS. The following chapters of this thesis will focus on three specific concepts, which will be discussed and further investigated. The first step is to select the three concepts that have the most advantages and are the most promising.

As already mentioned, summing up two relative NH_3 loadings makes no sense, so concept 1.1 will not be selected. Also, concept 4 will not be investigated further because the two separated controllers work against each other in certain situations. Concept 6 will also not be selected because it is not applicable at the moment and Concept 1.3 because with the combined model, the different properties are not considered. High costs and high calibration efforts are the reasons that concept 3.3 and concept 5 will also not be investigated. Finally, a comparison of the left concepts shows that concept 2 has the biggest disadvantage, because the NH_3 loading of the SCR catalyst is not considered and it can be expected that this concept has the worst conversion efficiency.

In conclusion it can be seen that concept 1.2, concept 3.1 and concept 3.2 are the most promising for controlling an SDPF-SCR based EAS. For a better understanding and readability, these three concepts are renamed as concepts A, B and C.

4 Simulation setup

Three simulations are performed for the evaluation of the different control concepts. The first one is a step test which should show the control behaviour, while the second and the third simulations are the non-road steady cycle (NRSC) and the non-road transient cycle (NRTC). These are regulated test procedures. The measurement data for these test procedures were provided by AVL List. In the following sections the simulation setup of all three tests is explained in further detail.

4.1 Step test

Two contrary OP are used for the step simulation. It is important to note that the loading setpoint does not step from one value to another, but the OP from the first to the second and again back to the first. The used OP are extracted from the NRSC and are listed in table 4.1.

For this test all needed parameters such as the K_p factors, the K_i factors or the optimal setpoint values and the precontrol values are optimized empirically. This should show the best possible transient response of the controlled system.

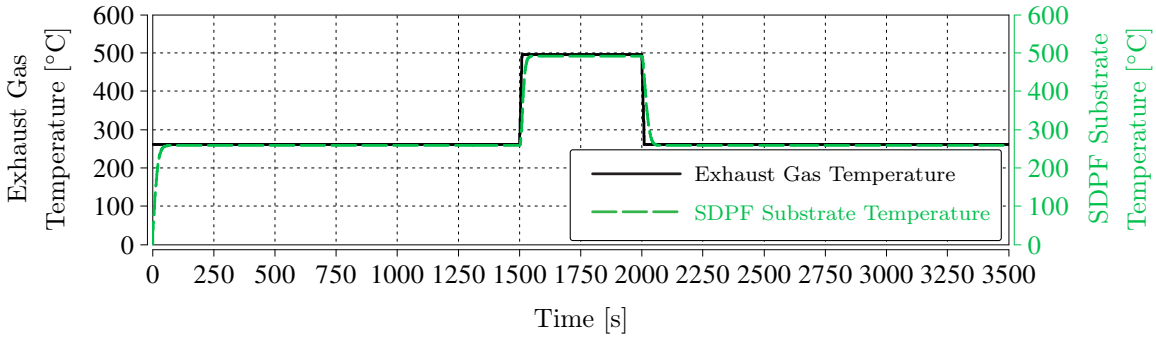

Figure 4.1: Temperatures during the step test

Figure 4.1 shows the exhaust gas temperature upstream the catalysts and the mean catalyst temperature of the SDPF. It can be seen that the catalyst temperature needs some time to reach its stationary value. Because of the slow system behaviour at cold

temperature and the comparability of the different concepts, for the first and the last part, a longer period has been chosen.

Nr:	T_{EG}	NO	NO_2	O_2	$\dot{m}_{EG}$	T_{Amb}	p_{Amb}
	°C	ppm	ppm	ppm	$\frac{kg}{h}$	°C	hPa
1	260	150	165	151803	645	25	970
2	495	855	145	64737	1026	25	970

Table 4.1: List of used OP for the step test

4.2 Non-Road Steady Cycle NRSC

The NRSC is a steady-state engine dynamometer test cycle and it is a special type of the ISO 8178 test cycles. It is the type C1 with its 8 different modes. The ISO 8178 is used in many countries such as Japan, the United States (US) or the European Union for type approval testing and emission certifications. It is an international standard for measuring exhaust emissions from non-road engines [24].

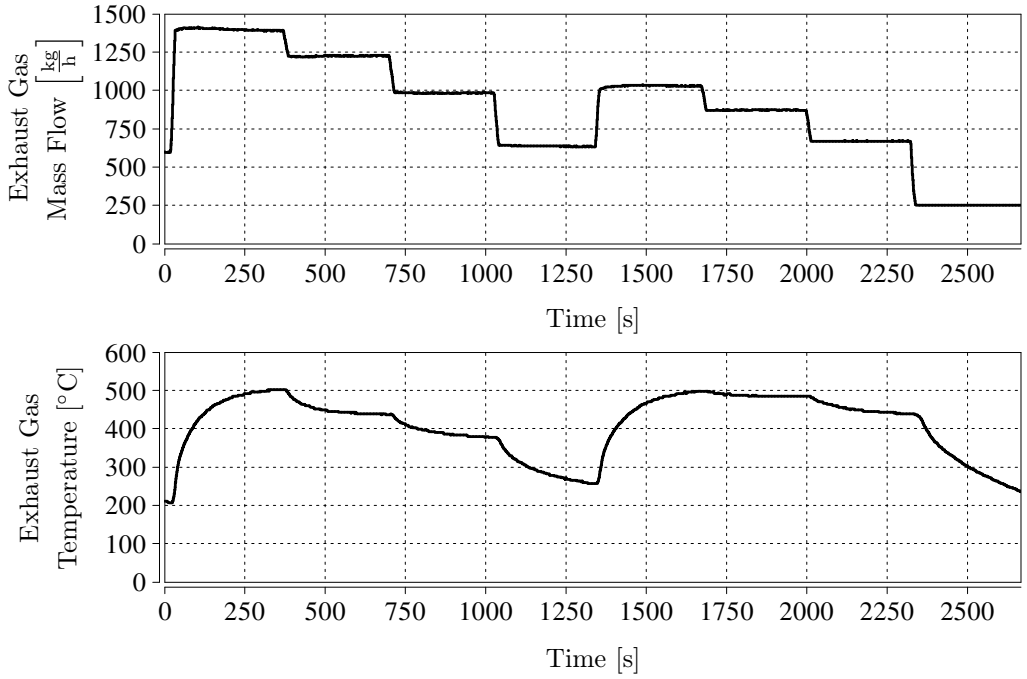

Figure 4.2: Exhaust gas temperature and mass flow during the NRSC test

To get an idea of this test cycle, figure 4.2 shows the exhaust gas temperature upstream the catalysts and the exhaust gas mass flow.

4.3 Non-Road Transient Cycle NRTC

The NRTC is an engine dynamometer transient driving test cycle which was developed by the EU and the US EPA. It is a transient driving cycle for mobile non-road diesel engines, also used for type approval testing and emission certifications in many countries of the world. For example in the European Union the NRTC test is included in the EURO Stage III/IV regulation. This test is always run twice to consider both a cold and a hot start [25].

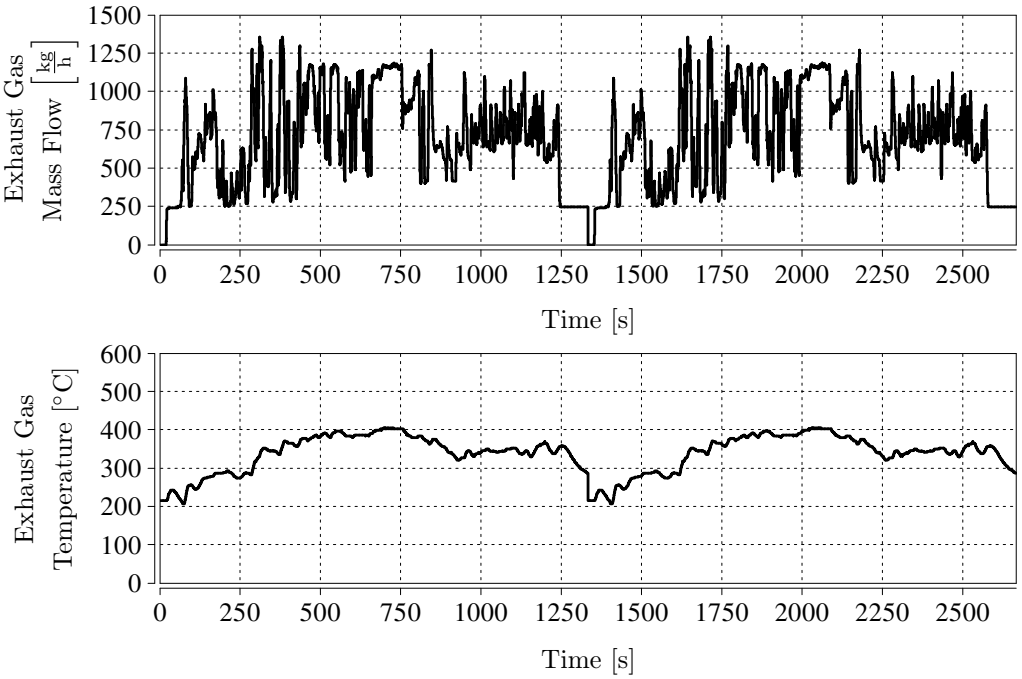

Figure 4.3: Exhaust gas temperature and mass flow during the NRTC test

Figure 4.3 illustrates the exhaust gas temperature upstream the catalysts and the exhaust gas mass flow for the NRTC test cycle .

5 Concept A

Firstly, the concept will be described in detail, highlighting the fact that two different controllers were used to control the ammonia loading. This will also be described in detail. Secondly, the results of the simulations will be illustrated and discussed. Finally, a comparison of these results will show the benefits and disadvantages of the two controllers.

5.1 Concept description

Figure 5.1 illustrates a block diagram of the control structure of concept A. It can be seen that the absolute ammonia loading m_{θ,NH_3} of the two catalysts is being controlled. The sum of the absolute ammonia loading of the two catalysts can be seen as the output parameter of the system. As the input parameter, the feedratio α, which is the ratio between the molar mass flow of NH_3 and NO_x upstream the SDPF, is more convenient as for example the ammonia mass flow or the ammonia concentration. The feedratio is defined by

$$\alpha = \frac{\dot{n}_{NH_3,SDPF,us}}{\dot{n}_{NO_x,SDPF,us}}$$

as already mentioned in section 2.3.

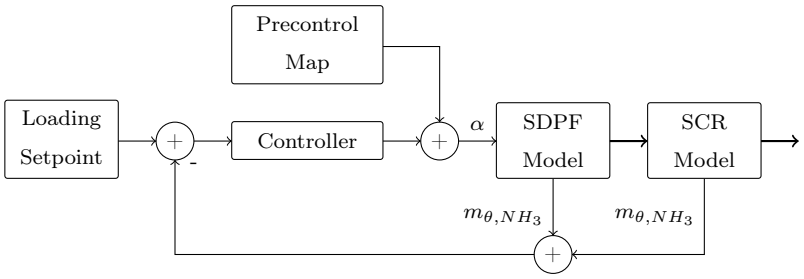

Figure 5.1: Block diagram of concept A

Systems with one input and one output are called SISO[18] systems. The system used here consisting of the SDPF and the SCR model can be seen as a SISO system because it can only be influenced by α although there are also other input and output parameters

[18]SISO = Single Input Single Output

like the concentration of the gaseous species up- and downstream the catalysts and others.

Two different controllers are used for controlling this system: On the one hand, a gain-scheduled PI-controller and on the other hand a so called Level-controller.

5.2 Gain-scheduled PI-controller

The controller consists of two main parts, which are the precontrol map and the scheduled PI-controller with anti wind-up measures. Figure 5.2 illustrates the block diagram. It shows that the scheduling maps - the K_p- and the K_i-map - as well as the precontrol and the loading setpoint map are depending on the average of the mean catalyst temperature of the SDPF and the SCR T_c, as well as the exhaust mass flow $\dot{m}_{EG}$. These are the parameters which have the biggest impact on the system behaviour. The average of the mean catalyst temperatures is calculated by

$$T_c = \frac{T_{c,SDPF} + T_{c,SCR}}{2}$$

where $T_{c,SDPF}$ is the mean SDPF catalyst temperature and $T_{c,SDPF}$ the mean SCR catalyst temperature. Usually the space velocity v_{space} is used instead of the exhaust gas mass flow. Because the overall ammonia loading of both catalysts is controlled and the space velocity of the two catalysts is different, this concept uses the exhaust gas mass flow.

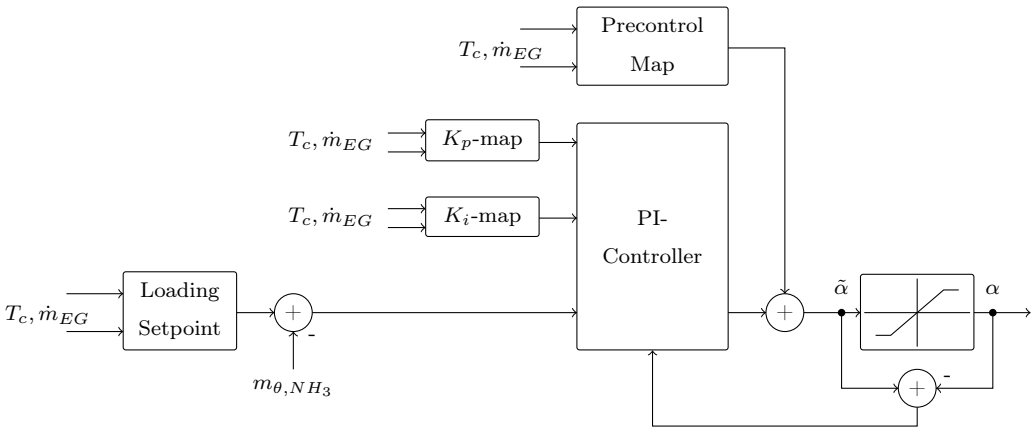

Figure 5.2: Block diagram of the gain-scheduled PI-controller

5.2.1 Precontrol and optimal loading setpoint calibration

The so called beta workflow from AVL List was used for the calibration of the precontrol map and the loading setpoint map. In order to do so, 30 different OP within the

usual operating area are defined. For each OP the stationary values of some required parameters are stored while the feedratio α is increased stepwise from 0 to 2. Table 5.1 shows a list of the defined OP.

Nr:	n	M	T_{EG}	NO	NO_2	O_2	$\dot{m}_{EG}$	T_{Amb}	p_{Amb}
	$\frac{1}{\text{min}}$	Nm	°C	ppm	ppm	ppm	$\frac{\text{kg}}{\text{h}}$	°C	hPa
1	1200	60	168	131	12	183724	320	25	970
2	1200	110	193	162	40	176066	327	25	970
3	1200	161	219	191	92	168996	335	25	970
4	1200	211	242	221	156	161986	344	25	970
5	1200	260	281	216	247	163815	348	25	970
6	1200	353	335	246	331	143167	370	25	970
7	1200	463	385	361	347	127605	398	25	970
8	1200	597	439	609	298	132106	424	25	970
9	1200	802	487	1008	247	95065	499	25	970
10	1200	1122	542	1603	172	74853	605	25	970
11	1500	92	197	136	28	176625	414	25	970
12	1500	138	221	153	65	170390	424	25	970
13	1500	184	246	173	105	164668	439	25	970
14	1500	225	265	196	141	159809	451	25	970
15	1500	277	293	211	187	160628	470	25	970
16	1500	369	333	245	240	152255	505	25	970
17	1500	482	380	310	259	144211	555	25	970
18	1500	686	435	545	244	128452	652	25	970
19	1500	1154	495	951	198	116289	922	25	970
20	1500	1471	523	1419	202	107806	1064	25	970
21	2100	17	187	75	7	183186	616	25	970
22	2100	78	214	116	25	176762	638	25	970
23	2100	136	240	139	52	171590	668	25	970
24	2100	197	273	161	90	167378	696	25	970
25	2100	264	295	193	119	163992	749	25	970
26	2100	445	355	255	177	148788	903	25	970
27	2100	695	398	375	192	139047	1172	25	970
28	2100	929	443	517	179	122716	1318	25	970
29	2100	1113	485	711	160	118121	1413	25	970
30	2100	1208	521	812	121	115241	1457	25	970

Table 5.1: List of operation points

For the calibration of the maps the following parameters are stored for each catalyst:

- NH_3 concentration upstream
- NH_3 concentration downstream
- NO_x concentration downstream
- Catalyst temperature
- Exhaust gas mass flow
- Space velocity
- Relative NH_3 loading
- Absolute NH_3 loading

To generate the maps, the tradeoff between NO_x conversion and NH_3 slip has to be considered. Therefore a cost function J is introduced.

$$J = \beta \cdot p \cdot x_{NO_x,ds} + (1 - \beta) \cdot q \cdot x_{NH_3,ds}$$

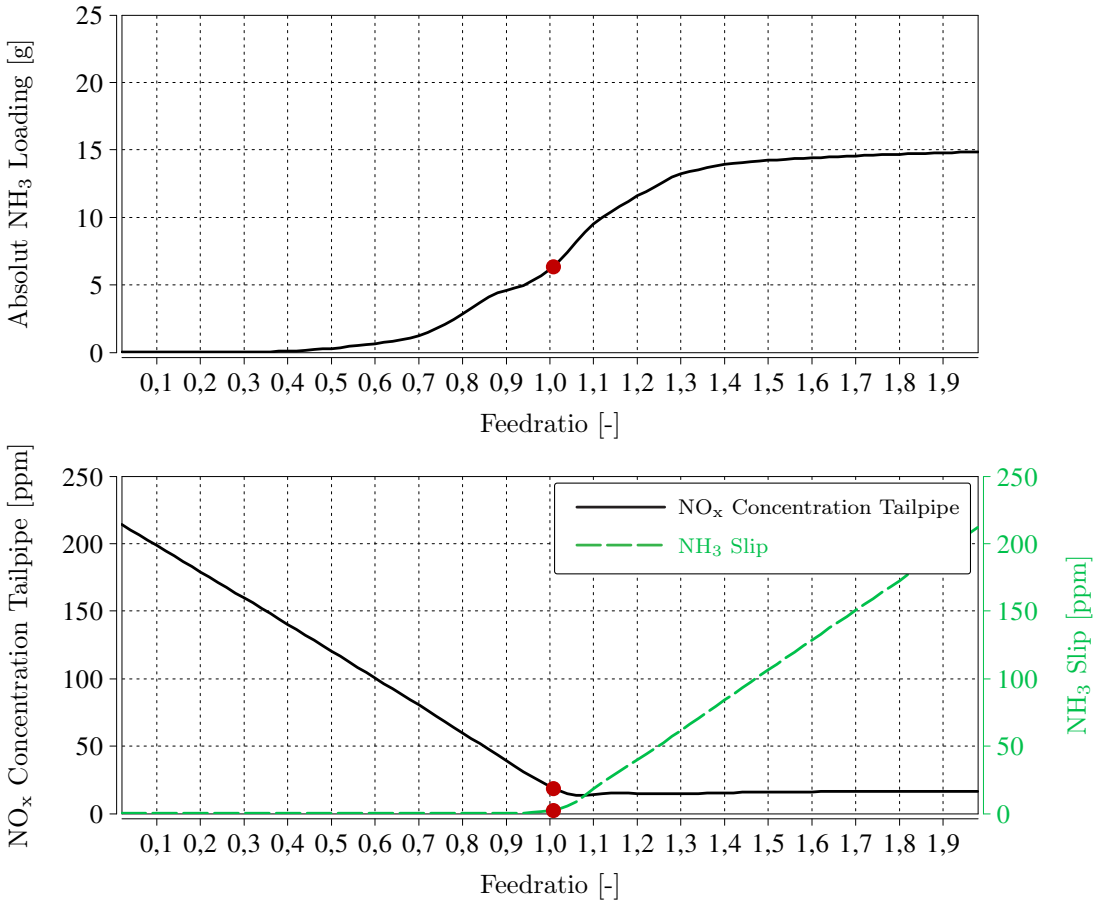

Figure 5.3: Stationary curve of OP12

The two parameters p and q are weighting parameters. To penalize high NH_3 slip stronger than NO_x tailpipe emission for the weighting parameters $p = 1$ and $q = 2$ is chosen. The third parameter of the cost function is called the tradeoff index β. It is defined for $\beta \in [0, 1]$. High β values lead to penalization of high NO_x tailpipe emission and low values for β lead to penalization of high NH_3 slip. With the index β it is easy to adjust the tradeoff between the NO_x conversion and the NH_3 slip [16].

An empirical value $\beta = 0.98$ was chosen for the tradeoff index since the focus of this thesis is the evaluation of different control concepts and not optimizing the tradeoff index. With the chosen β and the stored stationary values of the NO_x and the NH_3 concentrations downstream the SCR the cost function J, depending on α, can be

derived. Minimizing J leads to a specific value of the feedratio α and the other corresponding parameters. For OP12 the resulting optimal values are for example $\alpha = 1.007$ and $m_{\theta,NH_3} = 6.35g$. The bottom diagram (Figure 5.3) shows the stationary curve of the NO_x concentration downstream the SCR in black and the NH_3 slip in green. The top diagram shows the corresponding overall absolute NH_3 loading. In this plot the optimal values referred to the cost function J are marked by red dots. This process is performed with each of the 30 OP. With the gained information the desired loading setpoint and precontrol maps can be formed by interpolation between the optimal values and extrapolation in outside areas. The interpolation also contains smoothing so that the values in the maps can slightly differ from the optimal values. In figure 5.4 the resulting loading setpoint map is illustrated. It shows the big influence of the exhaust gas mass flow and the mean catalyst temperature.

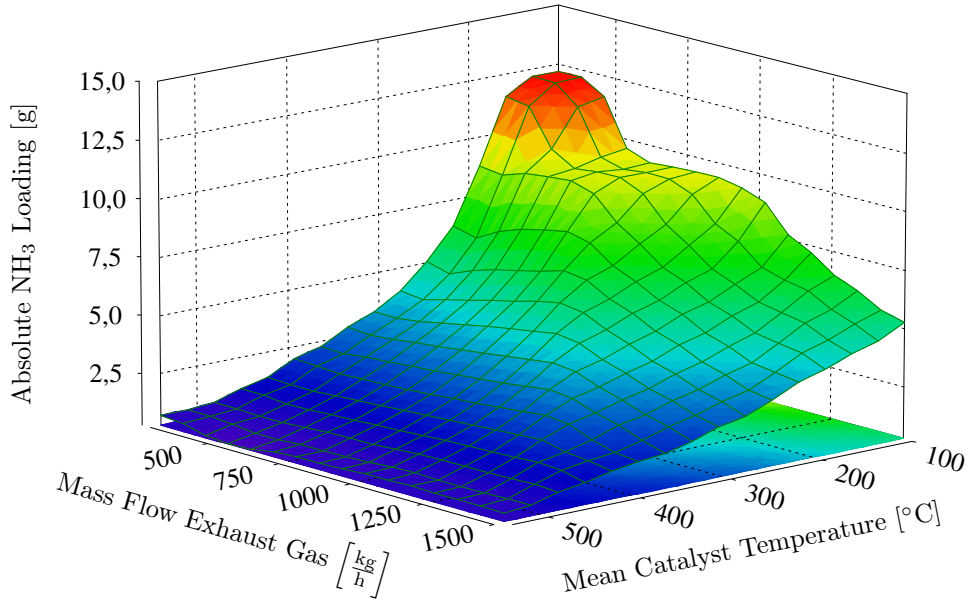

Figure 5.4: Loading setpoint map

Figure 5.5 shows the precontrol map. It can be seen that the optimal loading setpoint decreases with increasing temperatures while the feedratio through the precontrol increases in general.

5.2.2 Controller calibration

Since the controller is a gain-scheduled PI-controller (refer to figure 4.2) the control parameter maps for K_p and K_i have to be calibrated. As already mentioned, the control parameters depend - like the precontrol and the loading setpoint map - on the mean catalyst temperature T_c and the exhaust gas mass flow $\dot{m}_{EG}$. To get these maps for

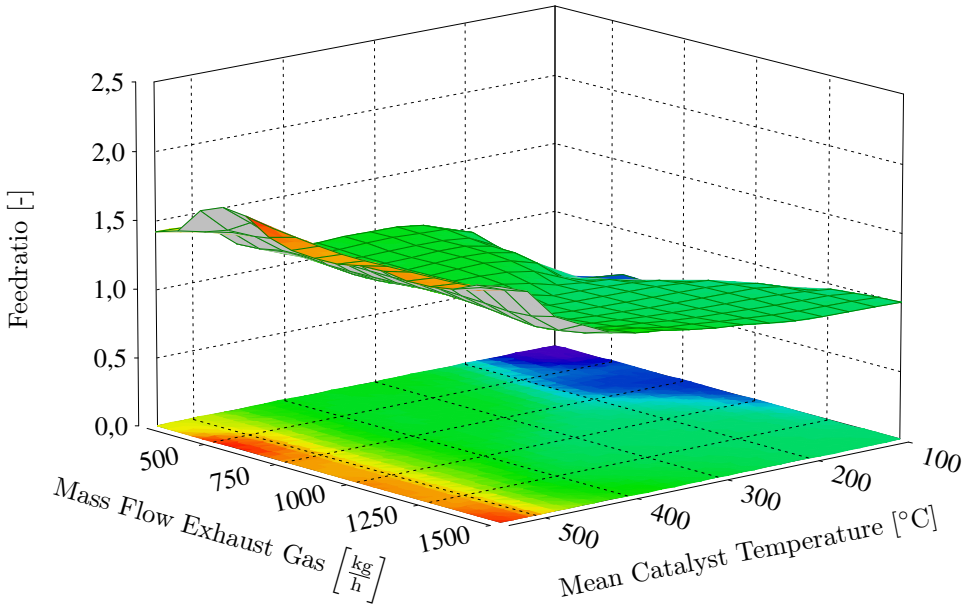

Figure 5.5: Precontrol map

each of the 30 OP, a simulation is done which provides the step response $p(t)$ of the system. In all simulations a feedratio step from zero to the corresponding value in the precontrol map is applied. As an example for the OP12 a step from $\alpha = 0 \rightarrow 1.007$ is performed.

With these step responses the system parameter can be estimated for each OP using an optimisation method. Here, the golden section search method is used to approximate the step response by a PT1-element which has the form

$$G(s) = \frac{\mu(s)}{\nu(s)} = \frac{k_\alpha}{1 + \tau \cdot s}. \tag{5.1}$$

With $G(s)$ the step response $g(t)$ can be computed. Since k_α is given by the stationary values of the step response and the input parameter step according to

$$k_\alpha = \left. \frac{m_{\theta,NH_3}(t)}{\alpha(t)} \right|_{t \rightarrow \infty}$$

only the time constant τ is left as an optimisation variable. The optimisation problem is therefore one-dimensional.

The cost function given by

$$f(\tau) = \int_0^{t_{end}} |p(t) - g(\tau, t)| \, dt$$

is used for the optimisation. Solving the optimisation problem

$$\min_{\tau \in \mathbb{R}} f(\tau)$$

leads to the desired system parameter τ. Figure 5.6 shows the step response of the system $p(t)$ and the step response of the estimation $g(t)$. It can be seen that the optimisation delivers a very good estimate with very low deviations. For the OP12 the estimated system parameter is $\tau = 1634.4$. Thus for the OP12, the system is approximated by

$$G(s) = \frac{k_\alpha}{1 + \tau \cdot s} = \frac{6.34}{1 + 1634.4 \cdot s}.$$

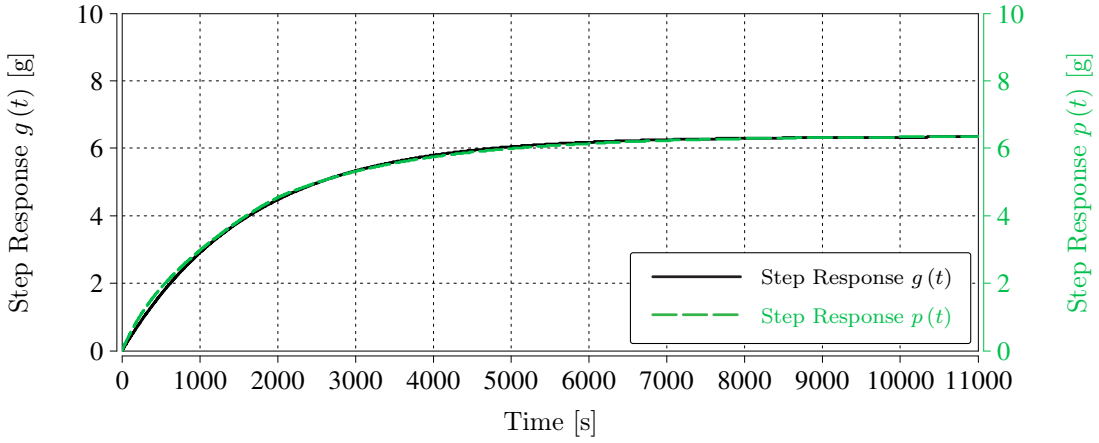

Figure 5.6: Comparison of the step response $p(t)$ with $g(t)$ for OP12

With the system parameters k_α and τ the control parameter K_p and K_i can be calculated. Usually the controller is determined by methods like Ziegler / Nichols or the frequency-domain method. Here, the so called inward approach is used to determine the controller parameters K_p and K_i of the desired PI-controller. For this method the overall transfer function $T_d(s)$ has to be defined, generally described according to

$$T_d(s) = \frac{\mu_{T_d}(s)}{\nu_{T_d}(s)} = \frac{\omega_0^2}{s^2 + 2 \cdot d \cdot \omega_0 \cdot s + \omega_0^2} \tag{5.2}$$

where ω_0 is the eigenfrequency and d the damping factor. For a successful controller determination the transfer function pair $(T_d(s), G(s))$ has to be implementable. Therefore some conditions have to be fulfilled:

- $\nu_{T_d}(s)$ has to be a Hurwitz-polynomial
- $\mu_{T_d}(s)$ has to include all unstable roots of $\mu(s)$

- $\deg\left(\nu_{T_d}\left(s\right)\right) - \deg\left(\mu_{T_d}\left(s\right)\right) \geq \deg\left(\nu\left(s\right)\right) - \deg\left(\mu\left(s\right)\right)$

The denominator $\nu_{T_d}\left(s\right)$ of the defined overall transfer function $T_d\left(s\right)$ is a Hurwitz-polynomial since d and ω_0 will be chosen positive. The choice of these two parameters will be explained later on. Also the second condition is fulfilled because the numerator $\mu\left(s\right)$ of the system $G\left(s\right)$ has no roots. A comparison of the two transfer functions 5.1 and 5.2 shows that the third condition holds too. Since all three conditions are fulfilled the transfer function pair $\left(T_d\left(s\right), G\left(s\right)\right)$ is implementable, although the implementability gives no information about the structure of the controller.

As it can be seen in figure 5.2 a unity-feedback configuration for the control system is used. With this configuration, the numerator of the overall transfer function cannot be chosen arbitrarily. It rather follows the calculation of the controller.

The transfer function of the desired PI-controller has the form

$$R\left(s\right) = \frac{b\left(s\right)}{a\left(s\right)} = \frac{b_1 \cdot s + b_0}{a_1 \cdot s + a_0}. \tag{5.3}$$

With the $G\left(s\right)$ the overall transfer function of the system can be calculated according to

$$T\left(s\right) = \frac{\mu_T\left(s\right)}{\nu_T\left(s\right)} = \frac{R\left(s\right) \cdot G\left(s\right)}{1 + R\left(s\right) \cdot G\left(s\right)} = \frac{b\left(s\right) \cdot \mu\left(s\right)}{a\left(s\right) \cdot \nu\left(s\right) + b\left(s\right) \cdot \mu\left(s\right)}.$$

This transfer function should be the defined overall transfer function $T_d\left(s\right)$. This leads to the equation

$$T\left(s\right) = \frac{b\left(s\right) \cdot \mu\left(s\right)}{a\left(s\right) \cdot \nu\left(s\right) + b\left(s\right) \cdot \mu\left(s\right)} \stackrel{!}{=} \frac{\mu_{T_d}\left(s\right)}{\nu_{T_d}\left(s\right)} = T_d\left(s\right).$$

The numerator and the denominator of this resulting equation can be separated according to

$$b\left(s\right) \cdot \mu\left(s\right) \stackrel{!}{=} \mu_{T_d}\left(s\right) \tag{5.4}$$

$$a\left(s\right) \cdot \nu\left(s\right) + b\left(s\right) \cdot \mu\left(s\right) \stackrel{!}{=} \nu_{T_d}\left(s\right). \tag{5.5}$$

The equation 5.5 is called Diophantine equation. Solving this equation delivers the desired controller parameter. As already mentioned, the numerator of the overall transfer function $T\left(s\right)$ cannot be chosen arbitrarily because equation 5.4 has to be fulfilled.

To solve the Diophantine equation the denominator, especially the two parameters d and ω_0 have to be defined. These two parameters can be estimated by defining the overshoot M_p and the rise time t_r. Since the step response of the controlled system should not show an overshoot for the first parameter $M_p = 1$ is chosen. The relation between M_p and d is shown in the appendix in figure A.1. Using this relation, the damping factor is given by $d = 1$.

The eigenfrequency ω_0 of the controlled system should be defined in such a way that the control variable does not exceed the control variable limit of $\alpha_{max} = 2$. Therefore

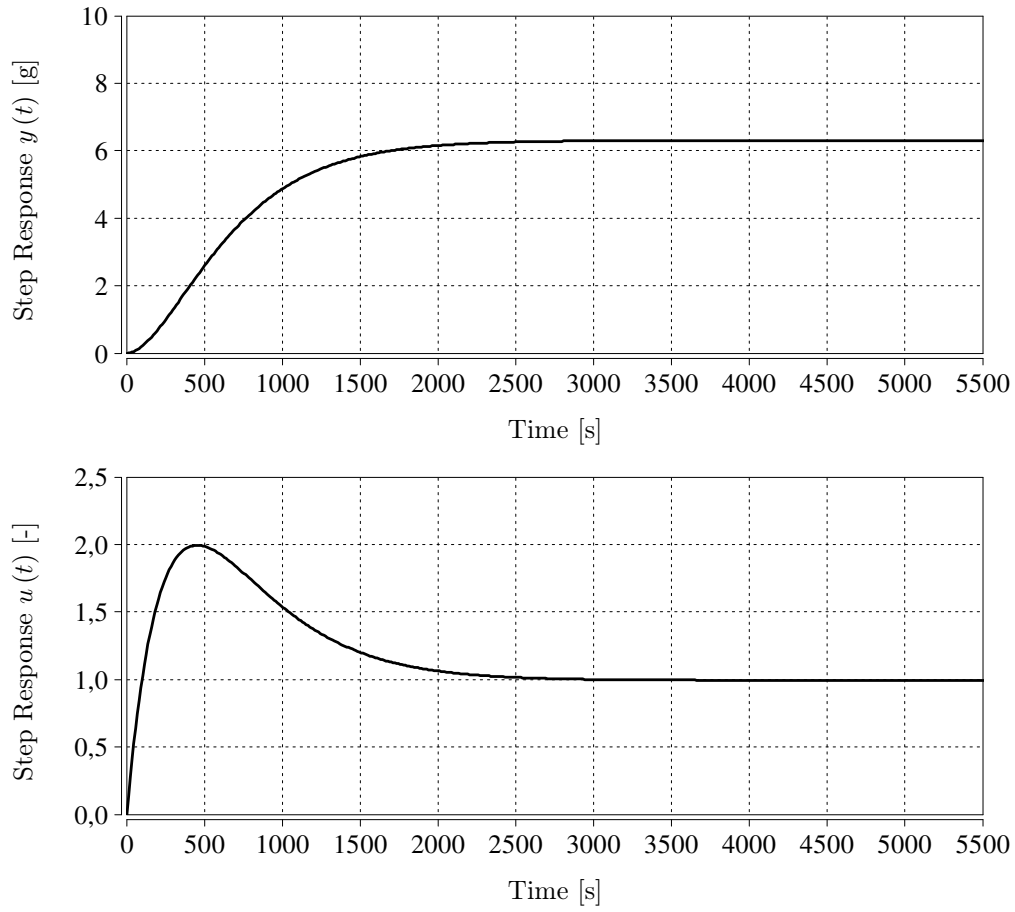

Figure 5.7: Step response of the controlled system

an iterative method is used. Within this method, the ω_0 is varied until the maximum of the control variable step response touches the limit at its maximum. For this iterative calculation an NH_3 loading step from zero to the corresponding value in the loading setpoint map is applied. In this case, a step from $m_{\theta,NH_3} = 0 \rightarrow 6.3$ is performed for the OP12. The step response $u(t)$ of the control variable can be calculated with the transfer function

$$T_u(s) = \frac{T_d(s)}{G(s)}.$$

Figure 5.7 shows the output variable step response $y(t)$ of the defined overall transfer function $T_d(s)$ and the corresponding step response of the control variable $u(t)$. It can be seen that the limit α_{max} is only touched but not exceeded. This method delivers the desired eigenfrequency, for example

$$\omega_0 = 2.819 \cdot 10^{-3} \frac{1}{s}$$

for the OP12. With the defined parameters d and ω_0, the resulting desired overall transfer function can be written as

$$T_d(s) = \frac{\mu_{T_d}(s)}{\nu_{T_d}(s)} = \frac{7.949 \cdot 10^{-6}}{s^2 + 5.639 \cdot 10^{-3} s + 7.949 \cdot 10^{-6}}.$$

Exemplary calculation of the control parameter

Since the desired overall transfer function is defined, the Diophantine equation (refer to 5.5) can be solved. Here the calculations are done exemplarily for the OP12. The Diophantine equation can be written in matrix format according to

$$\begin{bmatrix} \nu_0 & 0 & \mu_0 & 0 \\ \nu_1 & \nu_0 & \mu_1 & \mu_0 \\ 0 & \nu_1 & 0 & \mu_1 \\ 1 & 0 & 0 & 0 \end{bmatrix} \begin{bmatrix} a_0 \\ a_1 \\ b_0 \\ b_1 \end{bmatrix} = \begin{bmatrix} \nu_{T_d,0} \\ \nu_{T_d,1} \\ \nu_{T_d,2} \\ 0 \end{bmatrix}.$$

Inserting the determined parameter leads to the system of linear equations

$$\begin{bmatrix} 1 & 0 & 6.34 & 0 \\ 1634.4 & 1 & 0 & 6.34 \\ 0 & 1634.4 & 0 & 0 \\ 1 & 0 & 0 & 0 \end{bmatrix} \begin{bmatrix} a_0 \\ a_1 \\ b_0 \\ b_1 \end{bmatrix} = \begin{bmatrix} 7.949 \cdot 10^{-6} \\ 5.639 \cdot 10^{-3} \\ 1 \\ 0 \end{bmatrix}.$$

The solution of this system delivers the desired control parameter and thus the desired controller

$$R(s) = \frac{632.4 \cdot s + 1}{488.1 \cdot s} \tag{5.6}$$

for the OP12. The transfer function of this controller can also be written in the general PI-controller form

$$R(s) = K_p \frac{T_i \cdot s + 1}{T_i \cdot s} = K_p + K_p \cdot \frac{1}{T_i \cdot s} = K_p + K_i \cdot \frac{1}{s} = 1.2955 + 2.654 \cdot 10^{-3} \cdot \frac{1}{s}$$

where K_p is the proportional factor, T_i the integral time and K_i the integrating factor. The K_p and the K_i factors are determined for all thirty OP. With these values the K_p and the K_i maps can be generated by interpolation and extrapolation like described in the previous section for the precontrol map.

As already mentioned, the numerator of the over all transfer function results from the determined controller $R(s)$ with the chosen control structure. Since $\mu(s)$ is given by the estimated system $G(s)$ and $b(s)$ by the solution of the Diophantine equation the numerator of the resulting overall transfer function $T(s)$ results in

$$\mu(s) = b(s) \cdot \mu(s) = 5.027 \cdot 10^{-3} s + 7.949 \cdot 10^{-6}$$

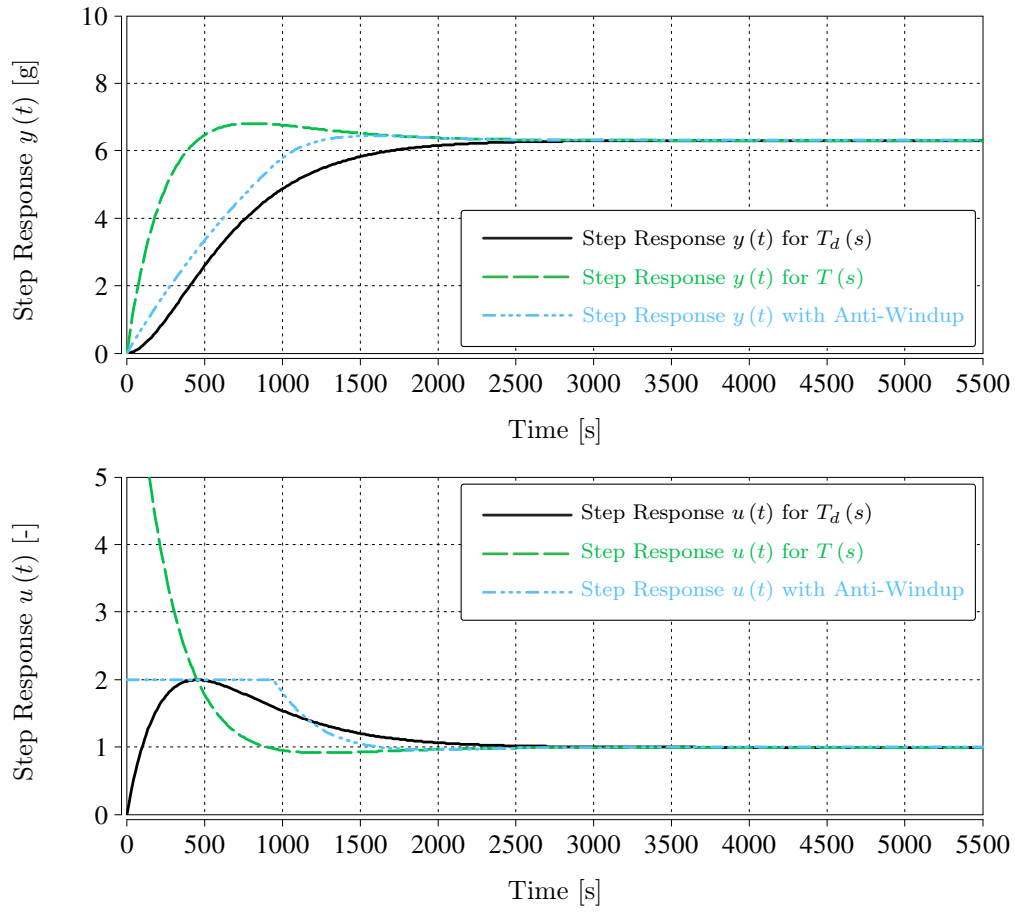

Figure 5.8: Comparison of the step responses for OP12

and thus the overall transfer function itself in

$$T(s) = \frac{5.027 \cdot 10^{-3} s + 7.949 \cdot 10^{-6}}{s^2 + 5.639 \cdot 10^{-3} s + 7.949 \cdot 10^{-6}}.$$

It can be seen that the numerator of $T(s)$ is now of first order. This leads to a different behaviour which is illustrated in figure 5.8. This figure shows the step responses of the output variable and the control variable of the desired and the resulting over all transfer function. Also the step response with anti-windup and precontrol is shown in the diagram. This step response shows a small overshoot which is acceptable for the control of the ammonia loading.

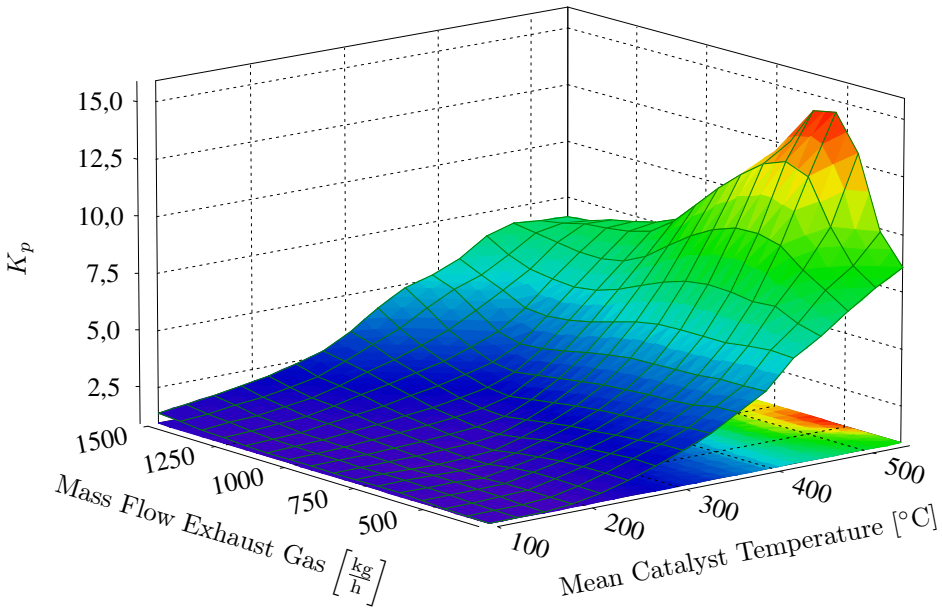

Figure 5.9: K_p map

The determined K_p map is illustrated in figure 5.9 and the corresponding K_i map in figure 5.10. It can be seen that the usage of a scheduled controller is necessary because especially with increasing catalyst temperatures, the speed of the system increases.

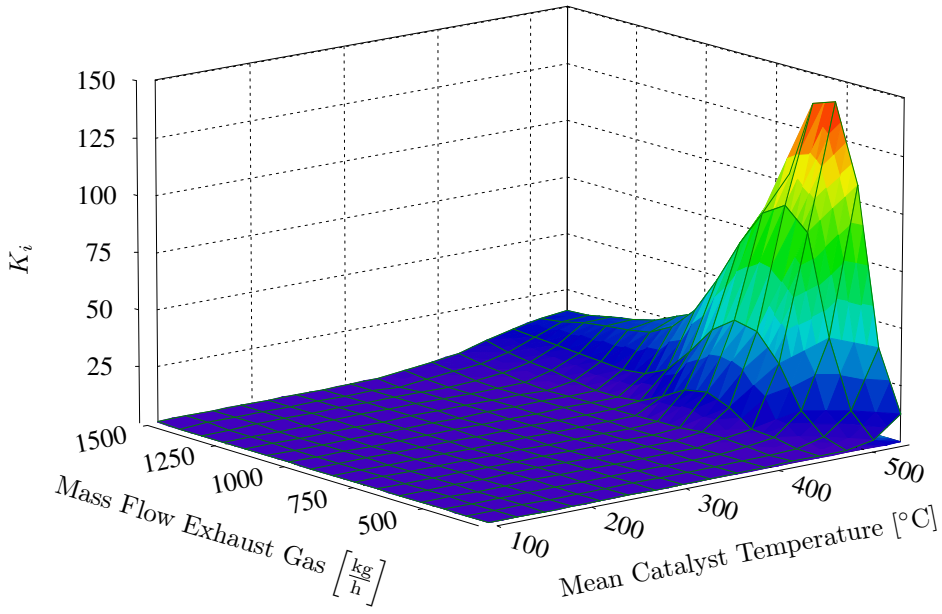

Figure 5.10: K_i map

5.3 Level-controller

In the previous section, the design of the used scheduled PI-controller was described. A so called Level-controller should be used for the first two concepts. This section shows the structure and the mathematical equations of this controller.

In this section all parameters are related to ammonia (NH_3). For convenience and readability, parameter names are simplified, as for example the ammonia mass flow upstream the SDPF $\dot{m}_{NH_3,SDPF,us}$ is written as $\dot{m}_{in}$ and the ammonia slip downstream the SCR $\dot{m}_{NH_3,SCR,ds}$ as $\dot{m}_{out}$.

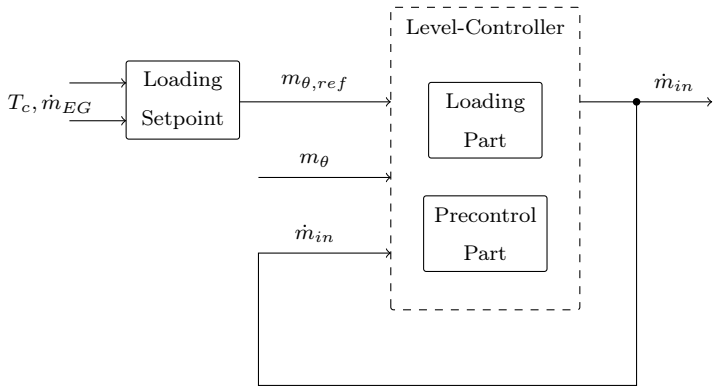

Figure 5.11: Block diagram of the gain-scheduled PI-controller

Figure 5.11 shows the block diagram of the Level-controller. It can be seen that it consists of two main parts: the ammonia loading part and the precontrol part.

5.3.1 Mathematical equations

The basis of this controller is the mass balance which can be written as

$$\frac{dm_\theta}{dt} = \dot{m}_{in} - \dot{m}_{out} - \dot{m}_{ox} - \dot{m}_{denox} \tag{5.7}$$

where m_θ is the overall ammonia loading, $\dot{m}_{in}$ the ammonia mass flow injected upstream the catalysts, $\dot{m}_{out}$ the ammonia mass flow downstream the catalysts, $\dot{m}_{ox}$ the oxidised ammonia and $\dot{m}_{denox}$ the ammonia which is reacting with the NO_x.

The injected ammonia consists of two parts according to

$$\dot{m}_{in} = \dot{m}_{in,\theta} + \dot{m}_{in,PC} \tag{5.8}$$

where $\dot{m}_{in,\theta}$ is the part of the injected NH_3 for the increase of the loading and $\dot{m}_{in,PC}$ the precontrol part.

Combining equation 5.7 and 5.8 delivers

$$\frac{dm_\theta}{dt} = \dot{m}_{in,\theta} + \dot{m}_{in,PC} - \dot{m}_{out} - \dot{m}_{ox} - \dot{m}_{denox}. \tag{5.9}$$

The precontrol part is chosen in such a way that a certain ammonia loading remains constant. This leads to the requirement

$$0 \stackrel{!}{=} \dot{m}_{in,PC} - \dot{m}_{out} - \dot{m}_{ox} - \dot{m}_{denox}.$$

The rearrangement of this equation delivers

$$\dot{m}_{in,PC} = \dot{m}_{out} + \dot{m}_{ox} + \dot{m}_{denox}. \tag{5.10}$$

Inserting this equation in 5.9 results in

$$\frac{dm_\theta}{dt} = \dot{m}_{in,\theta}. \tag{5.11}$$

It can be seen that $\dot{m}_{in,\theta}$ contributes an increase of the ammonia loading as it is desired. The combination of equations 5.7 and 5.10 leads to the following equation which describes another relation of the precontrol part.

$$\dot{m}_{in} - \frac{dm_\theta}{dt} = \dot{m}_{out} + \dot{m}_{ox} + \dot{m}_{denox} = \dot{m}_{in,PC} \tag{5.12}$$

Implementation of the Level-controller

Since the models of the catalysts are discrete models, the Level-controller is also implemented in a discrete form. The discretisation of equation 5.9 leads to

$$\frac{\Delta m_{\theta,k}}{T_s} = \dot{m}_{in,\theta,k} + \dot{m}_{in,PC,k} - \dot{m}_{out,k} - \dot{m}_{ox,k} - \dot{m}_{denox,k} \tag{5.13}$$

where $\Delta m_{\theta,k}$ is the difference between two consecutive values of the ammonia loading according to

$$\Delta m_{\theta,k} = m_{\theta,k+1} - m_{\theta,k}.$$

Multiplying equation 5.13 with the discretisation time T_s leads to

$$\Delta m_{\theta,k} = m_{in,\theta,k} + m_{in,PC,k} - m_{out,k} - m_{ox,k} - m_{denox,k}$$

where all terms are now related to one discrete time step. The corresponding discrete equation for the precontrol part (refer to 5.12) can be written as

$$m_{in,PC,k} = m_{in,k} - \Delta m_{\theta,k} = m_{in,k} - \left(m_{\theta,k+1} - m_{\theta,k}\right).$$

Since only values of the ammonia loading from the past are known, this equation has to be reformed according to

$$m_{in,PC,k-2} = m_{in,k-2} - \left(m_{\theta,k-1} - m_{\theta,k-2}\right).$$

To get the precontrol part of the controller, the following assumption is made:

$$m_{in,PC,k} \approx m_{in,PC,k-2}$$

The assumption says that the precontrol part does not change significantly over two time steps. This means that for the calculation of the precontrol part, the values of the last two time steps are used instead of the values of the present and the future time steps according to

$$m_{in,PC,k} = m_{in,k-2} - (m_{\theta,k-1} - m_{\theta,k-2})\,. \tag{5.14}$$

For the second part of the controller the equation 5.11 has to be discretised and multiplied by T_s which leads to

$$\Delta m_{\theta,k} = m_{in,\theta,k}$$

It can be seen that the whole mass $m_{in,\theta,k}$ is transferred to a change of the ammonia loading. Since a specific loading setpoint $m_{\theta,ref,k}$ should be reached, the difference between the setpoint and the loading value defines the ammonia mass $m_{in,\theta,k}$ for the loading increase. Also in this case, the actual loading value is not known, so the previous value is used according to

$$m_{in,\theta,k} = K_l \cdot (m_{\theta,ref,k} - m_{\theta,k-1}) = K_l \cdot m_{\theta,diff,k}. \tag{5.15}$$

The parameter K_l is used for the adjustment of the injection time. Without this parameter the whole loading difference $m_{\theta,diff,k}$ would be injected in one time step. Within this thesis $K_l = T_s$ was chosen which leads to an injection time of one second.

To get to the demanded control parameter $\dot{m}_{in,k}$ the two control parts have to be added and divided by the discretisation time T_s.

$$\dot{m}_{in,k} = \frac{(m_{in,PC,k} + m_{in,\theta,k})}{T_s}$$

The combination of this equation and the equations 5.14 and 5.15 leads to the overall controller equation

$$\dot{m}_{in,k} = \frac{m_{in,k-2} - (m_{\theta,k-1} - m_{\theta,k-2}) + K_l \cdot (m_{\theta,ref,k} - m_{\theta,k-1})}{T_s}$$

respectively to

$$\dot{m}_{in,k} = \dot{m}_{in,k-2} - \frac{m_{\theta,k-1} - m_{\theta,k-2}}{T_s} + \frac{K_l}{T_s} \cdot (m_{\theta,ref,k} - m_{\theta,k-1})$$

with $\frac{K_l}{T_s} = 1$. this factor can be neglected for the implementation, but here it is important for the right unit of the last term.

5.4 Simulation results

This section illustrates the simulation results of the step test, the NRSC and the NRTC. Firstly, the results of the PI-controller and the Level-controller will be presented. For the sake of completeness, the outcome of the step test with open-loop control will also be shown. Finally, the results will be compared and discussed.

5.4.1 Simulation results PI-controller

As already mentioned, two different controllers were used in concept A. This section shows the simulation results for the determined PI-controller.

Step test simulation results

Figure 5.12 shows the loading setpoint, the absolute ammonia loading and the corresponding feedratio for the step test. The bottom diagram also illustrates the NO_x and the NH_3 concentrations downstream the SCR catalyst. With the PI-controller a small overshoot in feedratio and ammonia loading can be seen at the beginning.

After 1500 seconds the step from the first OP to the second is performed. Thereby the catalyst temperature rises which requires a lower loading setpoint. It can be seen that in this period the feedratio decreases almost to zero and the NO_x concentration shows a huge peak. This peak comes from the increase of the NO_x concentration upstream the catalysts due to the OP step. The ammonia concentration shows a peak too, resulting from the rising catalyst temperatures which increases the speed of ammonia desorption. After 2000 seconds the setpoint rises again. In this period the feedratio is at its limit.

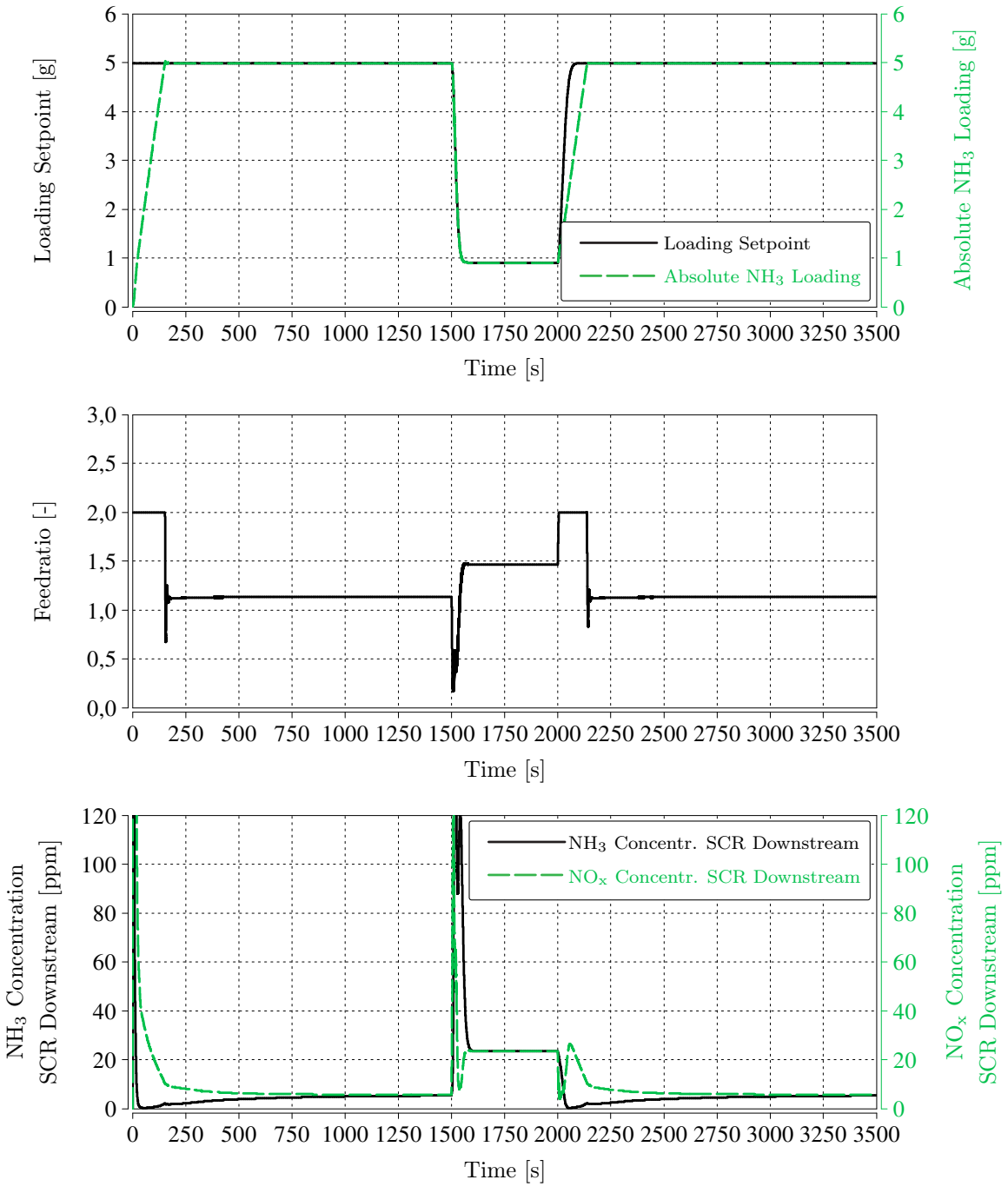

Figure 5.12: Step test simulation results with PI-controller

NRSC simulation results

Figure 5.13 shows the simulation results of the NRSC using the PI-controller. These plots show also the loading setpoint, the ammonia loading and the corresponding feedratio.

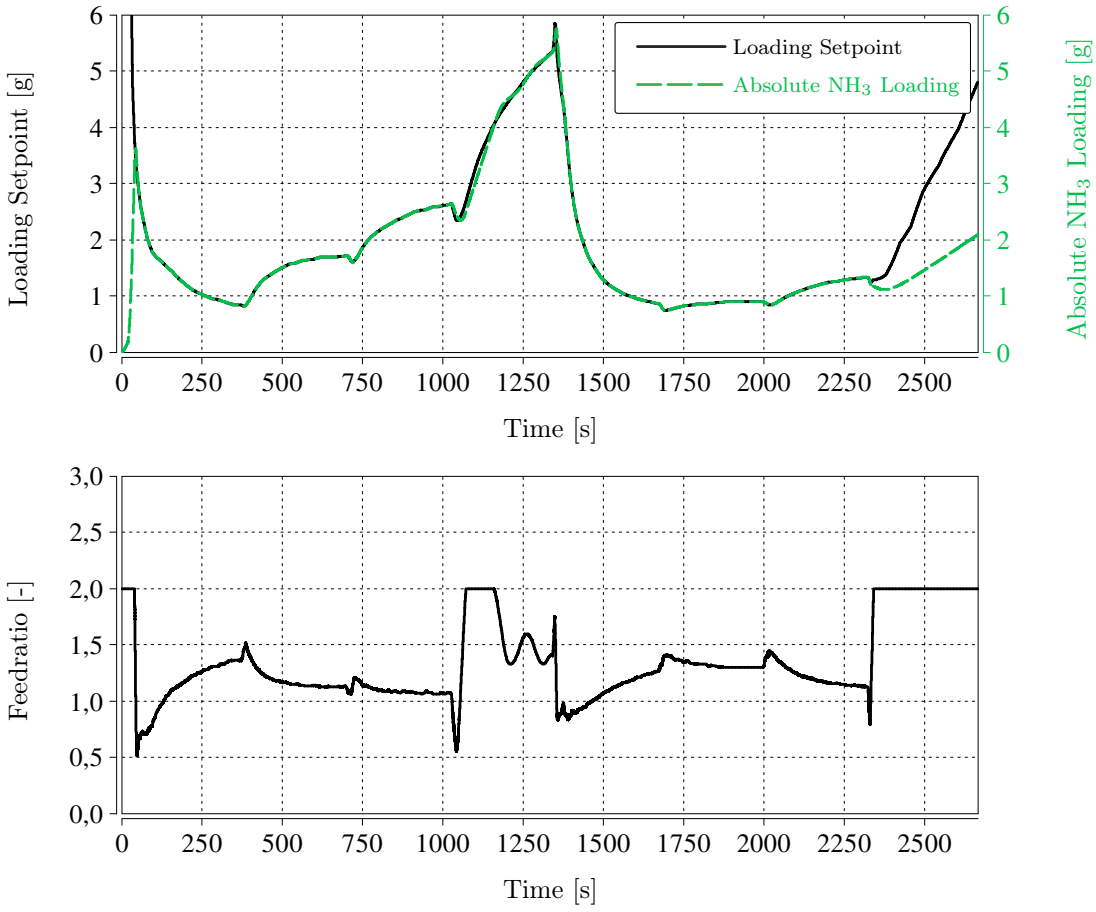

Figure 5.13: NRSC simulation results with PI-controller

It can be seen that the ammonia loading follows the setpoint with only small deviations. Some of these deviations lead from the feedratio limits which can be seen for example at the end of the simulation period.

NRTC simulation results

Figure 5.14 illustrates the NRTC simulation results. The top diagram also shows only small deviations between the ammonia loading and the loading setpoint. The reason for the ripple of the sepoint is mainly the fast change of the exhaust gas mass flow.

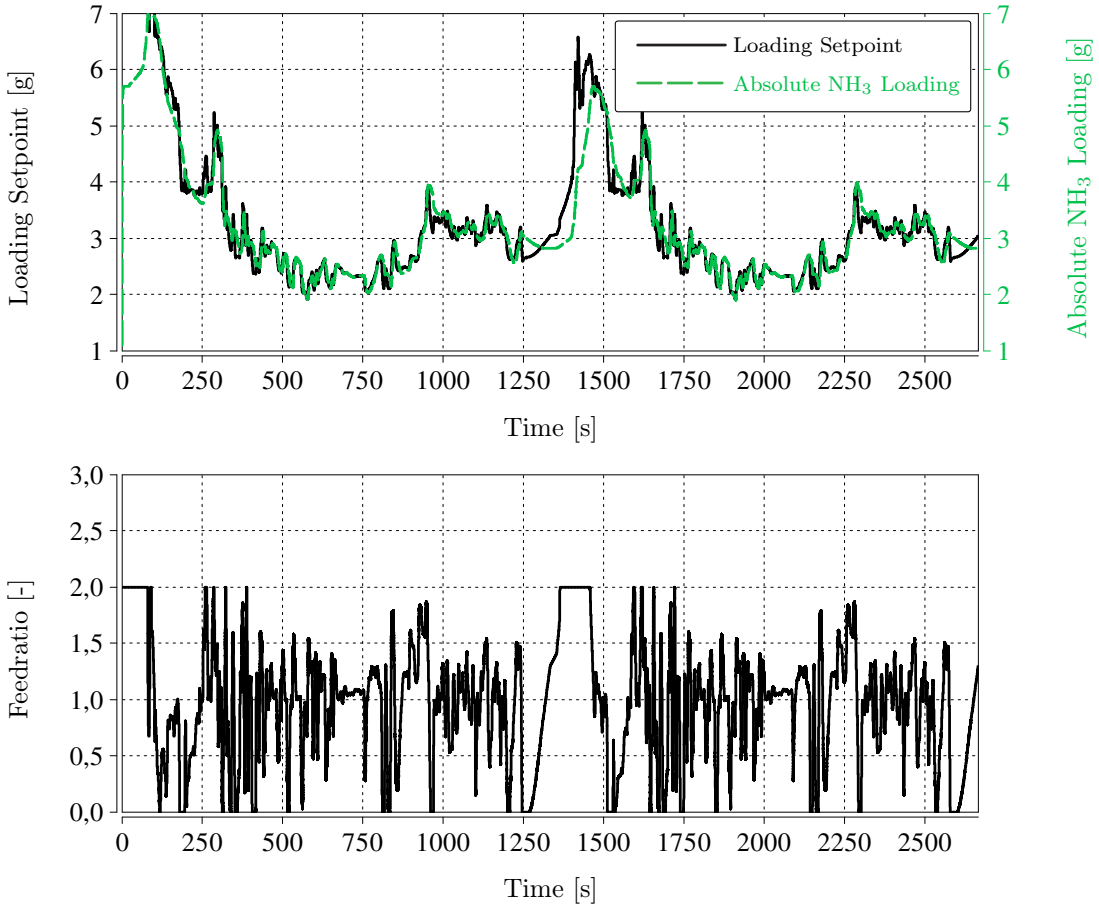

Figure 5.14: NRTC simulation results with PI-controller

5.4.2 Simulation results Level-controller

This section shows all relevant simulation results of concept A using the Level-controller.

Step test simulation results

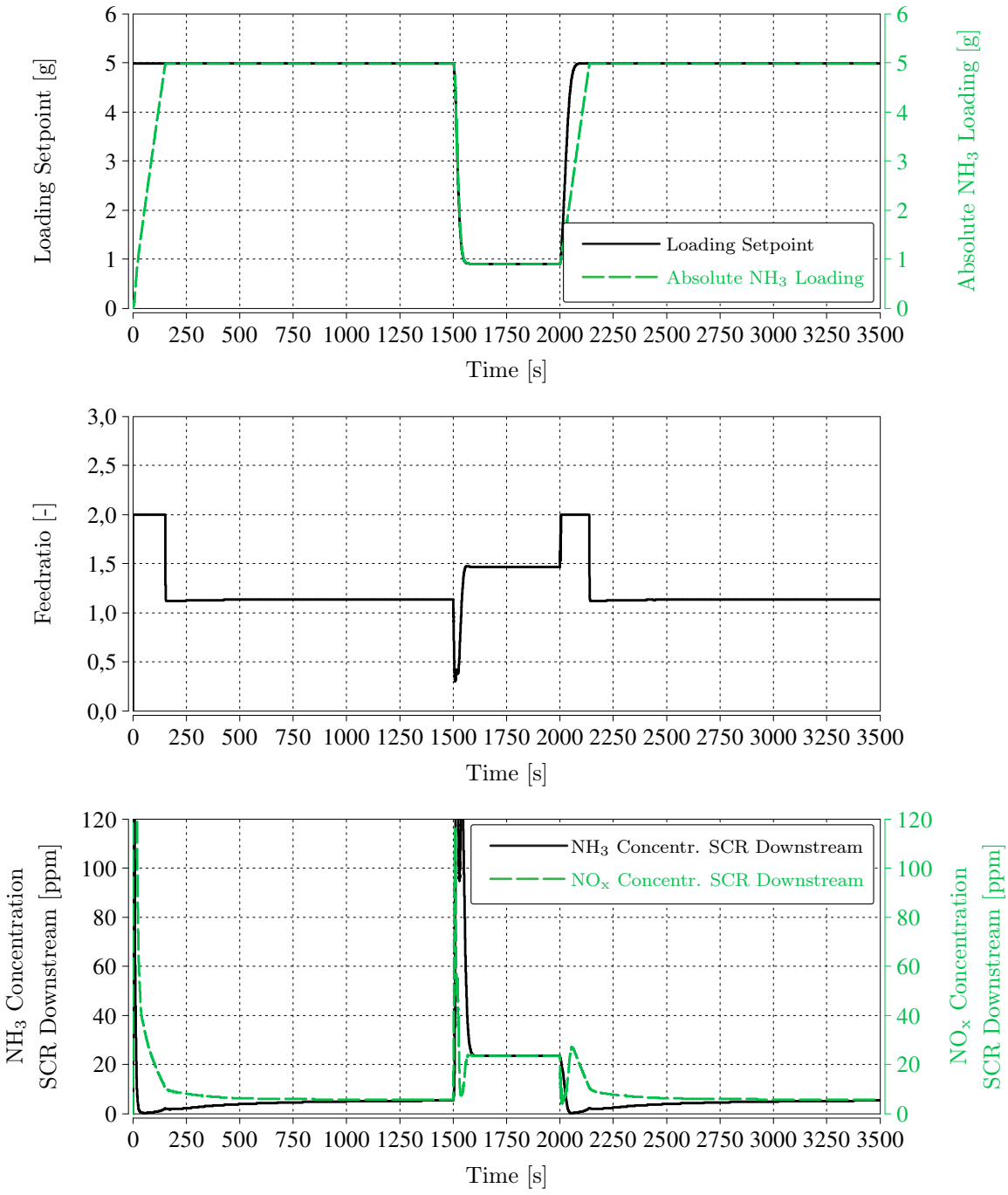

Figure 5.15: Step test simulation results with Level-controller

The simulation results for the step test show a very good control behaviour, which is illustrated in figure 5.15. It can be seen that the controller does not produce overshoots. The deviations between the shown ammonia loading and the loading setpoint come from the feedratio limitation. Apart from that, the loading follows almost exactly the setpoint.

NRSC simulation results

Figure 5.16 illustrates the results of the simulated NRSC. The top diagram also shows a nearly perfect match of the loading setpoint and the ammonia loading. The trend of the feedratio slightly differs from the corresponding test with the PI-controller.

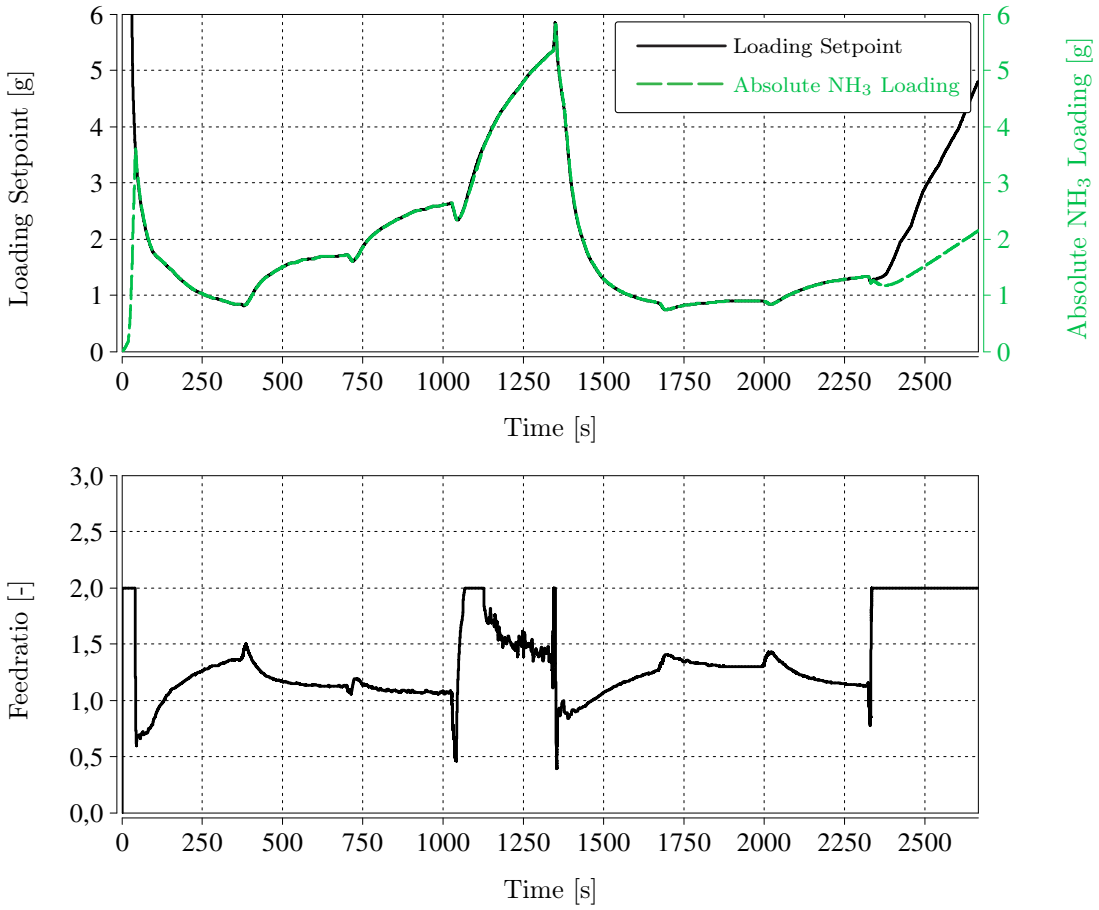

Figure 5.16: NRSC simulation results with Level-controller

NRTC simulation results

Figure 5.17 illustrates the simulation results of the NRTC. A comparison of the feedratio trend with the corresponding PI-controller test shows that the Level-controller reacts

faster and more strongly. As it can be seen, the Level-controller often operates in the limitation areas.

The top diagram of Figure 5.17 shows that the ammonia loading matches with the loading setpoint in most areas. Since the NRTC is a transient and fast changing test cycle, the control behaviour of the Level-controller seems very good.

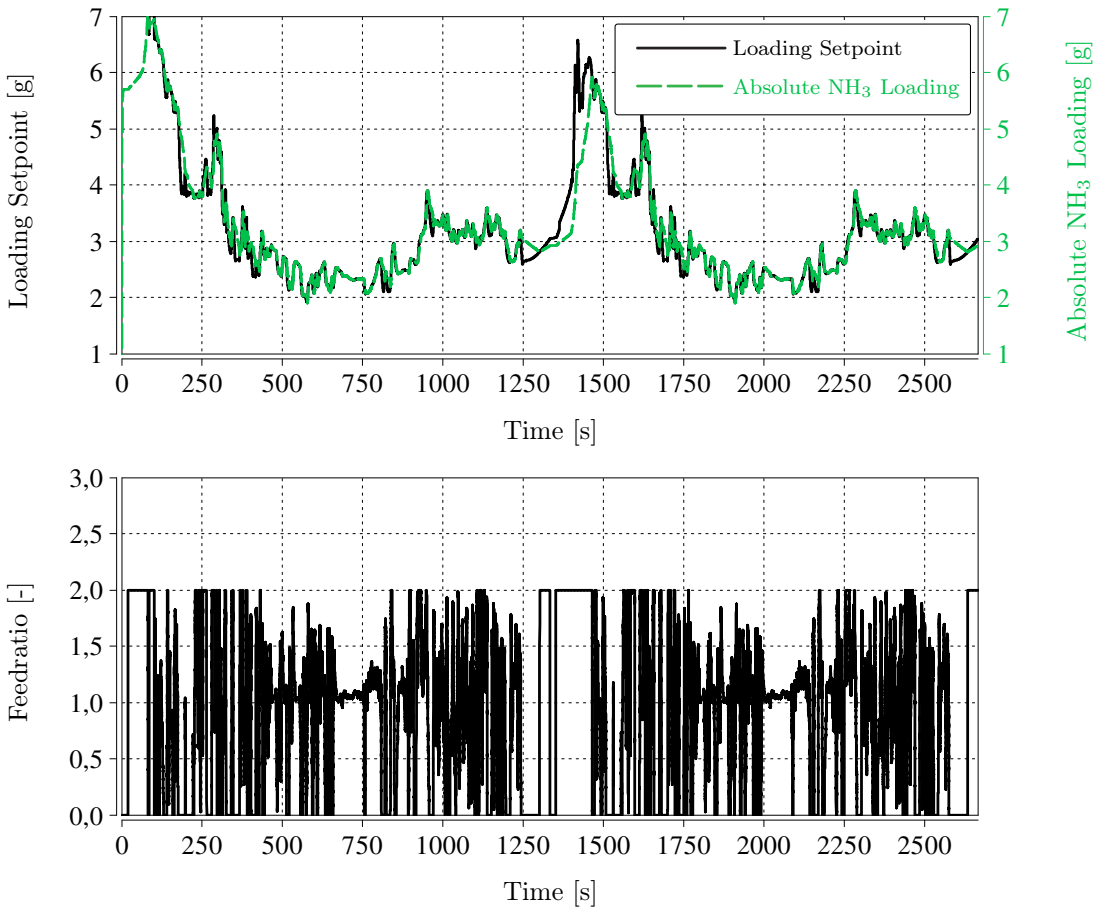

Figure 5.17: NRTC simulation results with Level-controller

5.4.3 Simulation results open-loop control

For completeness, the simulation results for the step test of the so called open-loop control are also presented here. For this control strategy, only the precontrol map is active and no controller is involved. Therefore, only the feedratio corresponding to the specific OP is used to control the ammonia loading.

Step test simulation results

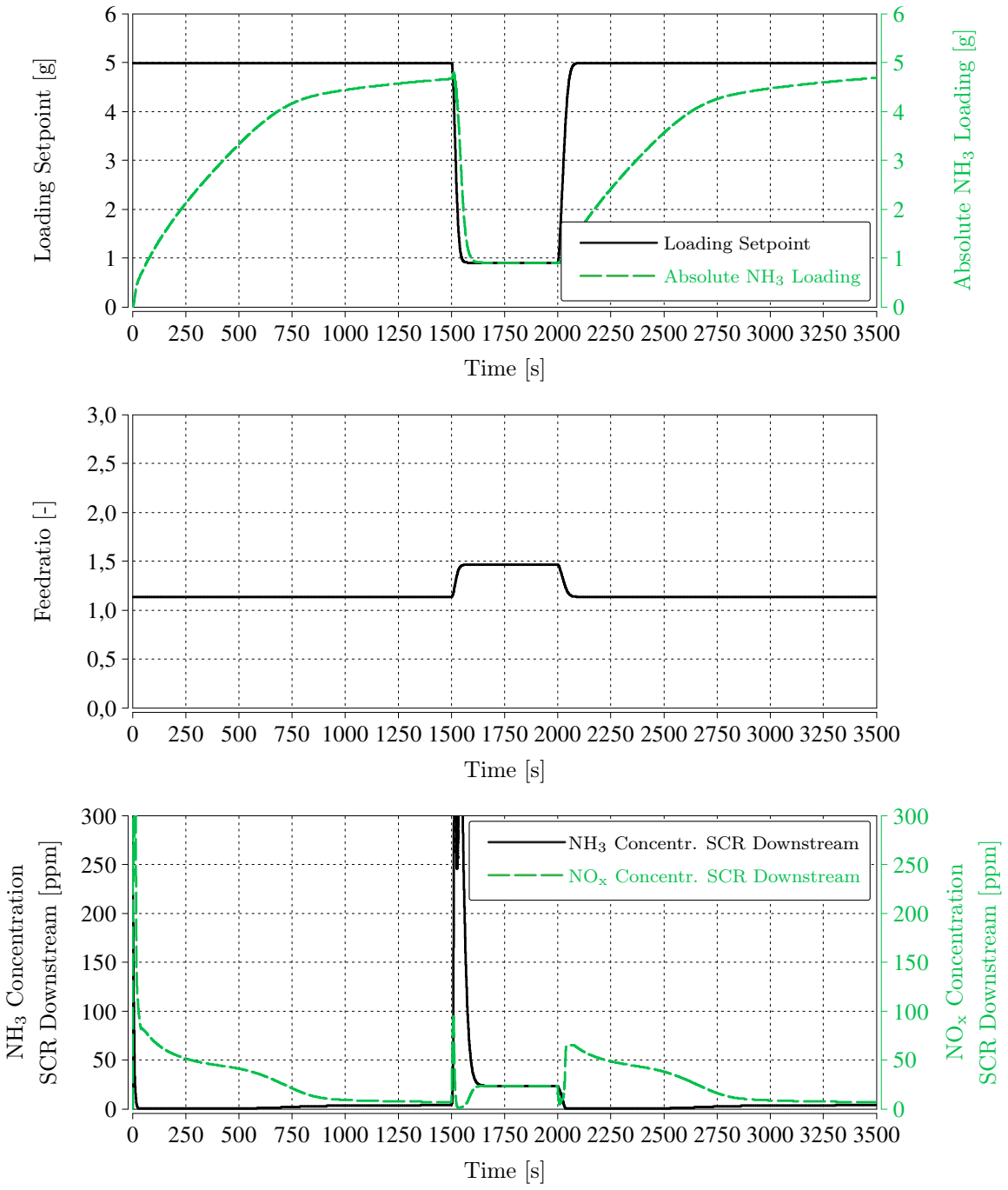

Figure 5.18: Step test simulation results with open-loop control

Figure 5.18 illustrates the simulation results for the step test with Open-Loop-Control. The top diagram shows the ammonia loading and the loading setpoint. It can be seen that without a controller the setpoint is not even reached during the first OP.

The bottom diagram shows the NH_3 slip and the NO_x concentration downstream the SCR catalyst. After about 500 seconds, the NO_x trend shows special behaviour. This is the point where NH_3 first breaks through the SDPF which leads to an ammonia loading of the SCR. Once the SCR is loaded with ammonia, the NO_x concentration downstream the SCR decreases.

Another interesting period is after about 1500 seconds, where downstream the catalysts a huge NH_3 concentration peak appears. This is because at rising catalyst temperatures, the loaded NH_3 desorbs and with this control strategy, there is no controller decrease the feedratio during this OP change. At this point it is important to mention that the range of the concentrations in this plot is more than twice as wide as in the figures before.

5.5 Discussion

In Section 5.4 it can be seen that concept A shows a very good control behaviour with few and small deviations between setpoint and ammonia loading. The differences between the results of the PI-controller and the Level-controller are marginal. Only the feedratio trends differ, however this has hardly an impact on the control quality.

The comparison of the accumulated mass of the different gas species upstream and downstream the catalysts shows that the Level-controller has a higher ammonia consumption with also higher ammonia slip but achieves a higher NO_x conversion. However, the differences are minimal. Another interesting insight is that the Level-controller shows no overshoots contrary to the PI-controller, which can be interpreted as an advantage.

It can be further noticed that a controller is needed to achieve satisfying results because using only the Open-Loop-Control strategy leads to very high ammonia slip and big deviations between setpoint and ammonia loading in wide areas.

6 Concept B

The second investigated control concept is described in the following section. Also here, two different controllers are used to control the ammonia loading. These two controllers and the parametrisation of the PI-controller are described in the previous chapter. Finally, the test simulation results are illustrated and discussed.

6.1 Concept description

Figure 6.1 shows the block diagram of concept B. It can be seen that the relative ammonia loading of the SCR catalyst θ_{NH_3} is controlled. The idea of this concept is that the loading of the SDPF catalyst follows the controlled SCR loading. The feedratio is used as the control parameter. The used PI-controller is a gain-scheduled controller as it is in concept A.

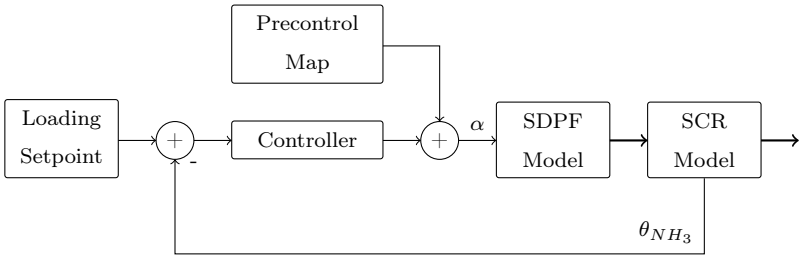

Figure 6.1: Block diagram of concept B

The precontrol map and the loading setpoint map are determined in the same way as described in section 5.2.1, with the difference that the mean catalyst temperature and the space velocity of the SCR catalyst are used as input parameters for all the maps. An estimated transfer function is used for the parametrisation of the K_p and K_i map. For each OP the system is approximated by the $\mathrm{PT1T_t}$ transfer function

$$G(s) = \frac{k_\alpha}{1 + \tau \cdot s} \cdot e^{-s \cdot T_t}$$

using an optimisation method. With the estimated system parameters τ and T_t the controller parameters K_p and K_i are determined by the so called *Chien, Hrones and Reswick tuning method*. The maps are formed by interpolation and extrapolation.

6.2 Simulation results

This section shows the simulation results of the step test, the NRSC and the NRTC for concept B. It includes the results for the PI-controller, the results for the level controller and a short discussion at the end.

6.2.1 Simulation results PI-controller

For each test simulation the ammonia loading, the setpoint and the corresponding feedratio are illustrated and shortly described.

Step test simulation results

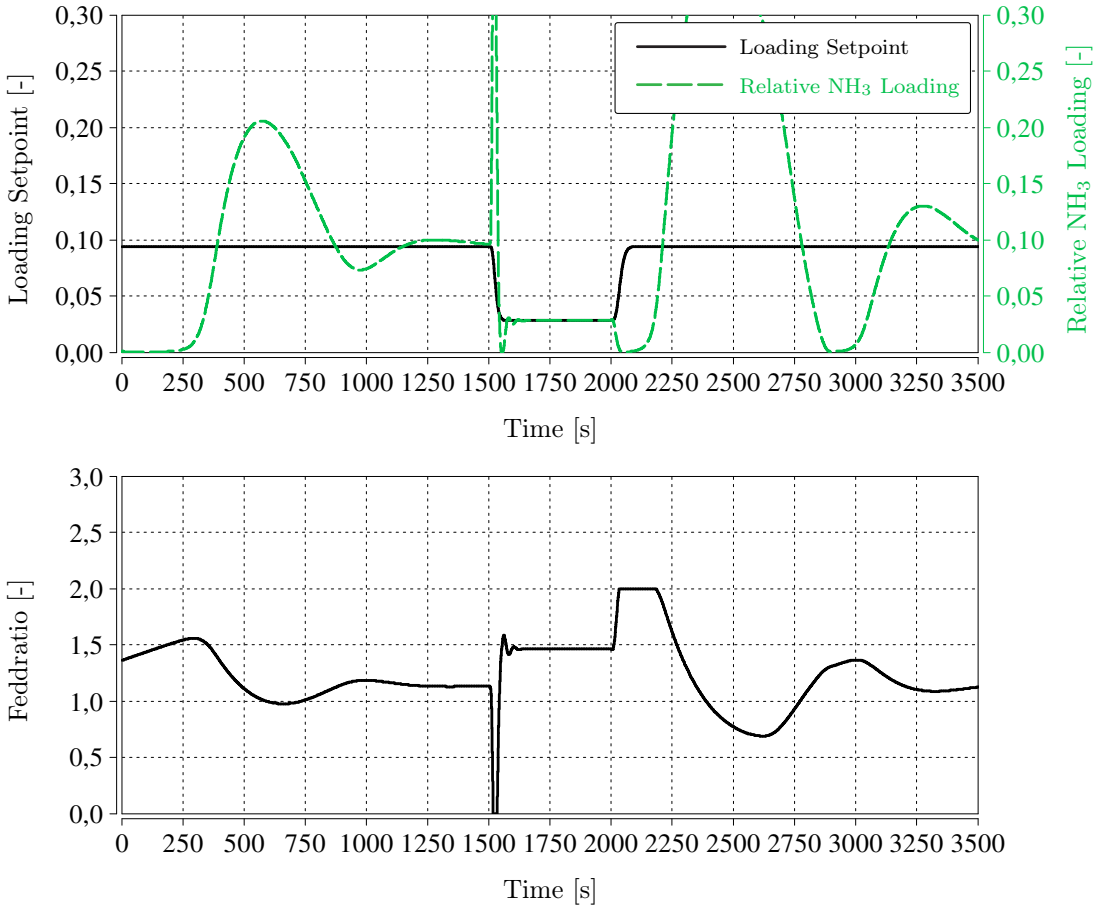

Figure 6.2: Step test simulation results with PI-controller

Figure 6.2 shows the simulation result of the step test. Compared to concept A, the relative ammonia loading of the SCR is controlled. Due to the SDPF in front of the

SCR, a time delay occurs from the beginning of the ammonia injection to the rise of the ammonia loading. This time delay limits the possible speed of the controller. In the top diagram, a huge overshoot of the ammonia loading can be seen, although the feedratio range is not exploited. The reason for this overshoot is the time delay. For the OP with higher catalyst temperatures this effect is rather rare, due to the smaller time delay.

NRSC simulation results

Figure 6.3 illustrates the simulation results of the NRSC. It can be seen that the controlled system is unstable in some areas of the NRSC. The reason for that is the already mentioned time delay and the small setpoint value.

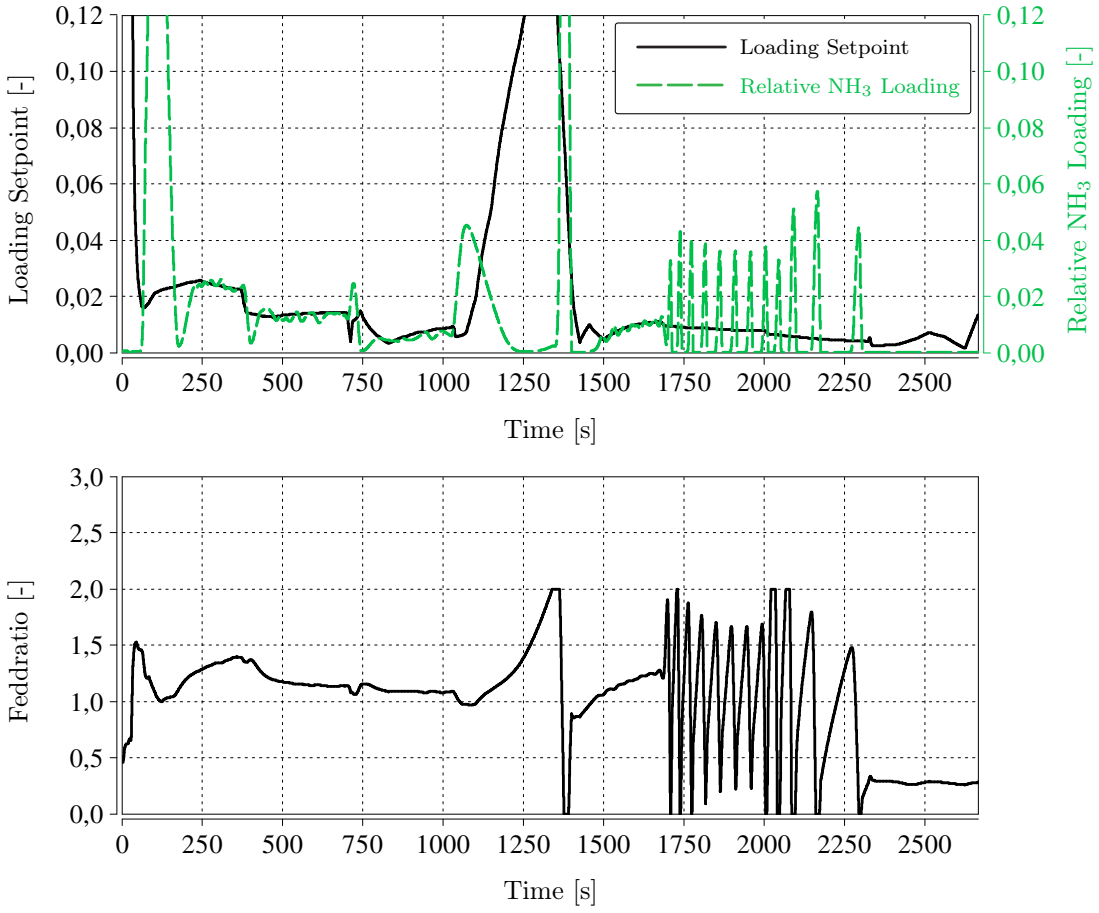

Figure 6.3: NRSC simulation results with PI-controller

NRTC simulation results

Figure 6.4 illustrates the NRTC simulation results. The top diagram contains the setpoint and the relative ammonia loading of the SCR catalyst, while the bottom diagram shows the feedratio trend. As it can be seen during this test cycle, the controller is not able to control the ammonia loading most of the time.

A comparison of the feedratio trend and the ammonia loading trend shows the mentioned time delay.

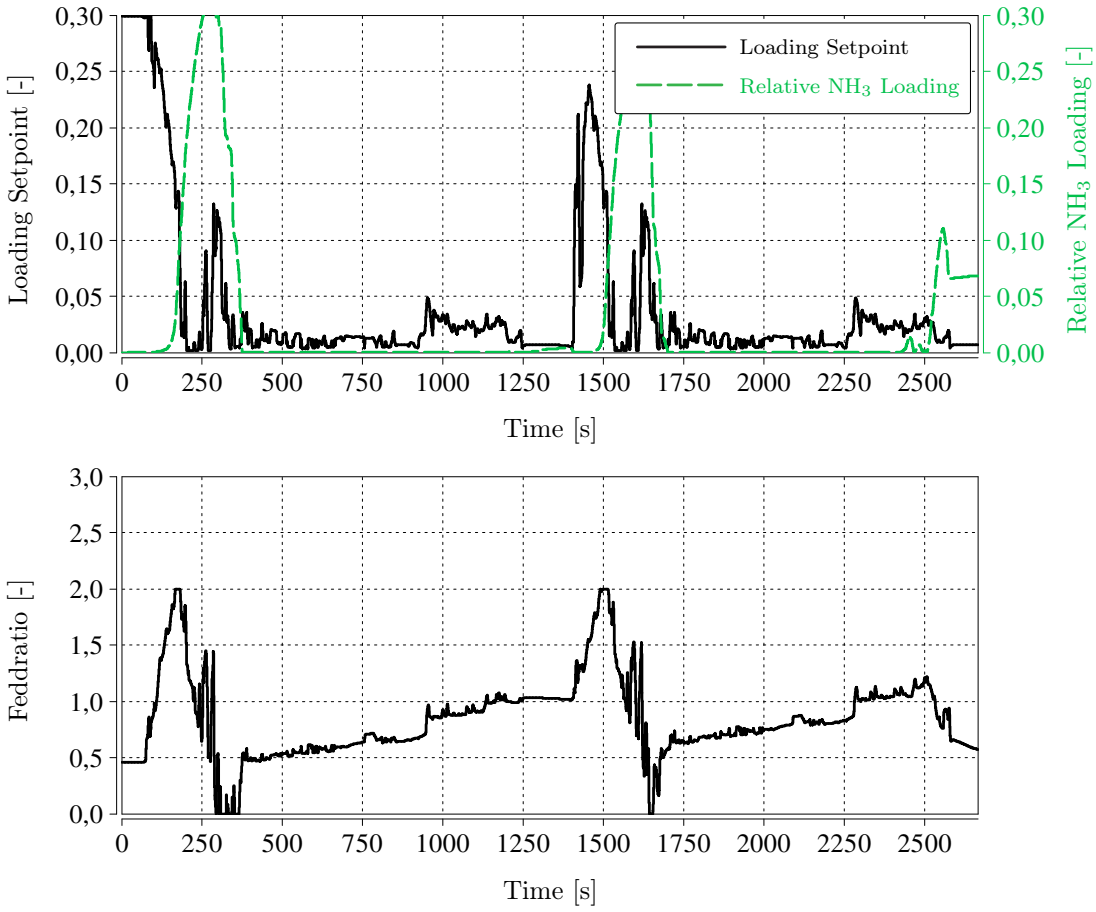

Figure 6.4: NRTC simulation results with PI-controller

6.2.2 Simulation results Level-controller

For the use of the Level-controller, only the results for the NRSC are illustrated because this test already shows that the controller is unstable.

NRSC simulation results

Figure 6.5 illustrates the simulation results for the NRSC. The trend of the ammonia loading shows that the Level-controller is not suitable for this concept, because it is oscillating and obviously unstable.

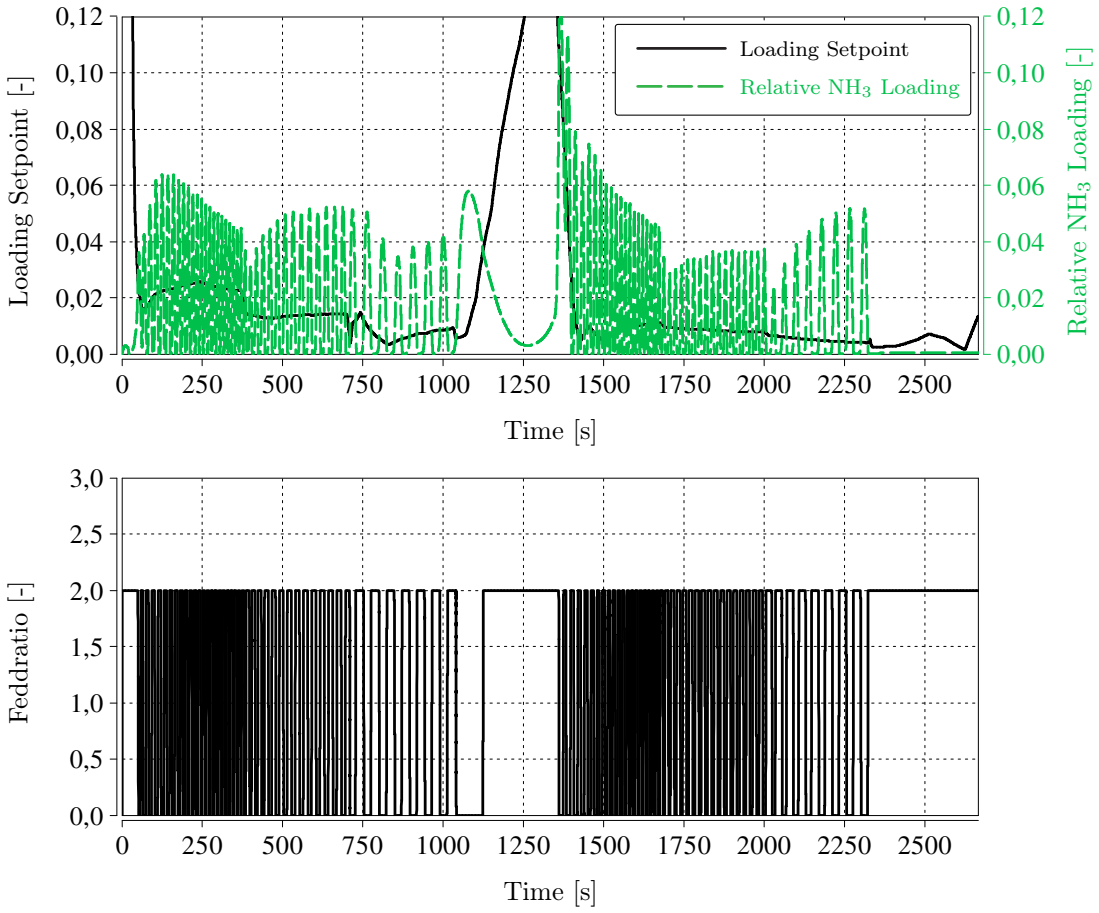

Figure 6.5: NRSC simulation results with Level-controller

6.3 Discussion

The results for this concept show that the Level-controller is not applicable. Because of the occurring time delay between the ammonia injection and the increase of the relative ammonia loading, the controller is oscillating. The time delay is also the reason for the bad control performance of the PI-controller, limiting the speed of the controller.

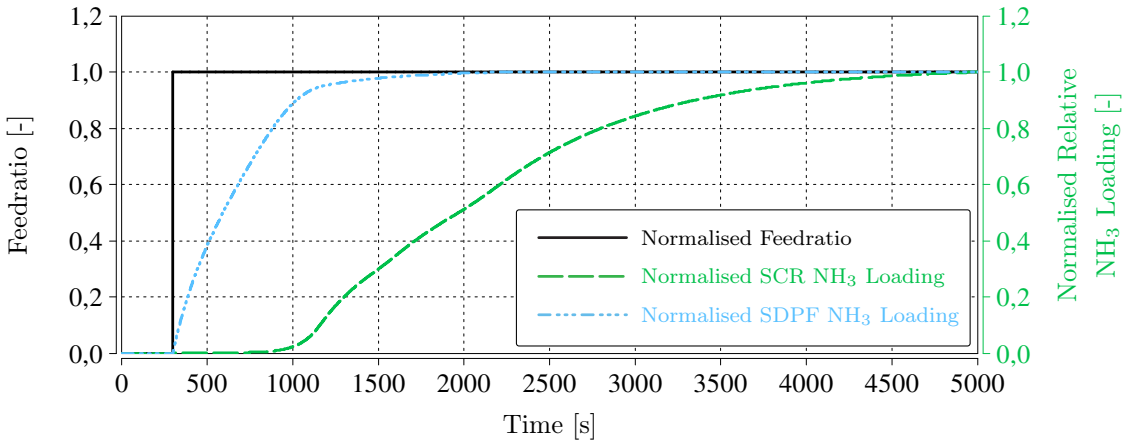

Figure 6.6: Time delay of SCR ammonia loading

Figure 6.6 shows a feedratio step and the corresponding relative ammonia loading trends of the SCR and the SDPF. All signal tends are normalised to one for a better understanding. This plot shows exactly what was mentioned before. Once the SDPF is loaded, the SCR loading increases, causing a time delay of about 800 seconds for this specific OP and feedratio step.

7 Concept C

The last investigated concept will now be described in detail, focusing on the cascaded PI-controller. Also the simulation results will be illustrated and discussed. Since this concept can be seen as a further development of concept B, a comparison between these two will be also included in the discussion.

7.1 Concept description

Figure 7.1 illustrates the block diagram of concept C. It shows the cascaded control structure with an inner and an outer control loop. The inner loop controls the NH_3 slip of the SDPF catalyst and the outer loop the relative ammonia loading of the SCR. Each loop has its own precontrol map. The output variable of the SCR controller is the desired demand of NH_3 slip downstream the SDPF. Both controllers are gain-scheduled PI-controllers just as in the previous concepts.

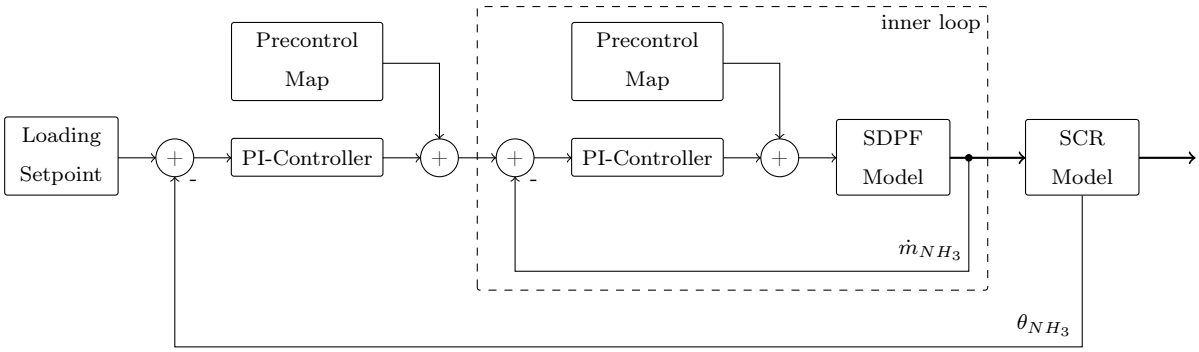

Figure 7.1: Block diagram of concept C

The loading setpoint map and the precontrol maps are determined as described in section 5.2.1. The input parameters of all maps are the corresponding mean catalyst temperatures and space velocities. Similar to concept B the parametrisation of the K_p and the K_i maps of the SDPF controller is done by the approximation of the transfer function and subsequently performing the *Chien, Hornes and Reswick tuning method*. For the parameter maps of the SCR controller, the desired overall transfer function is defined. An optimisation method determines the control parameters K_p and K_i. The maps are then formed by interpolation and extrapolation.

7.2 Simulation results

This section illustrates the results for the step test, the NRSC and the NRTC for concept C. Firstly, the results of the simulations will be shown and described. Since this is a cascaded controller, the actual value and the setpoint as well as the control variable trend of each of the two controllers is depicted. Finally, the results are discussed and compared with the results of concept B.

Step test simulation results

Figure 7.2 illustrates the simulation results for the outer control loop. The top diagram shows the loading setpoint and the relative ammonia loading of the SCR. The bottom diagram shows the demanded ammonia slip of the SDPF which is also the setpoint of the inner control loop. The ammonia loading shows just a small overshoot compared to concept B.

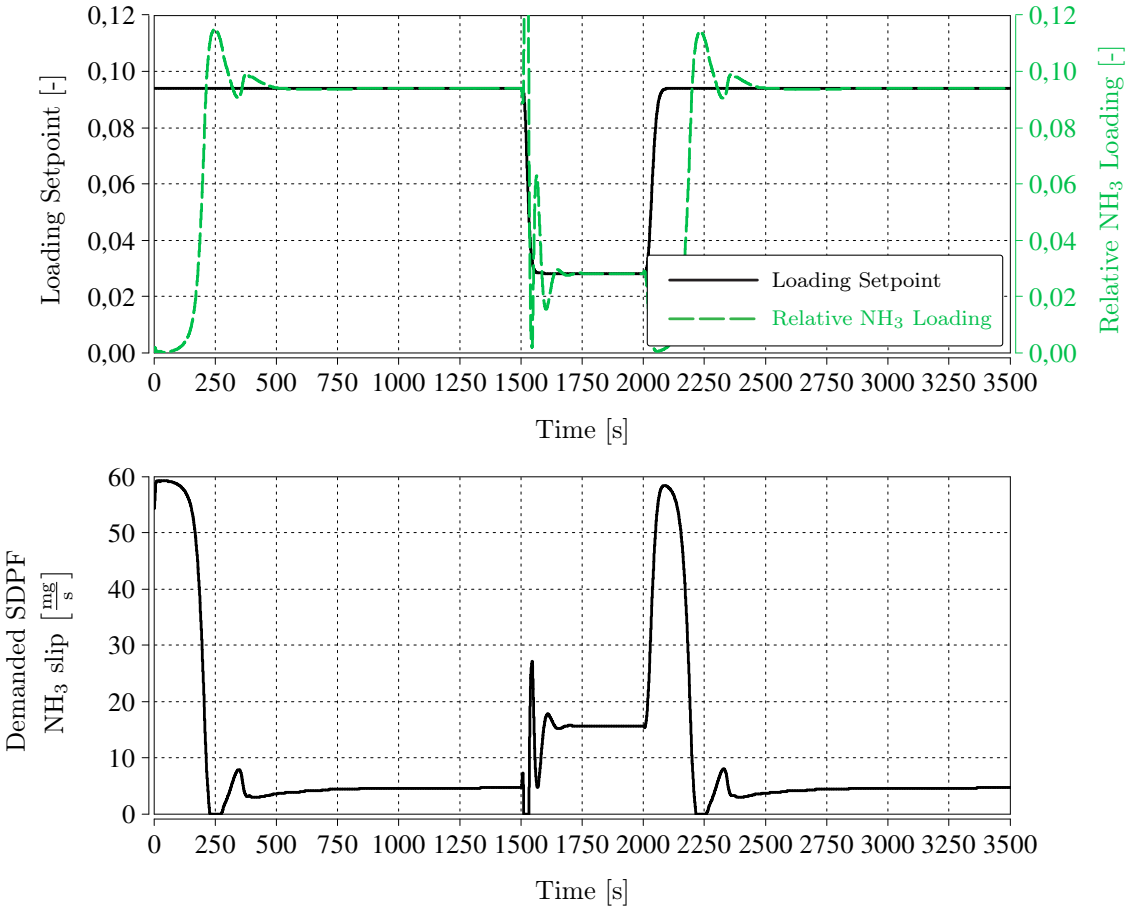

Figure 7.2: Step test simulation results of the outer loop

Figure 7.3 illustrates the results of the inner loop. The control variable signal of the outer loop is used as setpoint here. The top diagram shows that the controller works very well with just small deviations between demanded and actual ammonia slip.

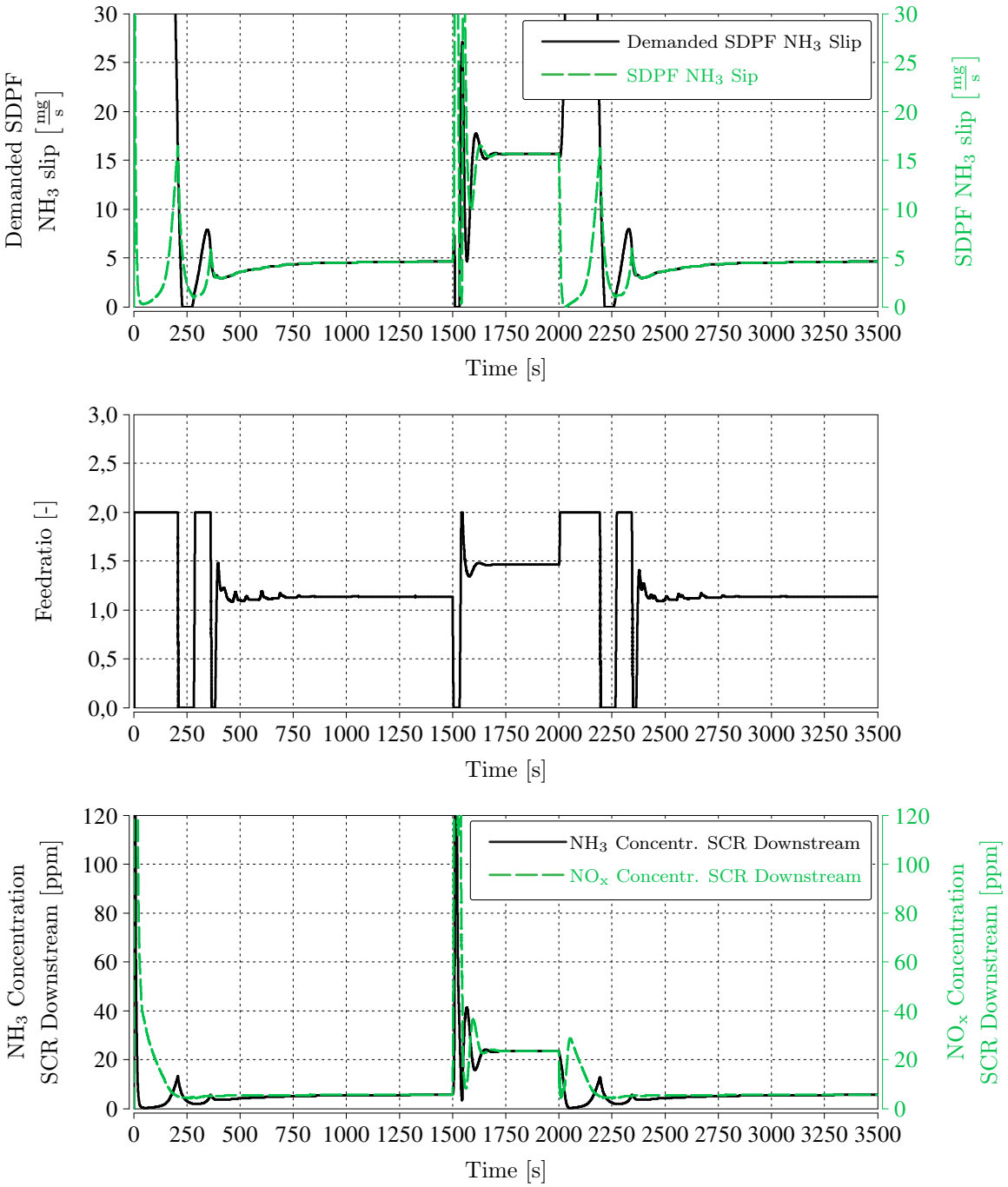

Figure 7.3: Step test simulation results of the inner loop

As it can be seen in the bottom diagram, the NO_x and NH_3 concentration downstream the SCR catalyst just slightly differs from those of concept A for the step test.

NRSC simulation results

Figure 7.4 shows the simulation results for the NRSC. It can be seen that the ammonia loading shows a ripple although the feedratio seems to remain relatively smooth. The reasons for that are the small loading setpoint values and the fact that even small changes of the feedratio have a serious impact on the relative ammonia loading of the SCR if the SDPF is fairly loaded.

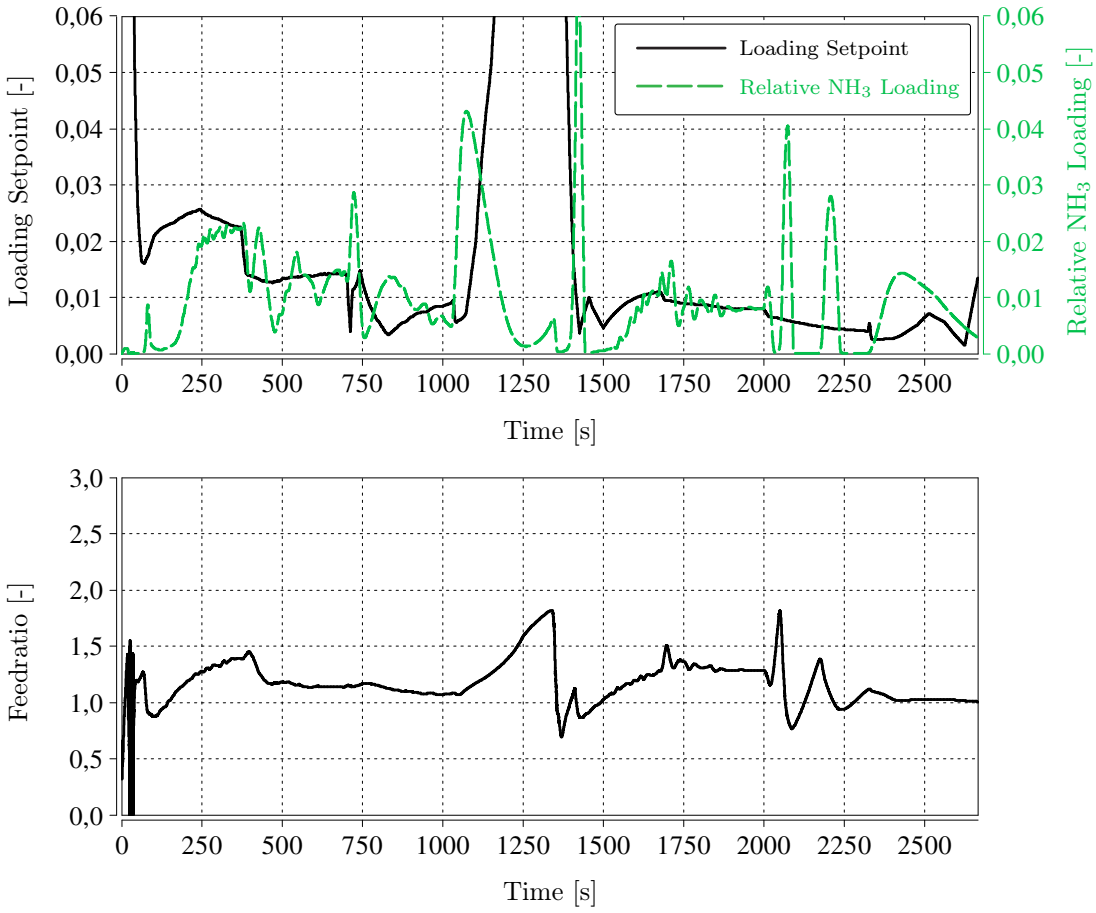

Figure 7.4: NRSC simulation results

NRTC simulation results

Figure 7.5 illustrates the simulation results of the NRTC. These plots shows that the relative ammonia loading of the SCR deviates massively from the setpoint. The reason

for that is that with this concept, there is still a time delay between the injection and the reaction of the loading. Another important influence on the control behaviour is NH_3 which desorbs from the catalyst surface of the SDPF. This process strongly depends on the catalyst temperature. Due to the low SCR loading setpoint, even a relatively small ammonia slip of the SDPF has a serious impact on the SCR ammonia loading.

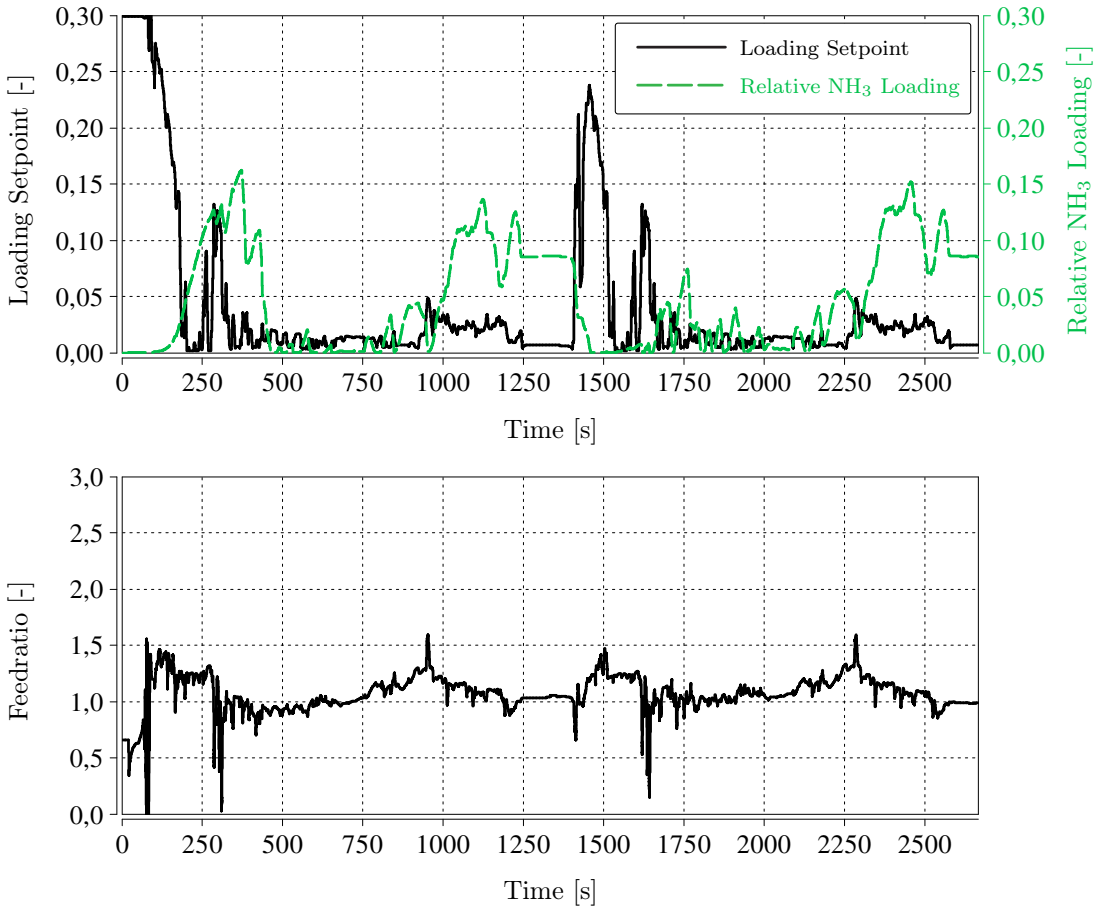

Figure 7.5: NRTC simulation results

7.3 Discussion

As already mentioned, this concept can be seen as a further development of concept B. Therefore a comparison of the simulation results for the step test is made and illustrated in figure 7.6. It can be seen that the cascaded strategy shows a strong improvement. Due to this control structure, the allowed feedratio range can be used better; the ammonia loading reaches the setpoint much earlier and also the overshoot

is minimized.

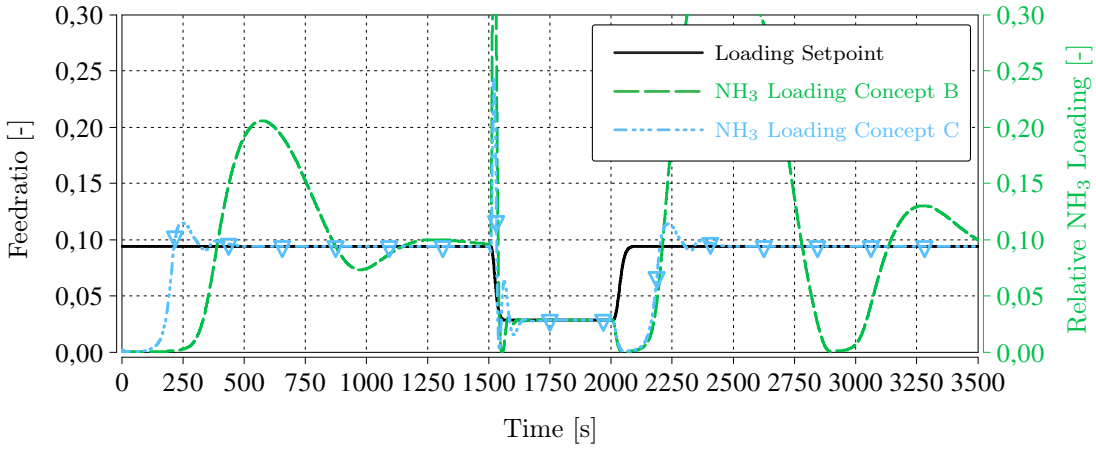

Figure 7.6: Step test comparison of concepts B and C

The simulation results in this section show that although the control concept achieved good results for the step test, the control performance during NRSC and the NRTC is not satisfying.

8 Comparison and conclusion

In this section, the control performances of the different control concepts are compared first. Beside the simulation trends, the relevant NO_x and the NH_3 accumulated mass upstream and downstream the catalysts is also compared. This shows how much ammonia is used, how much NO_x and how much NH_3 leaves the SCR, parameters which are commonly used to characterise the performance of the used control concepts.

The conclusion of this thesis will then finally make the end of this chapter.

8.1 Comparison simulation results

Figure 8.1 shows the normalised results of the step test for the different control concepts. It can be seen that concept A shows the fastest behaviour. The reason for that is that the absolute ammonia loading of the SDPF and the SCR is controlled. With the other two concepts, the relative ammonia loading of the SCR is controlled where a time delay occurs. Due to this fact, it is not possible to reach such fast step responses.

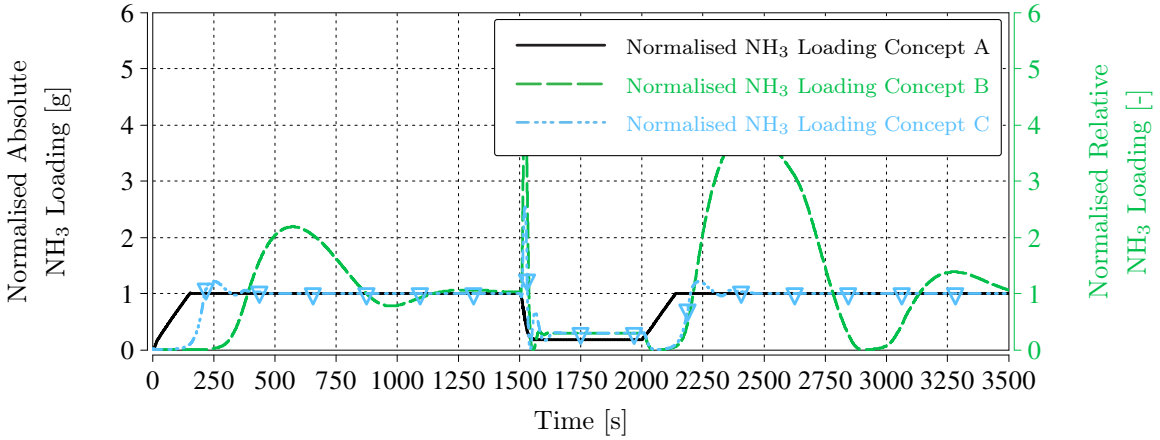

Figure 8.1: Comparison of the step test of all concepts

The relative ammonia loadings of the SDPF and the SCR are illustrated in figure 8.2. These plots show the loading distribution during the step test with concept A. As it can be seen, the SDPF gets loaded first. Once it is fairly loaded, the ammonia reaches the SCR. The loading distribution during the phase where the overall ammonia loading matches with the setpoint is also very interesting. In this phase, a redistribution takes

place; some of the ammonia leaves the SDPF and adsorbs on the surface of the SCR. Since in concepts B and C the loading of the SCR is controlled, this redistribution process does not occur.

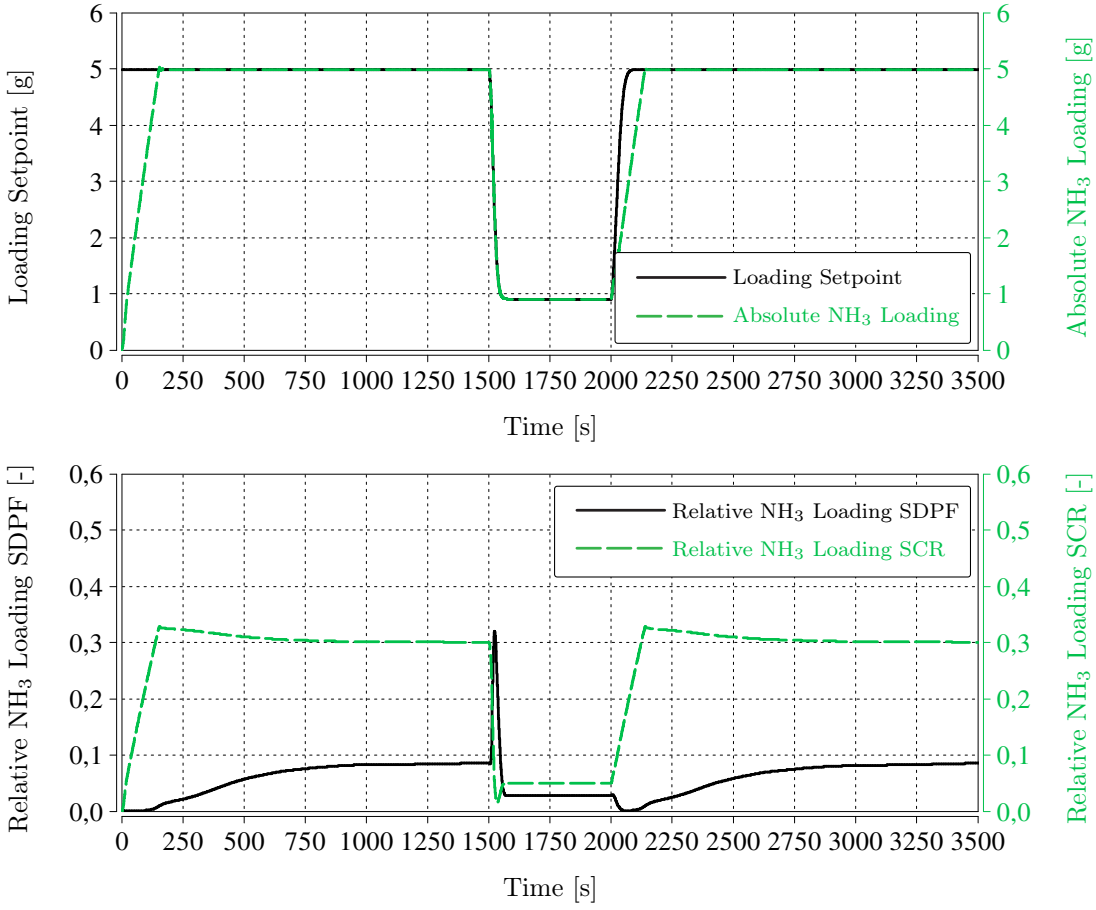

Figure 8.2: Loading distribution during the step test with concept A

Another interesting outcome of the comparison is the improvement of the control behaviour using a cascaded controller compared to concept B. This is already discussed in section 7.3 and illustrated in figure 7.6.

The following two tables contain the accumulated mass of the injected NH_3 $m_{NH_3,us}$, the ammonia slip $m_{NH_3,ds}$ and the NO_x downstream the SCR $m_{NO_x,ds}$ for the different control concepts with their different controllers. For the sake of completeness the values for the Open-Loop-Control are also given. Table 8.1 comprises the values for the step test and table 8.2 the values for the NRSC and the NRTC.

		Step Test		
		$m_{NH_3,us}$	$m_{NH_3,ds}$	$m_{NO_x,ds}$
		g	g	g
Concept A	PI	237.9	4.356	9.315
	Level	237.8	4.432	9.265
Concept B	PI	236.3	4.557	11.60
	Level	231.2	3.666	13.53
Concept C	PI	237.0	3.978	10.15
Open-Loop Control		234.7	5.508	21.76

Table 8.1: Accumulated mass for the step test

		NRSC			NRTC		
		$m_{NH_3,us}$	$m_{NH_3,ds}$	$m_{NO_x,ds}$	$m_{NH_3,us}$	$m_{NH_3,ds}$	$m_{NO_x,ds}$
		g	g	g	g	g	g
Concept A	PI	442.1	4.900	41.52	203.5	2.234	16.40
	Level	442.1	4.899	41.40	204.1	2.226	15.48
Concept B	PI	423.2	6.940	63.72	149.2	0.772	122.7
	Level	418.1	6.225	64.05	198.8	2.935	23.68
Concept C	PI	435.9	4.729	47.89	201.8	2.610	12.98
Open-Loop Control		473.1	14.92	24.32	208.1	4.101	21.75

Table 8.2: Accumulated mass for the NRSC and the NRTC

The comparison of all these values shows that concept A and concept C achieve the best results. Between these two concepts only small deviations occur related to the accumulated mass of the gas species.

8.2 Conclusion

For the control of an SCR-based EAS, a gain-scheduled PI-controller is used which is an established control concept of AVL List. The increasingly stringent regulations for pollutions caused by exhaust gas from all types of engines require new EAS concepts and arrangements of the catalysts. One possible EAS includes an SCR as well as an SDPF (refer to 1.5). Within this thesis, three different control concepts for this specific EAS have been investigated and evaluated.

The comparison of the test simulation results shows, that concept A has the best control performance. For all test cases, both deployed controllers show very little deviations between actual value and setpoint. Comparing the results of the different controllers indicates that the Level-controller has a slightly better performance; for example with no overshoots in the step test compared to the PI-controller. The accumulated mass of the different gas species only differ marginally.

Concept B shows the desirable control behaviour, essentially because of the occurring time delay. In the step test, the time delay causes immense overshoots of the actual value with regard to the setpoint, although the allowed control variable range is not

exploited. Also the results of the NRSC and NRTC indicate a not satisfactory control performance. Since the Level-controller shows an unstable control behaviour, it is not applicable in combination with this concept.

The cascaded control structure of concept C can be interpreted as a further development of concept B, since the same system parameter is controlled. This special structure definitely improves the control behaviour during step test. Although the results of the NRSC and the NRTC do not indicate such an improvement, the comparison of the accumulated mass values with concept A shows only small deviations. Anyway, the parametrisation and calibration effort of the cascaded PI-controller in this concept is rather large compared to concept A.

In summary, the Level-controller in combination with concept A delivers the best results and has the additional benefit of a very low calibration effort.

9 Outlook

In this thesis, all simulations were carried out without considering the DPF functionality of the SDPF, which means that the SDPF was never loaded with soot and ash. For further investigation, one could consider the influences of the DPF process. Since passive regeneration effects change the NO_2 to NO ratio, the influences on the optimal loading setpoint with regard to the tradeoff between NO_x conversion and NH_3 slip can be investigated. Also an analysis of the robustness of the control concept using the Level-controller is of great interest.

Another possible area of investigation is the consideration of the loading distribution of the two catalysts. With concept A only the overall ammonia loading is controlled. Since the distribution has influences on the conversion efficiency, maybe this effect can be considered in the Level-controller.

For the existing SCR-control concept, an adaptation function using real sensor signals is availably. This function would also make sense for controlling an SDPF-SCR based EAS in the form of a further development.

Bibliography

[1] Reif, K.: *„Dieselmotor-Management“*, Springer Vieweg Wiesbaden, 5. Auflage, 2012, ISBN 978-3-8348-2179-9

[2] Mollenhauer, K., Tschöke, H.: *„Handbuch Dieselmotoren“*, Springer-Verlag Berlin Heidelberg New York, 3. Auflage, 2007, ISBN 978-3-540-72164-2

[3] auto-presse.de: *„Weltweiter Kraftfahrzeugbestand: Milliardengrenze“*, http://auto-presse.de/autonews.php?newsid=22756, January 2008

[4] oica.net: *„The world's vehicles production in 2014“*, http://www.oica.net/wp-content/uploads//OICA-press-release-2015-03-04.pdf, March 2015

[5] ecomento.tv: *„Weltweit mehr als 740.000 Elektroautos, Markt-Wachstum ungebrochen“*, http://ecomento.tv/2015/03/24/mehr-als-740000-elektrofahrzeuge-weltweit/, March 2015

[6] Reif, K.: *„Abgastechnik für Verbrennungsmotoren“*, Springer Vieweg Wiesbaden, 1. Auflage, 2015, ISBN 978-3-658-09521-5

[7] Schwarz, C., Merker, G. P.: *„Grundlagen Verbrennungsmotoren“*, Vieweg + Teubner Wiesbaden, 4. Auflage, 2009, ISBN 978-3-8348-0740-3

[8] Basshuysen, R. v., Schäfer, F.: *„Handbuch Verbrennungsmotor“*, Springer Vieweg Wiesbaden, 7. Auflage, 2015, ISBN 978-3-8348-0740-3

[9] Eichlseder, H., Klüting, M., Piock, W.: *„Grundlagen und Technologien des Ottomotors“*, Springer-Verlag Wien New York, 2008, ISBN 978-3-211-25774-6

[10] Council Directive 88/77/EEC: *„Council Directive 88/77/EEC of 3 December 1987 on the approximation of the laws of the Member States relating to the measures to be taken against the emission of gaseous pollutants from diesel engines for use in vehicles“*

[11] Council Directive 91/542/EEC: *„Council Directive of 1 October 1991 amending Directive 88 / 77 / EEC on the approximation of the laws of the Member States relating to the measures to be taken against the emission of gaseous pollutants from diesel engines for use in vehicles“*

[12] Directive 1999/96/EC: *„Directive 1999/96/EC of the European Parliament and of the Council of 13 December 1999 on the approximation of the laws of the Member States relating to measures to be taken against the emission of gaseous and particulate pollutants from compression ignition engines for use in vehicles, and the emission of gaseous pollutants from positive ignition engines fuelled with natural gas or liquefied petroleum gas for use in vehicles and amending Council Directive 88/77/EEC“*

[13] Commission Regulation (EU) No 582/2011: *„Commission Regulation (EU) No 582/2011 of 25 May 2011 implementing and amending Regulation (EC) No 595/2009 of the European Parliament and of the Council with respect to emissions from heavy duty vehicles (Euro VI) and amending Annexes I and III to Directive 2007/46/EC of the European Parliament and of the Council“*

[14] Anderl, M. et al.: *„Emissionstrends 1990–2013“*, Umweltbundesamt GmbH Wien, 2015, ISBN 978-3-99004-354-7

[15] Queck, D., Hermann, O. E., Uchiyama, K.: *„Neue Technologien für Abgasnachbehandlung“*, Springer Fachmedien Wiesbaden, 1. Auflage, 2015, ISBN 978-3-658-08860-6

[16] Hollauf, B.: *„Model-Based Closed-Loop Control of SCR Based DeNOx Systems“*, Master's Thesis, FH Kärnten, 2009

[17] Calvo Zueco, S. et al.: *„Harnstoff-SCR-Systeme im Fokus: Neue Herausforderungen bei der Entwicklung von Abgasanlagen“*, Motortechnische Zeitschrift 68, 09/2007

[18] Becker, C., Härle, H. E., Ohrnberger, T.: *„14. Internationales Stuttgarter Symposium“*, Springer Fachmedien Wiesbaden, Band 1, 2014, ISBN 978-3-658-05129-7

[19] Fischer, S. et al.: *„Internationaler Motorenkongress 2015“*, Springer Fachmedien Wiesbaden, 2015, ISBN 978-3-658-08860-6

[20] Mihai, O. et al.: *„Evaluation of an Integrated Selective Catalytic Reduction-Coated Particulate Filter“*, Industrial and Engineering Chemistry Research 54, 12/2015

[21] Tronconi, E. et al.: *„Interaction of NOx Reduction and Soot Oxidation in a DPF with Cu-Zeolite SCR Coating“*, Emission Control Science and Technology 1, 5/2015

[22] Willems, F. et al.: *„Is closed-loop SCR control required to meet future emission targets?“*, SAE Technical Paper 2007-01-1574, 04/2007

[23] Zacher, S., Reuter, M.: *„Regelungstechnik für Ingenieure“*, Vieweg+Teubner Verlag | Springer Fachmedien Wiesbaden, 13. Auflage, 2011, ISBN 978-3-8348-0900-1

[24] dieselnet.com: *„ISO 8178“*, https://www.dieselnet.com/standards/cycles/iso8178.php, October 2001

[25] dieselnet.com: *„Nonroad Transient Cycle (NRTC)“*, https://www.dieselnet.com/standards/cycles/nrtc.php, July 2013

Appendix

Relationship overall transfer function

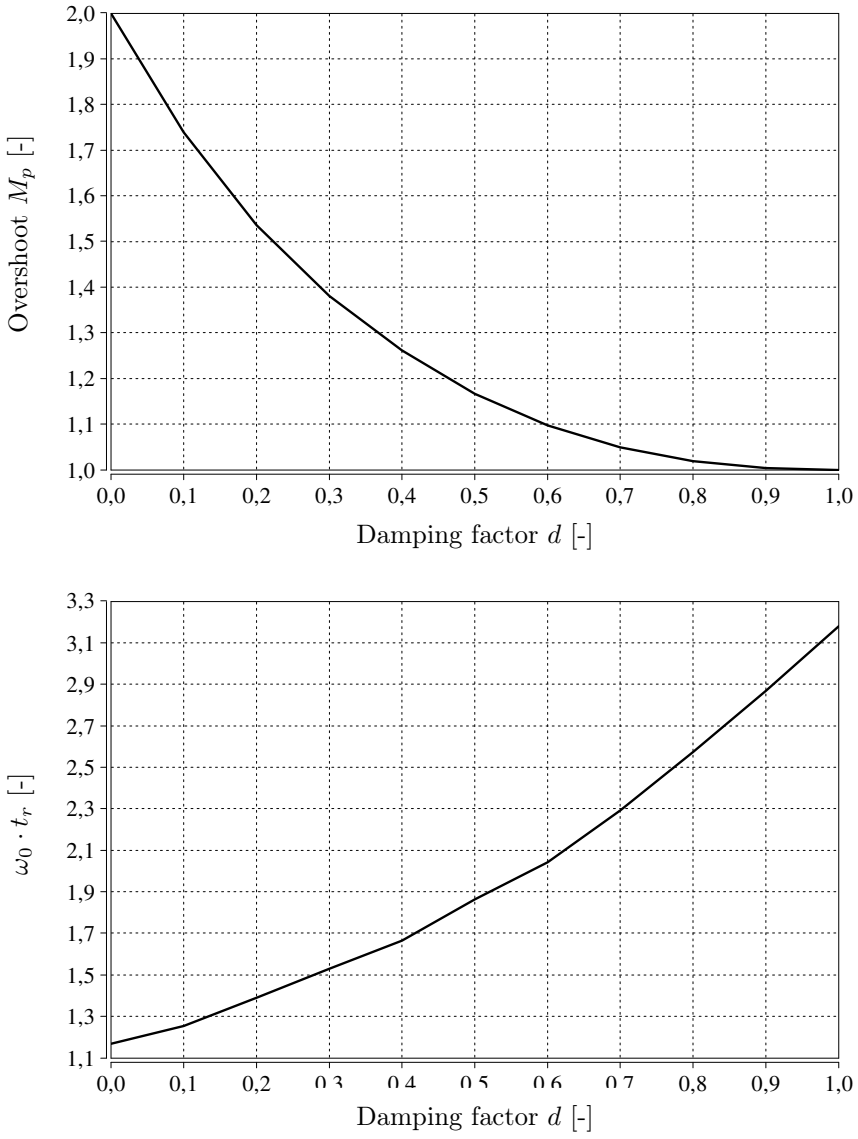

Figure A.1: Relationship between M_p, d, ω_0 and tr [16]